UNIVERSIDADE FEDERAL DE UBERLÂNDIA
FACULDADE DE ENGENHARIA QUÍMICA
PROGRAMA DE PÓS-GRADUAÇÃO EM ENGENHARIA QUÍMICA

ESTUDO DA HIDRODESOXIGENAÇÃO DO GUAIACOL EM FASE VAPOR SOBRE CATALISADORES DE PLATINA SUPORTADOS EM MATRIZES À BASE DE NIÓBIO: $xNb_2O_5/(100-x)Al_2O_3$ (x = 0, 5, 20, 100, % PESO) E $NbOPO_4$

Nathacha Kare Gonçalves Silva

Uberlândia – MG – Brasil
2018

UNIVERSIDADE FEDERAL DE UBERLÂNDIA
FACULDADE DE ENGENHARIA QUÍMICA
PROGRAMA DE PÓS-GRADUAÇÃO EM ENGENHARIA QUÍMICA

ESTUDO DA HIDRODESOXIGENAÇÃO DO GUAIACOL EM FASE VAPOR SOBRE CATALISADORES DE PLATINA SUPORTADOS EM MATRIZES À BASE DE NIÓBIO: $xNb_2O_5/(100-x)Al_2O_3$ (x = 0, 5, 20, 100, % PESO) E $NbOPO_4$

Nathacha Kare Gonçalves Silva

Orientador: Ricardo Reis Soares

Coorientador: Marcos Antonio de Souza Barrozo

Tese de Doutorado apresentada ao Programa de Pós-Graduação em Engenharia Química da Universidade Federal de Uberlândia como parte dos requisitos necessários para obtenção do título de Doutor em Engenharia Química na área de concentração em Desenvolvimento de Processos Químicos.

Uberlândia – MG – Brasil

2018

Dados Internacionais de Catalogação na Publicação (CIP)
Sistema de Bibliotecas da UFU, MG, Brasil.

S586e
2018

Silva, Nathacha Kare Gonçalves, 1988-
Estudo da hidrodesoxigenação do guaiacol em fase vapor sobre catalisadores de platina suportados em matrizes à base de nióbio [recurso eletrônico]: xNb2O5/(100-x)Al2O3 (x = 0, 5, 20, 100, % PESO) E NbOPO4 / Nathacha Kare Gonçalves Silva. - 2018.

Orientador: Ricardo Reis Soares.
Coorientador: Marcos Antonio de Souza Barrozo.
Tese (Doutorado) - Universidade Federal de Uberlândia, Programa de Pós-Graduação em Engenharia Química.
Disponível em: http://dx.doi.org/10.14393/ufu.te.2019.15
Inclui bibliografia.
Inclui ilustrações.

1. Engenharia química. 2. Processos químicos. 3. Catalisadores de platina. 4. Nióbio. 5. Química de biomassa. I. Soares, Ricardo Reis, 1965-, (Orient.). II. Barrozo, Marcos Antonio de Souza, 1961-, (Coorient.). III. Universidade Federal de Uberlândia. Programa de Pós-Graduação em Engenharia Química. IV. Título.

CDU: 66.0

Rejâne Maria da Silva – CRB6/1925

TESE DE DOUTORADO DE NATHACHA KARE GONÇALVES SILVA SUBMETIDA AO PROGRAMA DE PÓS-GRADUAÇÃO EM ENGENHARIA QUÍMICA DA UNIVERSIDADE FEDERAL DE UBERLÂNDIA COMO PARTE DOS REQUISITOS NECESSÁRIOS PARA OBTENÇÃO DO TÍTULO DE DOUTOR EM ENGENHARIA QUÍMICA, EM 07 DE JUNHO DE 2018.

BANCA EXAMINADORA:

Prof. Ricardo Reis Soares
Orientador (PPGEQ/UFU)

Prof. Marcos Antonio de Souza Barrozo
Coorientador (PPGEQ/UFU)

Dr. Vinicius Rossa
(PNPD-FEQ/UFU)

Dr. Robson de Souza Monteiro
(Catalysis Consultoria Ltda.)

Dr. Fábio Bellot Noronha
(INT)

Prof. Victor Luis dos Santos Teixeira da Silva
(PEQ/COPPE/UFRJ)

Aos meus familiares.

AGRADECIMENTOS

Sou grata a cada um que esteve no meu caminho durante esses quatro anos de doutorado. Cada pessoa me trouxe algo para celebrar ou para refletir. Tanta gente boa e querida com quem convivi nessa fase tão difícil da minha vida... Na conveniência de não citar todos os nomes e de não contar toda a história, agradeço:

À minha mãe e ao meu pai pela vida e pelo esforço amoroso em satisfazerem minhas necessidades; às minhas avós pelos sábios ensinamentos simples; à minha irmã pelas nossas partilhas engrandecedoras; aos meus familiares por me mostrarem a alegria da união e o desafio da vida em comunidade; às amigas e amigos pelo amparo e partilha de momentos leves; ao pessoal do laboratório pelas conversas, ajudas e trocas de saberes: Alexandra Pinho, Camilo Brandão, Carlos Pertensen, Celson Braga, Eduardo Piola, Fábio Gonçalves, Glenda Lopes, Izabela Lima, Isabela Munhoz, Kallyu Souza, Marina Fontes, Natan Tomaz, Roberta Martins, Ulisses da Silva, Vinicius Rossa e, em especial, ao amigo Franciel Bezerra e à querida amiga Ione Lucenir; aos estudantes e trabalhadores da Faculdade de Engenharia Química, da Faculdade de Engenharia Elétrica, do Instituto de Química e do Instituto de Física da UFU, por cada auxílio fornecido; ao professor Ricardo Soares por transmitir sua experiência no laboratório; ao professor Marcos Barrozo pela orientação e acolhimento vindos desde meu mestrado; aos engenheiros Robson Monteiro e Rogério Ribas pelo clima profissional e educativo das reuniões; à UFU e à FEQ pela infra-estrutura fornecida; à CBMM pelo custeio do projeto.

Há quem passe por um bosque e só veja lenha para a fogueira.

Leon Tolstói

TABLE OF CONTENTS

LIST OF FIGURES

LIST OF TABLES

RESUMO

Problemas oriundos da combustão de combustíveis fósseis, tais como a poluição local do ar, a mudança climática global e os conflitos entre países pelas finitas reservas fósseis estimularam a busca por fontes renováveis de energia. A biomassa lignocelulósica tem o potencial de ser transformada em combustíveis, aditivos de combustíveis e químicos sustentáveis na perspectiva de não-competição com a produção de alimentos. O produto bruto termoquimicamente tratado pela pirólise rápida da biomassa lignocelulósica apresenta propriedades indesejáveis derivadas do alto conteúdo de oxigênio e precisa ser refinado, de maneira análoga ao que acontece com o petróleo. A hidrodesoxigenação (HDO) é um dos processos que pode ser aplicado para refinar os vapores de pirólise não-condensados ou condensados (bio-óleo). Neste trabalho, a HDO de guaiacol (2-metóxifenol, $C_7H_8O_2$), composto modelo representativo da porção de lignina da biomassa, foi avaliado para funcionar como uma base para o desenvolvimento de estudos mais complexos. Inicialmente, uma análise termodinâmica da conversão de guaiacol foi realizada usando o *software* UniSim Design R400. Os resultados do equilíbrio químico revelaram que a maioria das reações era exotérmica e que a HDO de guaiacol não mostrou restrição termodinâmica para ocorrer. A parte experimental deste estudo envolveu a reação de guaiacol com hidrogênio à pressão atmosférica usando catalisadores à base de nióbio. O sistema catalítico testado foi composto por platina suportada em óxido de nióbio (Nb_2O_5), alumina (Al_2O_3), nióbia-alumina ($5\%Nb_2O_5/Al_2O_3$; $20\%Nb_2O_5/Al_2O_3$) e fosfato de nióbio ($NbOPO_4$). Os catalisadores foram caracterizados por difração de raios X (DRX), fisissorção de nitrogênio, quimissorção de CO e dessorção à temperatura programada de isopropilamina. A influência das condições operacionais como pressão parcial de hidrogênio, temperatura e velocidade espacial na atividade e seletividade foram analisadas. Foi observado que quanto maior o conteúdo de nióbia no suporte misto de nióbia-alumina maior foi a seletividade para fenol. O catalisador $Pt/NbOPO_4$ formou menos produtos desoxigenados do que Pt/Nb_2O_5. Pt/Nb_2O_5 preparado usando oxalato amoniacal de nióbio como precursor foi superior ao catalisador preparado usando ácido nióbico. Pt/Nb_2O_5 mostrou-se como o catalisador de melhor desempenho, o que foi atribuído à interação entre Pt e espécies NbO_x (interface metal-suporte).

Palavras-chave: fosfato de nióbio, guaiacol, hidrodesoxigenação (HDO), melhoramento da biomassa, nióbia.

ABSTRACT

Problems arising from fossil fuels combustion, such as local air pollution, the global climate change, and the conflicts between countries for finite fossil reserves stimulated the pursuit for renewable sources of energy. Lignocellusic biomass has the potential to be transformed in fuels, fuels additives, and sustainable chemicals in the perspective of non-competition with food production. The raw product thermochemically treated by fast pyrolysis of lignocellulosic biomass shows undesired properties derived from the high oxygen content and needs to be upgraded, in an analogue way as occurs with crude petroleum. Hydrodeoxygenation (HDO) is one of the processes that can be applied to upgrade the non-condensed or condensed (bio-oil) pyrolysis vapors. In this work, the HDO of guaiacol (2-methoxyphenol, $C_7H_8O_2$), model compound representative of the lignin portion of biomass, was evaluated to function as foundation for the development of more complex studies. Initially, a thermodynamic analysis of the guaiacol conversion was carried out using the software UniSim Design R400. The results of the chemical equilibrium revealed that most of the reactions were exothermic and that the HDO of guaiacol did not show thermodynamic restriction to occur. The experimental part of this study involved the guaiacol reaction with hydrogen at atmospheric pressure using niobium-based catalysts. The catalytic system tested was comprised by platinum supported on niobium oxide (Nb_2O_5), alumina (Al_2O_3), niobia-alumina ($5\%Nb_2O_5/Al_2O_3$; $20\%Nb_2O_5/Al_2O_3$), and niobium phosphate ($NbOPO_4$). The catalysts were characterized by X-ray diffraction (XRD), nitrogen physisorption, CO chemisorption, and temperature-programmed desorption of isopropylamine. The influence of operating conditions such as hydrogen partial pressure, temperature, and space velocity on both activity and selectivity were analyzed. It was observed that the higher the niobia loading in the niobia-alumina mixed support the higher was the selectivity for phenol. The $Pt/NbOPO_4$ catalyst formed less deoxygenated products than Pt/Nb_2O_5. Pt/Nb_2O_5 prepared using ammonium niobium oxalate as precursor was superior to the catalyst prepared using niobic acid. The Pt/Nb_2O_5 was the best performance catalyst, which was attributed to the interaction between Pt and NbO_x species (metal-support interface).

Keywords: biomass upgrading, guaiacol, hydrodeoxygenation (HDO), niobia, niobium phosphate

CHAPTER 1 – INTRODUCTION

1.1 Contextualization

Fossil fuels (coal, oil, and natural gas) are used as a dominant source of energy in the contemporary human society. 87% of the global energy supply comes from fossil fuels for transport, heat production, and electricity generation. Fossil energy provided progress, lowered territorial distances, and allowed a more comfortable life style. However, fossil fuels also produce negative impacts, such as local air pollution, emission of greenhouse gases [1], political and economic problems worldwide, since fossil fuel reserves are finite and unevenly distributed around the planet. In contrast, renewable sources of energy are abundant, better distributed around the world, and allow the development of zero-carbon or carbon-neutral technologies [2].

The global expansion of renewable energy use is strongly associated with environmental concerns arising from greenhouse gases emissions when fossil fuels are burned. The Intergovernmental Panel on Climate Change (IPCC) stated with 95% of certain that the current global warming is mainly caused by human activities. The atmospheric concentration of carbon dioxide, methane, and nitrous oxide increased due to anthropogenic greenhouse gas release. About 78% of the total greenhouse gases emissions increase from 1970 to 2010 are attributed to CO_2 emissions from fossil fuels combustion and industrial processes. It is extremely likely that anthropogenic factors contributed for more than half of the increase in global average surface temperature from 1951 to 2010. The impacts of temperature rising are many: species lost abundance and shifted both their geographic ranges and behavior patterns; the atmosphere and ocean became warmer; the sea level has risen, since the snow and ice quantity decreased; there was an increasing rate of ocean acidification; extreme weather events were observed (e.g., frequency/intensity of daily temperature extremes) [3]. In light of these evidences, countries agreed to work to keep global temperature rise below two degrees Celsius in the UN Paris Agreement on climate change that happened in 2015.

Brazil has been following the global trend for renewable energy pursuit some years ago. Initially, economic was the major driving force for the change, but recently environmental concerns became part of the country agenda. The economic driving force was the oil crisis in the 1970 decade, which affected the economy of many countries and stimulated the pursuit of alternative energy sources. Particularly in Brazil, the federal government instituted the National Fuel Alcohol Program (Proálcool) in 1975, through which encouraged the use of ethanol from sugar cane as automobile fuel. The environmental driving force for sustainable energy became more noticeable when Brazil hosted the first Conference on the Environment and Development (1992 Earth Summit), as well as the 2012 Rio+20 Conference. At Rio+20, it was agreed that an open working group would present its recommendations for achieving sustainable development. In 2015, world leaders participated of the United Nations Summit and adopted the 17 Global Goals for the 2030 Agenda for Sustainable Development. The Sustainable Development Goals (SDGs) must work out from 2016 to 2030, to substitute the Millennium Development Goals, which were on vigor since 2000. To ensure access to affordable and clean energy is one of the 17 SDGs [4].

Lignocellulosic biomass (e.g., sugar cane bagasse, grasses, wood) consists of a renewable energy source that displays the potential of being converted in sustainable fuels and chemicals [5,6]. Among the known thermochemical routes for biomass processing, fast pyrolysis stands out because of its simplicity and relatively low cost of operation [5,7]. The most interesting product from fast pyrolysis is bio-oil (condensed product) or the pyrolysis vapor (non-condensed product). However, the crude product from fast pyrolysis has limited applications because of its undesired properties derived from the high oxygen content [8,9]. Some methods were proposed to improve the quality of the crude product from fast pyrolysis, such as the addition of emulsifiers, filtration, solvent addition, and catalytic routes (zeolite cracking and hydrodeoxygenation) [5,8,10,11]. The upgrading of the crude product from fast pyrolysis in the scope of a biorefinery is an analogous approach to a petroleum refinery [12,13].

Hydrodeoxygenation (HDO) route can provide oils of higher grade than the zeolite cracking [11]. Therefore, HDO was chosen as the upgrading method for the crude fast pyrolysis product in this study. The HDO occurs over a catalyst in hydrogen environment at moderate temperatures (300–600 °C) with the aim of removing oxygen in the form of water (environmentally benign) [14–16]. The HDO of biomass-derived feedstocks can be carried out from near-ambient pressure in vapor phase to high pressure values in liquid phase. The high pressure upgrading increases the costs of operation, demands separation of both solvent

and catalyst, and is challenging due to the chemical and thermal instability of the liquid bio-oil [17–20]. Considering these facts, the HDO was carried out at atmospheric pressure and vapor phase in this study.

The current challenges of the HDO applied on lignocellulosic biomass upgrading include: (i) the complex composition of the feedstocks; (ii) the commercial unavailability of hydrogen from renewable sources; (iii) the many reactions in series and in parallel that occur along with the reactions of water release; (iv) the design of suitable catalytic systems. To circumvent the complex composition of the pyrolysis vapors, guaiacol (2-methoxyphenol, $C_7H_8O_2$) was selected as a model compound representative of the lignin-derived phenolic species from lignocellulosic biomass. The focus of this work was to study possible catalytic systems for the HDO of the lignin portion of biomass.

Research has been conducted with different catalysts to investigate the hydrodeoxygenation of the pyrolysis product. The bifunctionality of the catalysts has been discussed in terms of the existence of sites capable of activating hydrogen close to sites effective for C–O scission. It is believed that the most promising catalysts are the bifunctional because the existence of two different active sites can catalyze complementary reaction steps or can participate in the same step through interaction of different parts of an adsorbed molecule [21].

Noble metals, including Ru, Rh, Pd, and Pt, despite their high cost, are promising upgrading catalysts because they have the ability to activate hydrogen (supply atomic hydrogen to the reaction) and to conduct hydrogenation reactions. Furthermore, they do not deactivate in the presence of water and they are already used in commercial catalytic processes [21].

Phenolic compounds present in the pyrolysis product typically contain methoxy groups attached to the ring, which may produce low-value light gases in traditional hydrotreatment. A strategy to preserve the methoxy carbon is to incorporate acidity to the catalyst to allow transalkylation reactions. However, the acidity can lead to rapid catalyst deactivation, typically because phenolics strongly adsorb in acidic catalysts (e.g., zeolites). The introduction of a metal capable of dissociating hydrogen coupled with the acid function can reduce this problem, extend catalyst lifetime, and promote deoxygenation of OH groups. Alternatively to the zeolite/metal approach there is the possibility to incorporate a reducible oxide support [22].

Promising results were reported when the HDO of biomass related compounds was carried out using a noble metal supported on a reducible oxide (e.g., TiO_2, Nb_2O_5) [19,23–28].

A cooperative mechanism between the metal and the reducible support was inferred as the central cause of the good catalyst performance.

Niobium-based catalysts are typically stable and can provide high reactivity for reactions that either produce water or are conducted in aqueous environment [29]. It is valid to recall that the desired HDO process eliminates oxygen through water release from the molecules. Potential niobium-based supports are niobim oxide and niobium phosphate, which were tested in this study as catalytic supports. Nb_2O_5 can be used not only as catalytic support but also as a promoter, which is interesting to disperse the niobia of low surface area calcined at high temperatures (~ 500 °C). Moreover, the properties and molecular structures of the surface niobia can be very different from the bulk Nb_2O_5 phases and can influence the properties of the supports [30]. Alumina was chosen as the high surface area oxide support to be coated by niobia, thus the mixed support Nb_2O_5/Al_2O_3 was also evaluated.

1.2 Objectives

Considering what was previously exposed the general objective of this work was to study the performance of niobium-based catalysts on the hydrodeoxygenation (HDO) of guaiacol, model compound representative of the lignin portion of biomass.

The specific objectives were:

- To evaluate the thermodynamics of the HDO of guaiacol by simulation;
- To synthesize and to characterize the platinum supported catalysts over $xNb_2O_5/(100\text{-}x)Al_2O_3$ (x = 0, 5, 20, 100, wt.%) and $NbOPO_4$;
- To determine the effect of the niobia loading in the behavior of the Pt catalyst supported on Nb_2O_5/Al_2O_3;
- To compare the activity, stability, and selectivity of both the catalysts and pure supports;
- To evaluate the influence of the following operational conditions in the catalysts performance: H_2 partial pressure, temperature, and weight hourly space velocity (WHSV);
- To study the influence of different precursors of niobia (ammonium niobium oxalate and niobic acid) in the performance of the catalyst Pt/Nb_2O_5.

1.3 Structure of this work

This work is composed of 6 chapters. Chapters 3 to 5 are proposed partial papers to be submitted to journals. Chapter 1 introduces the general subject of this study, which is the hydrodeoxygenation (HDO) of a lignin-derived product, guaiacol, as a potential sustainable source of fuels and chemicals. Chapter 2 consists of a brief literature review about the subject of this thesis. Chapter 3 explores the thermodynamics of the HDO of guaiacol. Chapter 4 presents the promoting effect of niobia impregnation in alumina as a support for the platinum metal in the HDO of guaiacol reaction. Chapter 5 reveals the performance of the Pt catalysts containing niobium as support (Nb_2O_5 and $NbOPO_4$) and compares Pt/Nb_2O_5 catalysts prepared using different precursors of niobia. Chapter 6 covers the main conclusions of the present work as well as suggestions for future works. The Appendix contains supplementary information of the experimental part. Figures in Appendix are referred as Fig. A, Fig. B, etc.

CHAPTER 2 – LITERATURE REVIEW

2.1 Energy scenarios

The current global primary energy consumption by source is the following: crude oil (33.9%); coal (28.6%); natural gas (24.6%); traditional biofuels (7.3%); renewable sources (3.9%); nuclear (1.7%) [1]. Although fossil fuels are by far the most expressive energy source, it is noticeable the recent trend of both stabilization of global energy consumption and expansion of non-fossil fuel sources. A raise of 1.0% of world primary energy consumption was observed in 2016. This value is below than the 10-year average, which is 1.8%. In addition, the production of renewable power grew by 14.1% (excluding hydropower), of which more than half corresponded to wind power growth and one third came from solar energy growth [31].

Brazilian energy matrix is nowadays marked by the use of renewable energy due to the significance of hydropower. The most expressive sources used to produce electricity are hydroelectric power (61%), fossil fuel (17%), biomass (9%), wind (7%), and importation from Paraguay, Argentina, Venezuela, and Uruguay (5%). Sugar cane and the forest sector are responsible for 78% and 20%, in this order, by the power generated from biomass [32].

2.2 Biomass as energy source

Biomass is the only source of carbon known which is natural, renewable, and available in large quantity enough to be used as a substitute for fossil fuels. Biomass is renewable because it needs a short time to replace what is used for energetic purpose. On the contrary, fossil fuel coal, petroleum crude oil, and natural gas require millions of years to be formed in the earth, and their reserves are subject to depletion if the global demand increases in an accelerate way [33]. Biomass is easily available in many places around the world and contains negligible amounts of sulfur, nitrogen, and metals, unlike heavy oil [15].

From the energetic point of view, biomass can be considered as all renewable resource derived from organic matter of vegetable or animal origin, which can be used for

production of energy [34]. Aquatic and terrestrial vegetation, municipal solid waste, forest and agricultural residues, and some industrial wastes can all be classified as biomass. The basic principle of using biomass as a renewable resource comprehends (i) the capture of both solar energy and carbon (CO_2) from environment by the growing biomass and (ii) the conversion of biomass in fuels or thermal energy. The cycle completes when biomass or the product derived from it gets combustion, which is equivalent to release the solar energy previously captured and to turn back the carbon fixed during photosynthesis as CO_2 to the atmosphere [35].

Biomass feedstocks can be classified in the following general groups: i) amorphous sugars (e.g., starch, glucose), ii) triglycerides (e.g., vegetable oil), and iii) lignocellulosic biomass (the non-edible portion of biomass, e.g., bagasse, corn stover, grasses, wood). The last group comprehends the cheapest, most abundant, and fastest growing form of terrestrial biomass [6]. In addition, lignocellulosic biomass has the advantage of enabling the use of "second-generation" technologies for fuels production, which do not compete with the food productive chain. This consists of an alternative for the "first-generation" biofuels, such as bioethanol and biodiesel. The "third-generation" biofuels produced from microalgae and cyanobacteria are also being investigated [10,11,15,36,37]. It is worth to mention that ethanol and biodiesel are the liquid biofuels predominantly used in the recent times, marked by the blending with conventional fuels (gasoline and diesel) [2,15]. However, feedstocks with low land-use efficiency are used for the production of these biofuels. Besides the low impact in the land use, it is desirable that the feedstock used to generate energy also shows low water footprint and low carbon footprint. Lignocellulosic biomass fulfills the prerequisites mentioned and is available for use in the short term [38].

The three main components of lignocellulosic biomass are cellulose, hemicellulose, and lignin. Cellulose consists of a crystalline glucose polymer ($C_6H_{12}O_6$). Hemicellulose is a complex amorphous polymer of five-carbon sugars (xylose and arabinose) and six-carbon sugars (galactose, glucose, and mannose), but the xylose monomeric unit ($C_5H_{10}O_5$) prevails. Lignin is an aromatic amorphous polymer that gives structural integrity to the plant, since it acts as glue, which fills in the spaces between cellulose and hemicellulose. It is believed that the biosynthesis of lignin happens by the polymerization of primary monomers: p-coumaryl, coniferyl, and sinapyl alcohols [5,39]. The location and structure of the three main components of lignocellulosic biomass can be seen in Figure 2.1.

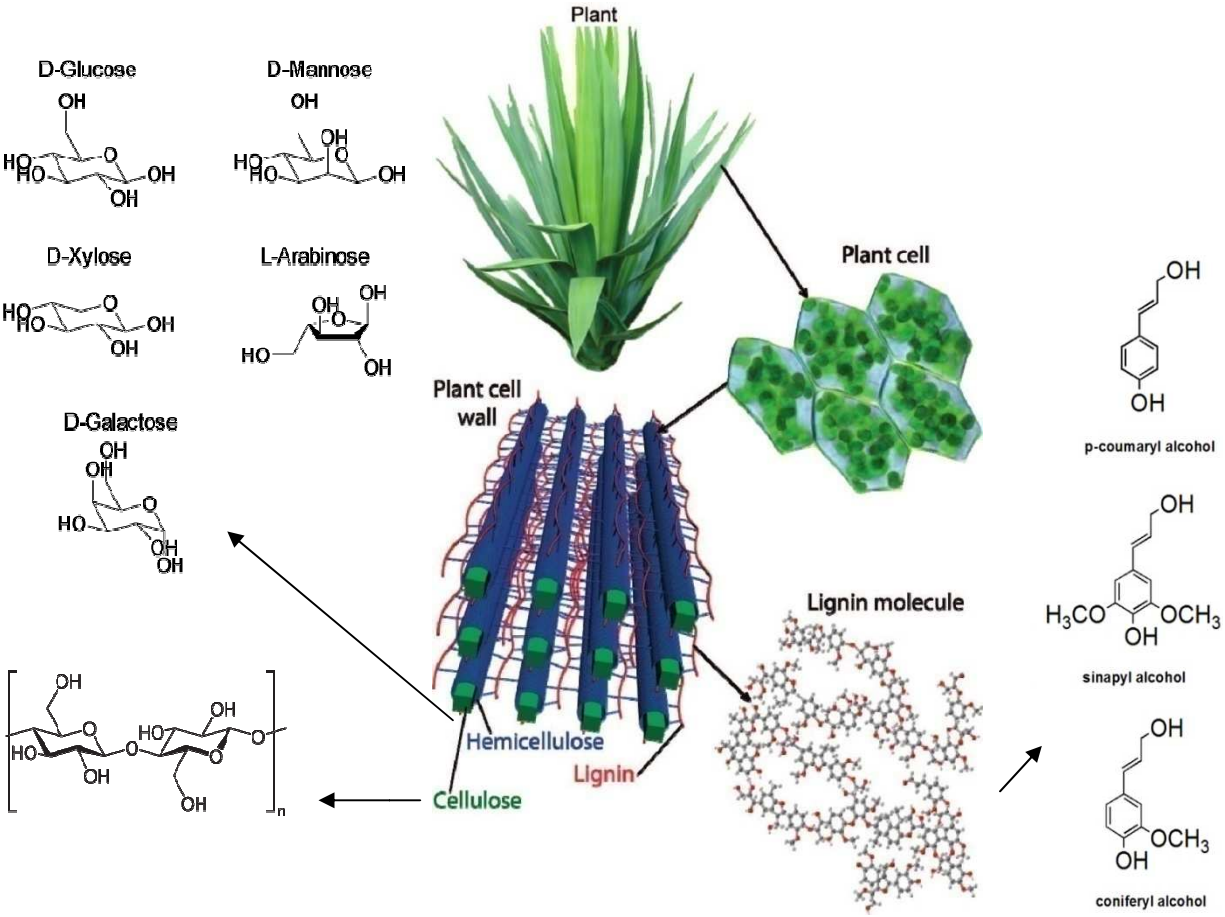

Figure 2.1 – Plant cell wall architecture. Adapted from ref. [39].

Biomass can be treated by biological (anaerobic digestion and fermentation) and thermal methods (combustion, gasification, pyrolysis, liquefaction) in order to produce fuels. Pre-treatment and hydrolysis are strategies of deconstruction of biomass that use both biological and chemical conversion [40]. In scope of thermochemical processes, i.e., decomposition of biomass by increasing temperature and/or pressure without catalyst [2], the direct combustion of biomass provide heat to generate steam and hence electricity. Gasification produces a fuel gas that can be combusted and used in an engine or turbine [40]. Fast pyrolysis and liquefaction allows that 50–90% of the biomass energy be converted in liquid, named bio-oil. Liquefaction is generally carried out at 50–200 atm and 250–325 °C. Fast pyrolysis typically occurs at 1–5 atm and 375–525 °C and it presents lower capital cost than liquefaction, which favors its commercialization [5]. The known processes for production of fuels from lignocellulosic biomass are shown in Figure 2.2.

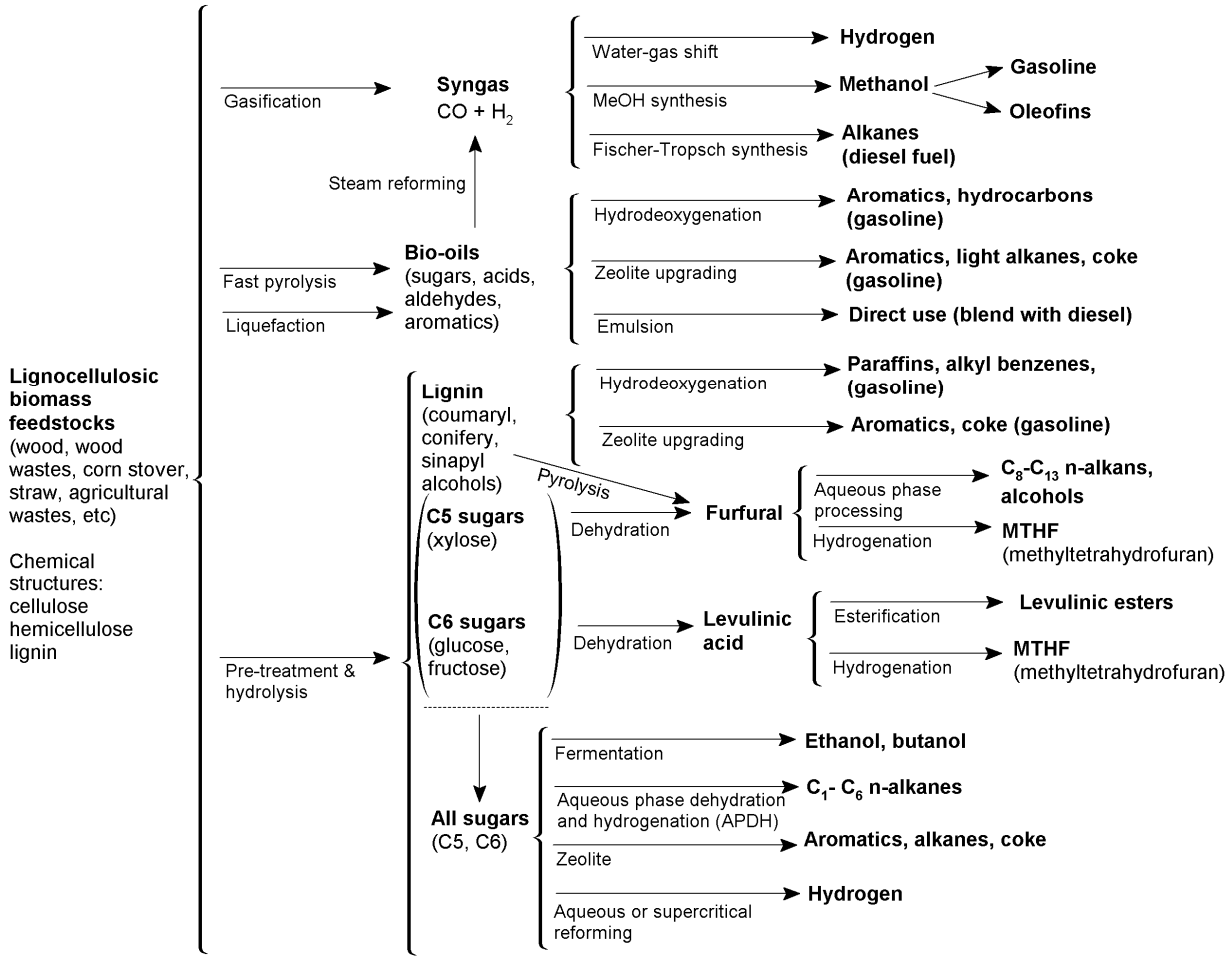

Figure 2.2 – Strategies for production of fuels from lignocellulosic biomass. Adapted from ref. [6].

2.3 Fast pyrolysis of biomass

The thermal decomposition through pyrolysis of organic materials in the absence of air gives gas, liquid, and solid as products. The proportions of the main products can be controlled by changing the reaction parameters (temperature, rate of heating, and vapor residence time). Lower temperatures (~400 °C) and longer vapor residence times (hours → days) favor the production of charcoal (carbonization) by the slow pyrolysis process. However, long residence times combined with high temperatures (~750–900 °C) increase biomass conversion to gas (gasification). Moderate temperatures (~500 °C) and short vapor residence times of less than 2 s characterizes the fast pyrolysis, which optimizes the liquid yields at up to 75 wt.% on a dry-feed basis [7,41]. Flash pyrolysis was found as a feasible route and is the most applied process to generate bio-oil [11].

All pyrolysis products are valuable and have application. However, bio-oil, the liquid product, is the most interesting compared to gas and charcoal because it offers a plenty of possibilities of being converted to fuel additives [10]. A fast pyrolysis system that maximizes

bio-oil production is comprised of an integrated series of operations which, conceptually, cover: i) preparation of the feed material (drying and grinding); ii) pyrolysis in the reactor; iii) char and ash separation, generally by cyclones; iv) gas-liquid separation and bio-oil collection [40]. Fast pyrolysis provides an increase in the energy density of raw biomass by roughly a factor of 7–8 [11]. Besides the high energy density, which implies in easier handling and transport compared to raw biomass, bio-oil has low nitrogen and sulfur content in relation to petroleum products meaning lesser air pollutant potential [42].

Bio-oils are mixtures comprised of more than 400 compounds derived from depolymerization and fragmentation reactions of cellulose, hemicellulose, and lignin. Bio-oil constituents belong to the groups of acids, esters, ethers, alcohols, ketones, aldehydes, sugars, furans, and phenolics. The phenolics come from the decomposition of lignin. The depolymerization of cellulose and hemicellulose forms sugars and furans. The remaining organic compounds may be formed from decomposition of the miscellaneous oxygenates, sugars, and furans. The identification of each compound in a bio-oil sample remains a challenge, but free hydrocarbons are rarely found, what suggests that oxygenates are expressive constituents [5,20].

The presence of oxygen in many bio-oil compounds is the primary reason for differences in the properties and behavior between hydrocarbon fuels and biomass pyrolysis oils, as can be seen in Table 2.1. High water content, high viscosity, poor ignition properties, corrosiveness, and instability are some undesired characteristics that challenge the use of bio-oils for fuel applications. The oxygen content of pyrolysis oils is usually 35–40 wt.%. This results in a heating value 50% lower than that of conventional fuels oils, besides the immiscibility with hydrocarbon fuels. The water content in bio-oils (15–30 wt.%) lowers its heating value and increases ignition delay compared to diesel fuels, but also reduces the oil viscosity, which favors pumping and atomization. During storage or handling, some compounds present in biomass oils can react with themselves, process that occurs slowly over time and it is called “aging”. The “aging” promotes undesirable changes in physical properties, such as increase of viscosity [8,9].

Emulsifiers added to crude bio-oil can be applied as a fuel additive for some boiler and engines [10]. However, the unfavorable characteristics of the crude liquid of pyrolysis make difficult its direct application. This fact is analogous to petroleum feedstocks, which must be refined in order to produce conventional fuels. The bio-oil quality could be upgraded by using simple physical methods, such as filtration (for char and alkali removal) and solvent addition (to reduce viscosity and increase chemical stability) [8]. Furthermore, more

elaborated routes were proposed for the upgrading of bio-oil, which includes hydrodeoxygenation (HDO), zeolite cracking, formation of emulsions with diesel, and conversion in synthesis gas by steam reforming [5,10,11], as previously shown in Figure 2.2. Unlike hydrodeoxygenation, hydrogen is not a requirement on zeolite upgrading, which results in drawbacks of poor hydrocarbon yield and catalyst deactivation. Hydrogen allows clean processing and less formation of coke [2]. HDO appears to be the best potential route compared to zeolite cracking, which produce oils of low grade [11].

Table 2.1 – Typical properties of wood pyrolysis bio-oil and of heavy fuel oil. Source: ref. [9].

Physical property	Bio-oil	Heavy fuel oil
Moisture content, wt.%	15 – 30	0.1
pH	2.5	–
Specific gravity	1.2	0.94
Elemental composition, wt.%		
C	54 – 58	85
H	5.5 – 7.0	11
O	35 – 40	1.0
N	0 – 0.2	0.3
Ash	0 – 0.2	0.1
Higher heating value (HHV) (MJ/kg)	16 – 19	40
Viscosity (at 50 °C), cP	40 – 100	180
Solids, wt.%	0.2 – 1	1
Distillation residue, wt.%	Up to 50	1

Two promising process designs for the catalytic upgrading of the pyrolysis oil are *ex situ* and *in situ* catalytic fast pyrolysis (CFP). On the first approach, the pyrolysis vapor is forwarded to a cyclone then it is sent, without heat exchange, to the reactor operating in vapor phase for deoxygenation. The difference of the *in situ* CFP is that the catalyst is placed inside the pyrolysis reactor. Both the techniques produce a stabilized bio-oil after condensation, which still may require further hydrotreating to achieve transportation fuel specifications. It is believed that to move from *ex situ* CFP to *in situ* CFP as a technology pipeline is a natural progression. However, research in the *ex situ* CFP allows the understanding of fundamental catalytic requirements for oxygen removal at pyrolysis conditions [20].

The separation of the many chemical functional groups present in bio-oil is challenging. Distillation is not effective because the increasing temperature accelerate polymerization and forms tar. The addition of a water/organic solvent mixture to bio-oil results in phase separation, but do not solve all problems since some compounds are

immiscible in both water and organic solvent. Another separation strategy consists of the sequential condensation of pyrolysis oil vapors (fractionation via staged condensation), in which the heavier products are condensed prior to the lighter ones. This approach allows some separation of the chemicals groups, but polymerization in the liquid phase may still be a problem. Alternatively, stages can be applied on the thermal processing of the solid biomass. In this method, the treatment at successively higher temperatures results in different vapor product streams, which can be catalytically upgraded in an individual manner. The fractionations strategies proposed are positive in the direction of dividing the complex biomass-derived feedstocks in a series of simpler stages [22]. The separation of the pyrolysis compounds is a field of research that requires more development.

2.4 Hydrodeoxygenation (HDO)

Hydrodeoxygenation process was chosen as the object of study of this work to be used as the strategy for upgrading the lignin-derived products from fast pyrolysis of biomass on vapor phase (*ex situ* catalytic fast pyrolysis). From another point of view, the HDO can also be applied as a subsequent step of the deconstruction of biomass through pretreatment or hydrolysis for lignin valorization [43], as showed in Figure 2.2. The individual treatment of each portion of biomass (cellulose, hemicellulose, and lignin) is a possible approach for a biorefinery, i.e., system similar to a petroleum refinery, but that uses biomass as primary feedstock [12,13].

In the context of catalytic hydroprocessing – the treatment of petroleum feedstocks with hydrogen gas –, the catalytic hydrodeoxygenation (HDO) refers to the conversion of the oxygen in the feed into water, which is environmentally benign. The HDO occurs simultaneously with several classes of reactions: hydrodesulphurization (HDS), hydrodenitrogenation (HDN), hydrogenation (HYD), and hydrodemetallization (HDM). The hydroprocessing aims to remove sulphur and nitrogen from organic compounds in petroleum feedstocks, in order to reduce SO_x and NO_x emissions, which cause air pollution. In addition, it avoids the poisoning of the catalysts by both S-compounds and N-compounds in the feeds. The removal of oxygen also occurs under hydrotreating conditions, although it is generally not a goal of this process. As the content of oxygen in conventional crudes is less than 2 wt.%, HDO is not an important step in the hydroprocessing of light fractions of petroleum. However, HDO plays a significant role during catalytic upgrading of heavy residues, shale

oil, tar sand, coal liquids, and especially in the treatment of biomass-derived feed, whose oxygen content may approach 50 wt.% [14,44].

The research about the catalytic hydrotreating of biomass-derived liquids began after the operation of the first pilot plant of wood liquefaction had started in 1979. The initial study published in 1983 was an attempt to produce gasoline from the liquefaction oil. The tests were performed in a batch reactor using phenolic model compounds. The advance of the studies revealed the difficulty of upgrading fast pyrolysis bio-oil because of its reactivity [45]. Initially, the conventional and commercial hydroprocessing catalysts used in petroleum industries [46] were tested in biomass upgrading, i.e., sulfided $CoO–MoO_3/\gamma\text{-}Al_2O_3$ (Co–Mo/Al_2O_3) and sulfided $NiO–MoO_3/\gamma\text{-}Al_2O_3$ (Ni–Mo/Al_2O_3). These catalysts were applied in earlier studies motivated by the idea of co-processing bio-oil in existing petroleum refineries [15,45,47]. However, some studies have shown that the hydrotreating approach used for petroleum feedstocks is not suitable for bio-oil [45]. An easy co-processing in the running hydrotreating units cannot be reproduced because the optimal industrial performance for petroleum feedstocks is not suitable for bio-oils [15]. In addition, hydrogen at high pressure (7–30 MPa) along with H_2S (to maintain a sulfided catalyst) is fed in conventional hydrotreating units at temperatures around 200–425 °C achieving near-complete conversion. On the other hand, significantly different operating conditions are used to produce the pyrolysis vapor through the *ex situ* catalytic fast pyrolysis (near-ambient pressure, 500 °C). Then, design of compressors to operate with pyrolysis vapor at 500 °C or high pressure hydropyrolysis will be required if high-pressure vapor upgrading is the process chosen. This approach increase the capital cost and still require research and development to be viable [20].

Bio-oils hydrotreating corresponds to a modification or extension of the conventional process applied in petroleum refineries [15]. The HDO of bio-oil is carried out in hydrogen environment with the presence of catalyst at moderate temperature (300–600 °C) to remove oxygen in the form of water. The following reactions may take place during the process: (i) dehydration caused by condensation polymerization reactions; (ii) decarbonylation (eliminates oxygen as CO); (iii) decarboxylation (eliminates oxygen as CO_2); (iv) dealkylation derived from the cleavage of the $C_{aromatic}O–CH_3$ bond, often demethylation (DME) through elimination of methane; (v) dealkoxylation eliminates oxygen as alcohol, in which demethoxylation (DMO) is often and releases methanol; (vi) hydrogenation (saturation of unsaturated components); (vii) hydrocracking and cracking, in which high molecular weight components are broke down into smaller molecules; (viii) transalkylation (methyl group transfer). Hydrogenolysis, as a general nomenclature, is related to the breakup of C–O

bonds [16,20]. Examples of these reactions are shown in Figure 2.3, in which the authors [20] refer to hydrodeoxygenation (HDO) as the reaction that eliminates water from the molecule after hydrogenation and attributed the direct deoxygenation (DDO) to the removal of water without prior hydrogenation. It is also common to find reference to HDO as the reaction that eliminates water from the molecule without prior hydrogenation. Different terminology for the reactions is commonly found in literature [21]. In the present work, the nomenclature adopted refers to HDO as the general treatment with hydrogen aiming the removal of oxygen comprised by different reactions in series and/or in parallel.

Once water is formed in the conceptual hydrodeoxygenation, at least two liquid phases (aqueous and organic) may be observed in the product. Two organic phases have also been reported, because some compounds had lower density than water [11]. However, the formation of different phases may be associated on both operating conditions and the conversion level reached on HDO. The liquid product of the present work exhibited a single homogeneous phase for the conversions range tested.

The technology for hydroprocessing lipid feedstocks has been developed for some companies, such as UOP Honeywell Co., Haldor Topsoe, Neste Oil Co., Tyson Foods, Inc., Valero Energy Corporation, ConocoPhillips, Toyota Motor Corporation (TMC), Hino Motors, the Tokyo Metropolitan Government, and Nippon Oil Corporation (NOC). The commercial production of green fuels (green diesel or jet fuel) by petroleum related companies is currently a reality [48]. For instance, the UOP/ENI Ecofining process is being applied in the United States and in Italy to produce green diesel or jet fuel through deoxygenation followed by isomerization [49]. Nest Oil is producing renewable fuels in refineries located in Finland, Singapore, and The Netherlands [50]. However, the technology and application concerning renewable fuels derived from lignocellulosic biomass are incipient, yet research is being conducted is this field. For instance, UOP LLC patented a process to produce aromatics useful in gasoline and diesel and chemical precursors for the chemical industry through treatment of lignin and cellulosic biomass under hydrogen atmosphere [51]. Several researches, including the ones conducted by Shell, Honeywell/UOP, PNNL (Pacific Northwest National Laboratory), and BTG (Biomass Technology Group) aiming the bio-oil hydrotreating were catalogued by Graça et al. [15].

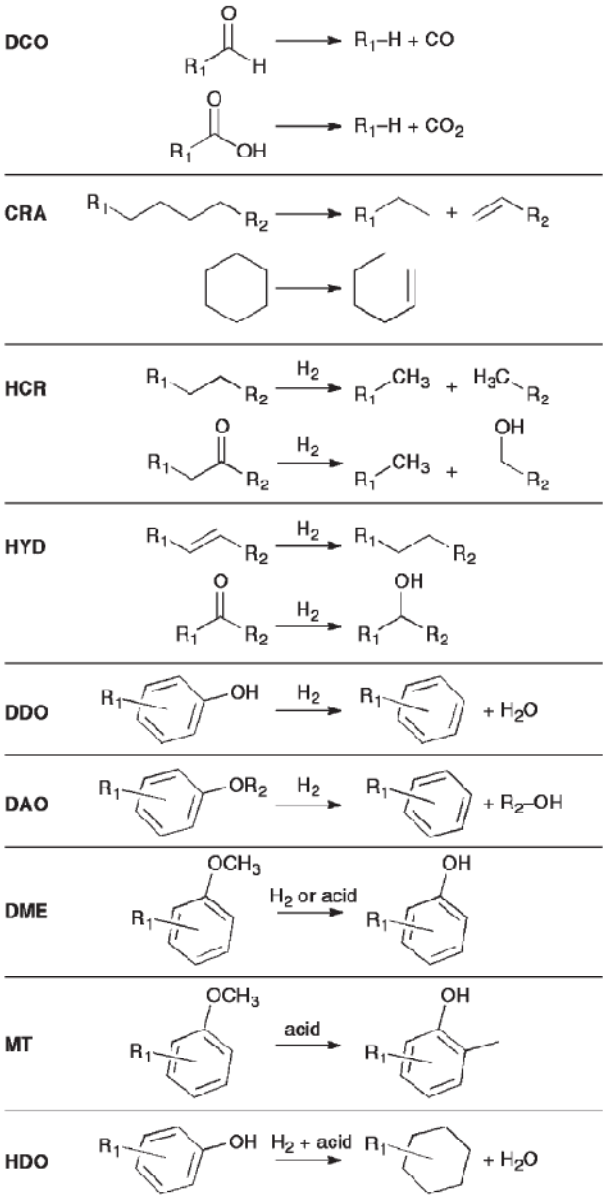

Figure 2.3 – Examples of reactions that can occur in catalytic bio-oil upgrading. Abbreviations: DCO (decarboxylation), CRA (cracking), HCR (hydrocracking), HYD (hydrogenation), DDO (direct deoxygenation), DAO (dealkoxylation), DME (demethylation), MT (methyl transfer reaction), HDO (hydrodeoxygenation). Source: ref. [20].

Some challenges found in the field of HDO include the design of suitable catalytic systems and the availability of sustainable hydrogen sources [16,37,43]. It is desirable to obtain deoxygenated products from biomass with maximum carbon and minimum hydrogen consumption. To achieve this goal catalysts should be developed for selectively cleave the C–O bonds [22,37]. Nowadays, 96% of hydrogen production is derived from fossil sources, in which 48% comes from steam reforming of natural gas [52]. However, studies have been conducted to obtain hydrogen from renewable sources, such as biomass [2,52–54]. It seems that the uncertainties for the application of the hydrogen energy derived from renewable

sources are caused by the lack of economic studies concerning the subject [52]. In the case of biofuels production, the cost of the fuel derived from lignocellulosic biomass (low feed cost) is mostly influenced by the processing, which is a combination of handling, treatment, conversion, and upgrading. On the other hand, the cost of fuel derived from petroleum is determined by the feed cost and shows low processing cost [20].

2.5 HDO of guaiacol

The complex composition of the bio-oil gives some challenges for the analysis aiming the identification of the components [55]. To circumvent this fact fundamental studies with model compounds have been developed in literature. These studies make it possible to simplify the reactants, to isolate transformations, and to clarify both the HDO reaction mechanisms and the catalysts active sites [16,20–22,37,56]. The idea is to understand the fundamental investigations of reaction pathways and kinetics then expand them to more complex compounds (with more functional groups) and to mixtures of compounds that can absorb competitively on catalytic sites [37]. The model compounds represent a structural class of the upgraded biomass derived feedstocks: lignin precursors represent bio-oil; sugars and sugar alcohols are representative of cellulose and hemicellulose; triglycerides and fatty acids derivatives are surrogates of lipids or fats/oils [56].

Bio-oil is comprised by about 30 wt.% of lignin-derived phenolic species [20], which are the lowest reactive compounds. Lignin typically decomposes from 280–500 °C during pyrolysis consisting of the more heat-resistant lignocellulosic biomass component compared to cellulose and hemicellulose [16]. Lignin valorization plays an important role in the modern biorefinery scheme, but it received little attention compared to the development of the triglycerides, cellulose, and hemicellulose valorization [37,39]. An overview of the carbohydrate-derived molecules possible conversion to chemicals and fuels was presented by Chheda et al. [57].

Lignin is currently considered a low-price waste product, which is available in large quantities and mostly burned for generation of process heat (e.g., sugarcane bagasse from lignocellulose-to-ethanol process and residue from pulp and paper industry). The methoxy-groups in lignin offer the opportunity to produce C1 compounds (e.g., methanol) in addition to low molecular weight aromatics. In fact, the only viable source to produce renewable aromatic compounds that are widely used nowadays is lignin. The research about the conversion of lignin to value added chemicals and fuels is incipient, since catalyst technology

applied to petroleum refining does not fit to the biomass substrates upgrading [16,37,39]. The conversion of the phenolic compounds present on lignin is appealing due to their similarity to gasoline [22]. The applications of macromolecular lignin, like carbon fibers, polymer modifiers, adhesives, and resins were not the focus of this study.

The pyrolysis applied for lignin valorization may be employed for the decomposition of the lignocellulosic biomass into carbohydrate (water-soluble) and pyrolytic lignin (water-insoluble) fractions. In this case, methods for separating the lignin-derived compounds from the bio-oil mixture are necessary. Another possibility is to carry out pyrolysis of the dry isolated lignin derived from other biomass fractionation process. The conversion of lignin to low molecular weight chemicals is more difficult compared with carbohydrates. This fact can be attributed to the complex structure of lignin that counts on the presence of different linkages between the monomers and also to the thermal and oxidative instability of lignin fragments [38].

The lignin model compounds are often found after the depolymerization of the lignin polymer. The study of these model compounds may help on the development of lignin valorization to high-value chemicals. In addition, the analytical challenge is smaller in model compounds studies relative to lignin polymer, which simplifies the analysis of both the reaction networks and the catalytic performance [39]. Guaiacol (2-methoxyphenol, $C_7H_8O_2$) has been considered a good representative of the lignin portion of bio-oil because it incorporates two different oxygenated functions (hydroxyl and methoxy groups) [37]. Moreover, its elemental composition (H/C/O ratios) is close to the lignin bio-oils [18]. Guaiacol was the model compound chosen as object of study of the present work. It is worth to mention that research is being developed with other compounds representative of the lignin portion of biomass, for instance the simpler compounds phenol and anisole [37].

The reaction pathways of guaiacol conversion depend on the catalyst used and on the operating conditions (temperature, pressure) in which the process is carried out. Figure 2.4 shows the reaction pathways for the HDO of guaiacol catalyzed by platinum supported on γ-Al_2O_3 and gives a notion of the possible products that can be formed.

HDO of guaiacol tests carried out in a fixed-bed reactor at 250–300 °C and 1 or 8 atm using Ni_2P/SiO_2 as catalyst revealed the strong influence of pressure on products distribution. At 1 atm direct deoxygenation was the predominant pathway to produce benzene with a selectivity of 62% for a guaiacol conversion of 83%. However, at 8 atm prehydrogenation followed by deoxygenation prevailed to produce cyclohexane (selectivity = 91%; guaiacol conversion = 100%) [58]. Another study analyzed the pressure effect using

diphenyl ether as model compound and Pt/20%Nb_2O_5–Al_2O_3 as catalyst at 200 °C. The increasing pressure from 5 to 30 bar increased the conversion from 38–75%. Furthermore, the selectivity of cyclohexane increased when the pressure was raised, while the formation of benzene and phenol declined. The authors argued that pressure determined the reaction pathways: direct hydrogenolysis of diphenyl ether occurred at low pressures while at high pressures the aromatic ring was prior hydrogenated and then deoxygenated [26]. These results indicate that operation at lower pressures seems to reduce hydrogen consumption by avoiding the saturation of the aromatic ring.

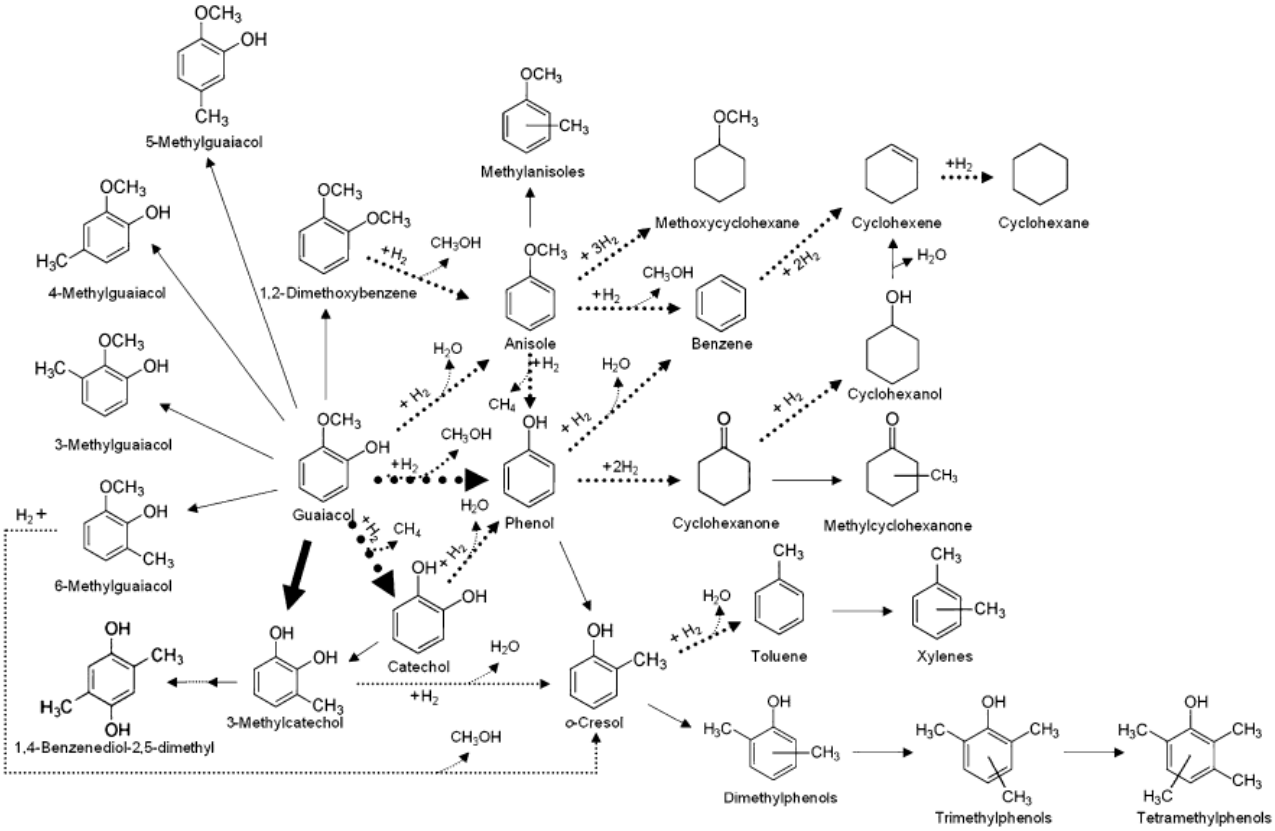

Figure 2.4 – Reaction network for the conversion of guaiacol over Pt/Al_2O_3 at 573 K. The reaction classes identified and classified by the authors were: hydrogenation, hydrogenolysis, and hydrodeoxygenation (in dotted arrows); in solid arrows: transalkylation and dehydration. Bold arrows refer to reactions kinetically most significant. Source: ref. [59].

The HDO at vapor phase and atmospheric pressure was chosen for this study based on the idea of hydrodeoxygenate the pyrolysis vapor without condensate it, in order to work around the chemical and thermal instability of the liquid bio-oil as well as to circumvent the costs with high pressure operation [17–19,23]. Besides the simplicity of not using high-pressure tolerant equipment, the HDO at atmospheric pressure avoid the consumption and the separation of solvent [18]. Table 2.2 shows the experimental conditions of previous works

about the HDO of guaiacol at lower pressures, with the intention to give a notion of the process variables range generally applied.

Table 2.2 – Some experimental conditions of earlier studies in the HDO of guaiacol at low pressure.

Catalyst	T (°C)	P (atm)	Operating conditions*	Main results	Ref.
Pt/Al_2O_3	300	1.4	0.015 mL/min guaiacol; 30% H_2/N_2 (100 mL/min) 0.001–0.100 g of catalyst	Rate constant to remove the methoxy group from guaiacol: 4.4 L (g of catalyst)$^{-1}$ h^{-1}	[60]
Pt/MgO	300	1.4	3% guaiacol with 29% H_2 in He	Major products: phenol, cyclopentanone, and catechol, whose selectivities were: 0.51; 0.17; 0.25, respectively	[61]
Fe/SiO_2	350 400 450	1	73 mL/min H_2, 7.5 mL/min Ar, 239 µL/h guaiacol, 100 mg of catalyst (standard run)	38% of benzene and toluene yield was achieved	[18]
Ru/C; Ru/SiO_2 Ru/Al_2O_3; Ru/TiO_2	400	1	H_2/Guaiacol = 60 mol/mol 15–200 mg of catalyst 0.8 < WHSV < 91	The activity on a per-weight basis followed the sequence: Ru/TiO_2 > Ru/C > Ru/Al_2O_3 > Ru/SiO_2	[23]
Pt/C; Pd/C; Rh/C; Ru/C	300	1	0.025 mL/min guaiacol 100 mL/min H_2:N_2 = 1 0.5 g of catalyst (standard runs)	Pt/C catalyst showed superior deoxygenation activity and stability and its optimum operating temperature was 300 °C	[62]
Ni_2P/SiO_2 (Ni/P= 1, 2, 3)	300	1	Guaiacol/H_2/N_2= 0.02/30.01/69.97 1 < WHSV < 21	The Ni/P = 1 sample displayed the highest deactivation rate of guaiacol conversion (~78 %) while the Ni/P = 3 sample had the lowest (~46 %)	[63]
Ni_2P/ASA Ni_2P/FCC Ni_2P/ZSM-5	425 450	1–3	H_2/Guaiacol = 143 0.7 mol% guaiacol in 100 mL/min H_2 10s < contact time < 50s	Order of activity: Ni_2P/ASA > Ni_2P/FCC > Ni_2P/ZSM-5	[64]

* WHSV [h^{-1}] = weight hourly space velocity = g guaiacol / (h × g catalyst)

2.6 Catalysts for the HDO process

Different types of materials have been tested aiming the hydrodeoxygenation of biomass-derived feedstocks, including supported metals (noble, non-noble, sulfides, phosphides, carbides, and nitrides) [37]. The first studies used conventional hydroprocessing metal sulfide catalysts, including MoS_2 and supported CoMoS and NiMoS. They are kept in the sulfided form because the reaction environment of petroleum feedstocks contains H_2 and H_2S (this last is formed in HDS reactions). However, biomass is almost absent of sulfur then the supported metal sulfides would not be stable in contact with water and oxygen-containing compounds formed. They would be converted into oxide forms, unless a sulfur source was added to the feed (H_2S for instance). The disadvantage of adding a sulfur source would be that the product would produce pollutant sulfur oxides to the atmosphere after combustion [37].

Further studies were carried out with different catalytic systems at different operating conditions. The traditional industrially γ-alumina support generally provides high activity for the HDO process. However, this acidic support also leads to coke formation. Supports which display more resistance to coke formation and high selectivities in HDO were also evaluated, such as C, ZrO_2, SiO_2, MgO. Deposits of carbonaceous material (coke) were the most reported cause of deactivation of catalysts in the HDO process. But sintering, loss of surface area of active sites, and poisoning by biomass-derived compounds containing nitrogen and phosphorus were also observed [37].

A cooperative mechanism exists in a bifunctional catalyst comprised by a noble metal supported on a reducible oxide, as illustrated in Figure 2.5 for the Pt/Nb_2O_5 catalyst applied on the HDO of carboxylic acids. The cooperation between Pt, NbO_x species, and acidic sites in the case of the $Pt/NbOPO_4$ catalyst was explained as the promoters of effectiveness on the HDO of raw woody biomass [65]. However, a search in literature resulted in no study related to the HDO of guaiacol at atmospheric pressure with catalysts containing niobium.

A great challenge of the research concerning the HDO as a strategy for biomass upgrading is to develop a catalyst which is active, selective to oxygen removal that preserves C–C bounds, and which shows minimum deactivation.

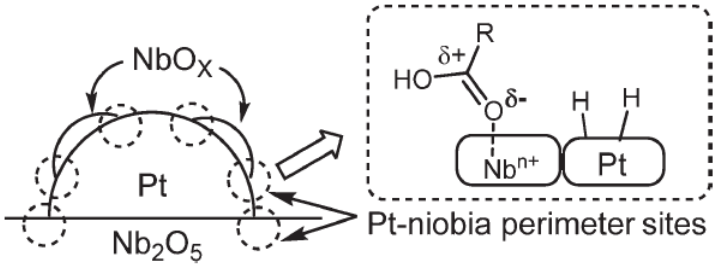

Figure 2.5 – Proposed cooperative mechanism for the HDO of carboxylic acids using Pt/Nb_2O_5 in a partially SMSI state. Source: ref. [24].

CHAPTER 3 – THERMODYNAMIC EQUILIBRIUM ANALYSIS OF THE VAPOR PHASE HYDRODEOXYGENATION OF GUAIACOL

The thermodynamic analysis allows to verify the viability of a chemical reaction and to determine the maximum conversion possible, i.e., the equilibrium conversion. Previous works that reported data related to the thermodynamics of the HDO of guaiacol investigated some representative reactions of the process [11,18,58,66] or selected possible compounds to determine the chemical equilibrium by the minimization of the Gibbs free energy [18,58]. The non-catalytic HDO of guaiacol was also computationally evaluated within the framework of the density functional theory (DFT). Thus, standard thermodynamic and kinetic parameters of five possible pyrolytic pathways of guaiacol were calculated, based on DFT methods, in order to understand the substituent effect of the methoxy group [67]. Moreover, thermochemistry data (e.g., the activation energy requirement) were determined for each reaction of the three reaction schemes selected, aiming as products catechol, anisole, benzene, and cyclohexane from the guaiacol conversion [68].

A better understanding about the HDO of guaiacol on the thermodynamic point of view, considering the possible reaction pathways involved on the formation of target products (benzene, toluene, phenol) and also taking account the operating conditions of the lignin pyrolysis vapors upgrading is still required. In this study, a thermodynamic equilibrium analysis of commonly reported reactions in the HDO of guaiacol literature was performed to determine the most stable reaction routes. This task occurred by the comparison of the values of the chemical equilibrium constant (or equilibrium conversion) of each reaction and by performing a multiple reactions simulation (MRS). Furthermore, the influence of the variables temperature, hydrogen to guaiacol molar ratio, and inert concentration on the equilibrium composition was evaluated by the minimization of the Gibbs free energy method.

3.1 Simulation methods

The thermodynamic equilibrium of the HDO of guaiacol was calculated by two approaches using UniSim Design R400 [69]. One was the equilibrium constants method, the other was the minimization of the Gibbs free energy method, both applied at isothermal conditions using PRSV (Peng-Robinson-Stryjek-Vera) as thermodynamic model for solving the software modules "Equilibrium Reactor" and "Gibbs Reactor" (UniSim terminology), respectively.

In the former analysis ("Equilibrium Reactor") the equilibrium constants were determined using the database and correlation of the pure component Gibbs Free Energy, which is valid/accurate for a temperature range of 25–426.85 °C according to the information provided by the UniSim Design user manual [70]. Therefore, the data obtained out of this temperature range should be analyzed with caution. Some primary and secondary reactions from the conversion of guaiacol and hydrogen proposed by previous works [11,17,59,71,72, 73,74,75] were studied, and they are shown in Table 3.1. The reaction classes included direct deoxygenation (DDO), transalkylation (TRA), demethylation (DME), demethoxylation (DMO), hydrogenation (HYD), and dehydration (DHD). This nomenclature was assumed based on the work of Bui et al. [47] and Wu et al. [63].

The experimental conditions and the type of catalyst used give direction to the sequence of the reactions from Table 3.1 that may occur. Some examples of experimental results conducted in fixed bed reactors are described in the following lines to give more understanding about this fact. The zeolite HY (solid acid catalyst) did not produced deoxygenated products in the conversion of guaiacol carried out at 573 K and 1.4 bar. The predominant compounds were catechol, 1,2-dimethoxybenzene and methylguaiacols, formed by methyl-group transfer (TRA) reactions [59], typical route of acid catalysts [17]. The catalysts $CoMoS/Al_2O_3$ and $CoMoS/TiO_2$ produced catechol and methane by guaiacol DME, and then phenol was formed in the sequence at 573 K and 4 MPa of H_2. However, when the support was changed by ZrO_2, phenol and methanol were produced directly from guaiacol through DMO [76]. A bimolecular transalkylation path between guaiacol and phenol was verified in the reaction catalyzed by Pt–Sn/CNF/Inconel conducted at atmospheric pressure and 673 K [17].

In the second type of analysis, guaiacol, hydrogen, and nitrogen were fed into the "Gibbs Reactor" and possible products were selected, without any reaction specified. The products considered were the 13 compounds present on the reactions from Table 3.1: anisole,

benzene, catechol, cyclohexane, cyclohexene, cyclohexanol, cyclohexanone, o-cresol, methane, methanol, phenol, toluene, and water. The critical, physical, and chemical properties of these substances were available in the software. The thermodynamic parameters (e.g., heats of formation, entropies, heat capacities) were determined by the software. We are aware that other substances not mentioned in this list may also be formed, such as methylated both guaiacol and catechol products, double-ring aromatic compounds (from condensation reactions), CO_x, and products derived from decarbonylation/ring closing reactions (e.g., cyclopentanone). However, the focus of this work was to study the simplest reactions that can lead to target products, e.g., aromatics typical of chemical industry and oxygen free compounds. A partial HDO can produce useful chemical intermediates (phenol and cyclohexanone) [60] and a complete hydrodeoxygenation is interesting for the formation of BTX (benzene, toluene, and xylene) [18].

Depending on pyrolysis operating conditions different product distribution can be obtained from lignin. For example, the suitable conditions for production of monomeric phenols (e.g., guaiacol, syringol, and their alkyl-derivatives) are small particle size, low residence time, reduced pressure, and moderate temperature [77]. The pyrolysis conditions are crucial for the development of a proper catalytic reactor coupled to the pyrolysis process. The upgrading process of liquid bio-oil faces some challenges, because bio-oil shows chemical and thermal instability. The initial composition of the pyrolysis vapors is different from the liquid product after the condensation step. Besides, the hydrotreatment of bio-oil in the liquid phase demands costs with high pressure operation and, otherwise, evaporation of bio-oil has the disadvantage of fouling pipes [17–19]. Although improved catalyst stability can be achieved with high pressure operations, as hydrogen pressure increases, hydrogenation of the aromatic ring may occur before deoxygenation, thus leading to higher hydrogen consumption [62]. An alternative route is to hydrodeoxygenate the pyrolysis vapor without condensate it [17–19]. The reactor for lignin pyrolysis vapors upgrading operating at atmospheric pressure should be at a temperature around 673 K to guarantee a minimum condensation of the vapors [75]. Besides, the reactor must receive as feed not only the vapors formed due to the lignin decomposition, but light gases as CO_2, H_2, CO, CH_4, and the fluidization gas (for the typical pyrolysis performed in a fluidized bed) [78]. It is worth to mention that the HDO of lignin pyrolysis vapors is different from the HDO process developed in the conditions typical of crude oil hydrotreatment (high pressures of pure H_2 and temperatures about 473–573 K) [75].

Considering these information, the simulations in this work were performed at the pressure of 1 atm and at the temperature range from 500 to 1000 K (guaiacol boiling point is

478 K at 1 atm). The HDO of guaiacol catalytic studies at atmospheric pressure generally use diluted solutions, which avoid thermal polymerization reactions [79]. In this study, different proportions between guaiacol and hydrogen in the feed were analyzed, with the presence of an inert substance (nitrogen) or not.

Table 3.1 – Reactions selected for the thermodynamic analysis of the HDO of guaiacol process.

Reaction ID	Reaction	Route*
R1	guaiacol + H_2 ⇄ catechol + CH_4	DME
R2	guaiacol + H_2 ⇄ anisole + H_2O	DDO
R3	guaiacol + H_2 ⇄ phenol + CH_3OH	DMO
R4	guaiacol + $2H_2$ ⇄ phenol + H_2O + CH_4	DME+DDO
R5	guaiacol + H_2 ⇄ o-cresol + H_2O	DDO
R6	guaiacol + $2H_2$ ⇄ toluene + $2H_2O$	DDO
R7	guaiacol + $2H_2$ ⇄ benzene + H_2O + CH_3OH	DMO+DDO
R8	guaiacol + $12H_2$ ⇄ $7CH_4$ + $2H_2O$	DDO
R9	guaiacol + phenol ⇄ catechol + o-cresol	TRA
R10	guaiacol + phenol ⇄ catechol + anisole	TRA
R11	phenol + H_2 ⇄ benzene + H_2O	DDO
R12	phenol + $2H_2$ ⇄ cyclohexanone	HYD
R13	phenol + $3H_2$ ⇄ cyclohexanol	HYD
R14	phenol + $4H_2$ ⇄ cyclohexane + H_2O	DDO
R15	anisole + H_2 ⇄ phenol + CH_4	DME
R16	anisole ⇄ o-cresol	TRA
R17	anisole + H_2 ⇄ benzene + CH_3OH	DMO
R18	anisole + $2H_2$ ⇄ benzene + H_2O + CH_4	DME+DDO
R19	catechol + H_2 ⇄ phenol + H_2O	DDO
R20	catechol + $2H_2$ ⇄ benzene + $2H_2O$	DDO
R21	o-cresol + H_2 ⇄ phenol + CH_4	DME
R22	o-cresol + H_2 ⇄ toluene + H_2O	DDO
R23	cyclohexanone + H_2 ⇄ cyclohexanol	HYD
R24	cyclohexanol + H_2 ⇄ cyclohexane + H_2O	DDO
R25	cyclohexanol ⇄ cyclohexene + H_2O	DHD
R26	benzene + $3H_2$ ⇄ cyclohexane	HYD
R27	cyclohexene + H_2 ⇄ cyclohexane	HYD

* Abbreviations for the reaction routes are: direct deoxygenation (DDO), demethylation (DME), demethoxylation (DMO), transalkylation (TRA), hydrogenation (HYD), and dehydration (DHD).

3.2 Simulation results and discussion

3.2.1 Chemical equilibrium analysis: HDO of guaiacol reactions

Figure 3.1 illustrates the reaction network selected (Table 3.1) for the chemical equilibrium analysis of the HDO of guaiacol. For each reaction *"i"* it is shown the chemical equilibrium constant (K_i) determined at 573 K, which is only a function of temperature and the standard states of the reactants and products [80]. It could be noted that guaiacol primary reactions (R1–R7) were thermodynamically favorable at 573 K, since they showed high equilibrium constant values ($10^4 < K_i < 10^8$). The bimolecular transalkylation (TRA) between guaiacol and phenol giving anisole and catechol (R10) would be the most stable path compared to the reaction R9, in which catechol and o-cresol are formed, since $K_{10} = 9.7 \times 10^7 > K_9 = 3.9 \times 10^4$. Moreover, the demethylation (DME) followed by the direct deoxygenation (DDO) route (R4) [71] had a higher equilibrium constant value than the demethoxylation (DMO) route (R3) for guaiacol decomposition ($K_4 = 4.9 \times 10^8 > K_3 = 3.9 \times 10^5$). This means that the formation of methane was more favorable than methanol along with phenol on the conversion of guaiacol. Same trend of superior methane stability was noted for anisole decomposition into benzene, which is represented by reactions R17 and R18 ($K_{18} = 9.3 \times 10^6 > K_{17} = 0.0003$). This result is consistent with literature data since, in general, methane is more expressively produced than methanol in the catalytic reaction of the HDO of guaiacol at atmospheric pressure [63,81]. It is noteworthy that methanol may not be expressively detected in the product stream also because it can be decomposed into CO and H_2 [82].

Table 3.2 shows the chemical equilibrium constants and the equilibrium conversions as a function of temperature for reactions from Table 3.1. Most of the reactions exhibited an exothermic behavior, since both the equilibrium constant and the conversion diminished with increasing temperature, while the adiabatic equilibrium temperature has risen in relation to the feed temperature. The exceptions were reactions R10 (transalkylation between guaiacol and phenol producing catechol and anisole) [17] and R25 (dehydration of cyclohexanol forming cyclohexene), which behaved endothermically. It was found good proximity between our values and the results from Olcease et al. [18] for the Gibbs free energy change of reactions R6, R7, and R26 (relative deviation < 10%).

The reactions in which guaiacol was reagent (R1–R10) had higher equilibrium constant values ($10^3 < K_i < 10^8$) than the remaining secondary reactions ($10^{-7} < K_i < 10^8$) for the temperature range of 500–700 K (Table 3.2). As a large value of the equilibrium constant

indicates that the reaction will proceed in the direction of the products, this result implies that guaiacol is more reactive than the secondary products (except catechol in reaction R20). This fact was experimentally proved by the reactivity comparison test between guaiacol and anisole [17]. Although most reactions presented high values of equilibrium constant, the activation energy requirements of some reactions are high and they may not occur in real life without the use of suitable catalysts [68].

The hydrogenation of the ring reactions (R12, R13, R23, R26, and R27), typically exothermic, were strongly disfavored with increasing temperature and showed low values of both equilibrium constant and conversion, as expected. This result is coherent with experimental data from literature, since hydrogenation products such as cyclohexane, cyclohexene, methoxycyclohexanol, and cyclohexanol were not abundant in the HDO of guaiacol reactions conducted at atmospheric pressure and moderate temperatures (523–723 K) [17,18,59,63,72,79]. However, as the equilibrium composition is influenced by temperature, pressure, and presence of inert [80], hydrogenation products are commonly produced in the conversion of guaiacol performed in pressurized reactors operating at lower temperatures (see for instance ref. [83]).

Moon et al. [58] performed a thermodynamic simulation using the Gibbs free energy minimization method over the temperature and pressure ranges of 300–1000 K and 1–100 atm, respectively, by the selection of six compounds: anisole, cyclohexane, cyclohexanol, guaiacol, methoxy-cyclohexane, and phenol. They explained that cyclohexane was the most thermodynamically favorable molecule at lower temperatures, while benzene was the most stable compound at the elevated temperature values. Furthermore, the authors' experimental data of the HDO of guaiacol revealed benzene as the most abundant product at 1 atm, but at 8 atm the selectivity changed toward cyclohexane using Ni_2P/SiO_2 as catalyst at 523–573 K. These results indicate that the HDO process for lignin derived products is promising at vapor phase and atmospheric pressure. This process is promising not only because it may avoid the challenge of upgrading the instable liquid bio-oil and reduce costs with high pressure operation, but also because the formation of hydrogenation products would be reduced, as well as the consumption of hydrogen, which is a crucial point for a biorefinery. An interesting HDO process must promote high oxygen removal without much hydrogen spending neither high carbon loss as light gases.

DME, DMO, and DDO reactions in which guaiacol was the reagent were put together into the "Equilibrium Reactor" in order to analyze a multiple reactions simulation (MRS) by feeding guaiacol and hydrogen at different proportions (guaiacol molar fraction in

the feed equal to 1%, 25%, 50%, 75%, and 99%) and temperatures (500–1000 K). Although a diluted stream of guaiacol in the feed is the condition typically employed in the experimental works, it was desired to study the influence of the guaiacol to hydrogen molar ratio. Four case studies were analyzed, and their respective groups of reactions were the following:

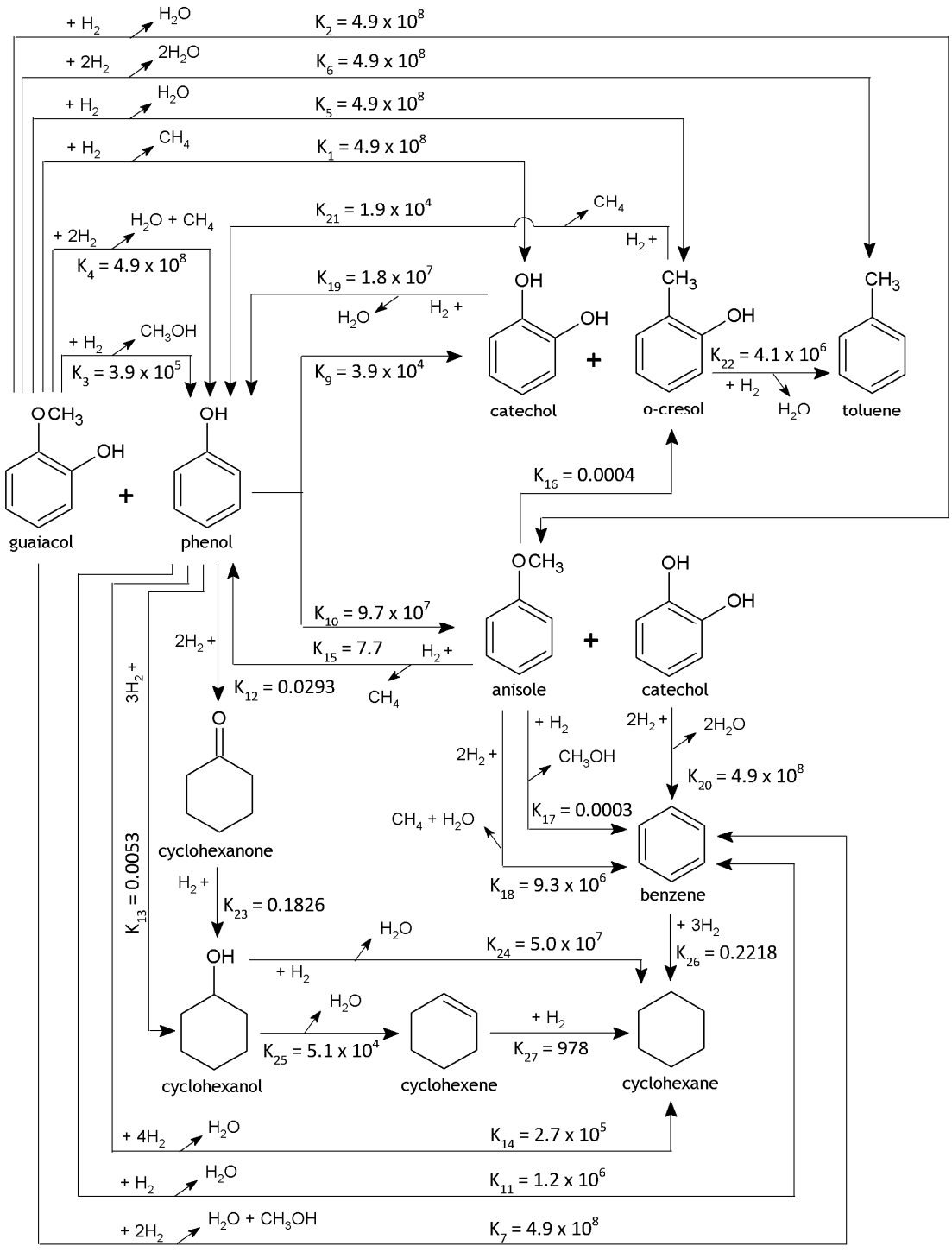

Figure 3.1 – Reaction pathways studied in the thermodynamic simulation of the HDO of guaiacol. The chemical equilibrium constant K_i for each reaction i from Table 3.1 was determined at 573 K on the basis of activity (dimensionless). Simulation conditions: 1 atm, stoichiometric feed, isothermal "Equilibrium Reactor" (UniSim terminology).

Table 3.2 – Simulated chemical equilibrium constant and equilibrium conversion (in brackets) as a function of temperature for reactions from Table 3.1, determined at isothermal conditions and stoichiometric feed.

	Equilibrium constant* and equilibrium conversion (%)					
Reaction	500 K	550 K	600 K	650 K	700 K	750 K
R1	4.9×10^{8} (100)	4.9×10^{8} (100)	3.0×10^{8} (100)	6.6×10^{7} (100)	1.8×10^{7} (100)	6.0×10^{6} (100)
R2	4.9×10^{8}(100)	4.9×10^{8}(100)	4.9×10^{8}(100)	4.9×10^{8}(100)	4.9×10^{8}(100)	4.9×10^{8}(100)
R3	2.0×10^{6}(100)	6.2×10^{5}(100)	2.4×10^{5}(100)	1.0×10^{5}(100)	5.2×10^{4}(100)	2.8×10^{4}(99)
R4	4.9×10^{8}(100)	4.9×10^{8}(100)	4.9×10^{8}(100)	4.9×10^{8}(100)	4.9×10^{8}(100)	4.9×10^{8}(100)
R5	4.9×10^{8} (100)	4.9×10^{8} (100)	4.9×10^{8} (100)	4.9×10^{8} (100)	4.9×10^{8} (100)	4.9×10^{8} (100)
R6	4.9×10^{8} (100)	4.9×10^{8} (100)	4.9×10^{8} (100)	4.9×10^{8} (100)	4.9×10^{8} (100)	4.9×10^{8} (100)
R7	4.9×10^{8} (100)	4.9×10^{8} (100)	4.9×10^{8} (100)	4.9×10^{8} (100)	4.9×10^{8} (100)	4.9×10^{8} (100)
R8	4.9×10^{8}(87)	4.9×10^{8}(87)	4.9×10^{8}(87)	4.9×10^{8}(87)	4.9×10^{8}(87)	4.9×10^{8}(87)
R9	2.0×10^{5}(100)	6.2×10^{4}(100)	2.4×10^{4}(99)	1.1×10^{4}(99)	5.5×10^{3} (99)	3.1×10^{3} (98)
R10	4.5×10^{6}(100)	4.0×10^{7}(100)	2.5×10^{8} (100)	4.9×10^{8} (100)	4.9×10^{8} (100)	4.9×10^{8} (100)
R11	8.9×10^{6}(100)	2.1×10^{6}(100)	6.5×10^{5}(100)	2.3×10^{5}(100)	9.6×10^{4}(100)	4.4×10^{4}(100)
R12	2.2×10^{0}(40)	1.0×10^{-1}(4)	7.7×10^{-3} (0)	8.5×10^{-4} (0)	1.3×10^{-4} (0)	2.4×10^{-5} (0)
R13	3.0×10^{0}(43)	3.3×10^{-2} (1)	7.5×10^{-4} (0)	3.0×10^{-5} (0)	1.9×10^{-6} (0)	1.6×10^{-7} (0)
R14	4.9×10^{8}(99)	3.1×10^{6}(97)	1.9×10^{4}(93)	2.4×10^{2} (82)	5.6×10^{0}(62)	2.1×10^{-1}(33)
R15	3.4×10^{3}(98)	4.4×10^{1}(87)	1.2×10^{0}(52)	5.2×10^{-2}(19)	3.5×10^{-3} (6)	3.3×10^{-4} (2)
R16	4.4×10^{-2} (4)	1.6×10^{-3} (0)	9.4×10^{-5} (0)	8.5×10^{-6} (0)	1.1×10^{-6} (0)	1.7×10^{-7} (0)
R17	2.7×10^{-2}(14)	1.0×10^{-3}(3)	6.6×10^{-5} (1)	6.1×10^{-6} (0)	7.7×10^{-7} (0)	1.2×10^{-7} (0)
R18	4.9×10^{8}(100)	9.5×10^{7}(100)	7.5×10^{5}(99)	1.2×10^{4}(97)	3.4×10^{2} (92)	1.5×10^{1}(80)
R19	1.4×10^{8}(100)	3.2×10^{7}(100)	9.2×10^{6}(100)	3.2×10^{6}(100)	1.3×10^{6}(100)	5.6×10^{5}(100)
R20	4.9×10^{8} (100)	4.9×10^{8} (100)	4.9×10^{8} (100)	4.9×10^{8} (100)	4.9×10^{8} (100)	4.9×10^{8} (100)
R21	7.6×10^{4}(100)	2.8×10^{4}(99)	1.2×10^{4}(99)	6.1×10^{3}(99)	3.3×10^{3}(98)	2.0×10^{3}(98)
R22	3.1×10^{7}(100)	7.3×10^{6}(100)	2.2×10^{6}(100)	7.7×10^{5}(100)	3.1×10^{5}(100)	1.4×10^{5}(100)
R23	1.4×10^{0}(35)	3.3×10^{-1} (13)	9.8×10^{-2} (5)	3.5×10^{-2} (2)	1.5×10^{-2} (1)	6.9×10^{-3} (0)
R24	4.6×10^{8}(100)	9.5×10^{7}(100)	2.5×10^{7}(100)	8.0×10^{6}(100)	3.0×10^{6}(100)	1.3×10^{6}(100)
R25	1.1×10^{4}(100)	3.3×10^{4}(100)	8.0×10^{4}(100)	1.7×10^{5}(100)	3.1×10^{5}(100)	5.2×10^{5}(100)
R26	1.6×10^{2}(84)	1.5×10^{0}(31)	2.9×10^{-2} (1)	1.0×10^{-3} (0)	5.8×10^{-5} (0)	4.7×10^{-6} (0)
R27	4.1×10^{4}(100)	2.8×10^{3}(98)	3.1×10^{2}(94)	4.8×10^{1} (86)	9.7×10^{0}(69)	2.4×10^{0}(46)

* Determined using the activity of the components (dimensionless).

i) MRS1: R1 (formation of catechol by DME), R2 (formation of anisole by DDO), R3 (formation of phenol by DMO), and R5 (formation of cresol by DDO);

ii) MRS2: R1, R2, R4 (formation of phenol by DME+DDO), and R5;

iii) MRS3: R1, R2, R3, R5, R6 (formation of toluene by DDO), and R7 (formation of benzene by DMO+DDO);

iv) MRS4: R1, R2, R4, R5, R6, and R7.

Both the case studies MRS1 and MRS2 are comprised by the reactions which form not fully deoxygenated products commonly obtained from catalytic experiments, which are catechol, phenol, anisole, and cresol. The difference is that MRS1 considers the DMO of guaiacol to produce phenol, while MRS2 is comprised by the DME+DDO routes [71,75]. Since phenol is a common product reported in catalytic HDO of guaiacol, it seemed plausible to carry out a comparison between the DMO and DME+DDO routes. In MRS3 the reactions which lead to benzene and toluene were added to MRS1 reaction set, while MRS4 was comprised by the MRS2 reaction set plus the oxygen-free compounds. The reactions selected were independent and guaiacol was the reagent of each one. The global independent reactions of guaiacol → cyclohexanone, guaiacol → cyclohexanol, guaiacol → cyclohexane, and guaiacol → cyclohexene were not analyzed. This simplification was carried out since hydrogenation products were not thermodynamically favorable at the conditions tested, as mentioned in section 3.1.

Table 3.3 shows the equilibrium conversion as a function of both temperature and guaiacol molar fraction in the feed for the case studies MRS1 and MRS2. Considering MRS1, it was observed that the release of methanol from guaiacol to form phenol (R3) was not a thermodynamically viable route compared to the formation of catechol + CH_4 (R1), anisole + H_2O (R2), and cresol + H_2O (R5). The highest equilibrium conversion value for reaction R3 was 3% at the lower temperature (500 K). The raise in temperature from 500 to 1000 K decreased the equilibrium conversion of R1 from 40% to 2% and increased the conversion of R2 from 29% to 95% for a guaiacol molar fraction in the feed from 1 to 50%. This means that higher temperatures favored anisole formation (along with cresol) and were prejudicial for catechol. The conversion values for reaction R5 were similar to R2 until 800 K, then a fall in conversion occurred from 900–1000 K. It is worth to mention that the transalkylation of anisole to cresol (R16) was not a viable route in the temperature range tested (Table 3.2). The fall in conversion of reaction R5 at 900 and 1000 K seems to be associated to the strong negative influence of temperature of both equilibrium constant and conversion of reaction R16. The product distribution at the equilibrium was independent of the guaiacol molar fraction in the feed up to 50%. However, the conversion values strongly dropped when an excess of guaiacol was fed. The conversion for each individual reaction was three times higher at 50% guaiacol molar fraction compared to 75% guaiacol in the entire temperature range. At 99% of guaiacol the conversion was below 0.5%, which indicates that the group of reactions selected would not be converted using a pure guaiacol stream. This result is coherent, since hydrogen is also reagent in the individual stoichiometric reactions (Table 3.1).

Table 3.3 – Simulated equilibrium conversion as a function of both temperature and guaiacol molar fraction in the feed for the multiple reactions simulations (MRS1 and MRS2)[a] performed at isothermal conditions.

%	Equilibrium conversion for MRS1 [c]							Equilibrium conversion for MRS2 [d]						
GUA[b]	Reaction	Temperature (K)						Reaction	Temperature (K)					
		500	600	700	800	900	1000		500	600	700	800	900	1000
1	R1	40.4	35.2	12.0	4.6	2.8	1.6	R1	1.0	0.6	0.0	0.0	0.0	0.0
1	R2	28.5	31.9	43.7	47.5	84.9	95.4	R2	1.0	1.0	1.0	1.0	1.0	1.0
1	R3	2.6	1.0	0.6	0.4	0.3	0.2	R4	97.1	97.4	98.0	98.0	98.9	99.0
1	R5	28.5	31.9	43.7	47.5	12.0	2.7	R5	1.0	1.0	1.0	1.0	0.1	0.0
25	R1	40.4	35.2	12.0	4.6	2.8	1.6	R1	21.5	15.6	1.4	0.2	0.0	0.0
25	R2	28.6	31.9	43.7	47.5	84.9	95.4	R2	17.7	18.9	21.6	21.9	30.9	32.8
25	R3	2.6	1.0	0.6	0.4	0.3	0.2	R4	43.1	46.6	55.3	56.1	64.7	66.2
25	R5	28.5	31.9	43.7	47.5	12.0	2.7	R5	17.7	18.9	21.6	21.9	4.4	0.9
50	R1	40.3	35.2	12.0	4.6	2.8	1.6	R1	41.4	35.5	12.0	4.6	2.8	1.6
50	R2	28.6	31.9	43.7	47.5	84.9	95.4	R2	29.3	32.2	44.0	47.7	85.1	95.6
50	R3	2.6	1.0	0.6	0.4	0.3	0.2	R4	0.0	0.0	0.0	0.0	0.0	0.0
50	R5	28.6	31.9	43.7	47.5	12.0	2.7	R5	29.3	32.2	44.0	47.7	12.0	2.7
75	R1	13.4	11.7	4.0	1.5	0.9	0.5	R1	13.8	11.8	4.0	1.5	0.9	0.5
75	R2	9.5	10.6	14.6	15.8	28.3	31.8	R2	9.8	10.7	14.7	15.9	28.4	31.9
75	R3	0.9	0.3	0.2	0.1	0.1	0.1	R4	0.0	0.0	0.0	0.0	0.0	0.0
75	R5	9.5	10.6	14.6	15.8	4.0	0.9	R5	9.8	10.7	14.7	15.9	4.0	0.9
99	R1	0.4	0.4	0.1	0.0	0.0	0.0	R1	0.4	0.4	0.1	0.0	0.0	0.0
99	R2	0.3	0.3	0.4	0.5	0.9	1.0	R2	0.3	0.3	0.4	0.5	0.9	1.0
99	R3	0.0	0.0	0.0	0.0	0.0	0.0	R4	0.0	0.0	0.0	0.0	0.0	0.0
99	R5	0.3	0.3	0.4	0.5	0.1	0.0	R5	0.3	0.3	0.4	0.5	0.1	0.0

[a] MRS (multiple reactions simulations) was performed by inserting together a group of independent reactions in the "Equilibrium Reactor" (UniSim terminology); [b] Guaiacol molar fraction in the feed stream (guaiacol + H_2); [c] MRS1 was comprised by reactions R1 (guaiacol + H_2 ⇄ catechol + CH_4), R2 (guaiacol + H_2 ⇄ anisole + H_2O), R3 (guaiacol + H_2 ⇄ phenol + CH_3OH), and R5 (guaiacol + H_2 ⇄ cresol + H_2O); [d] MRS2 was comprised by reactions R1, R2, R4 (guaiacol + $2H_2$ ⇄ phenol + H_2O + CH_4), and R5.

The carbon-oxygen bonds present in the guaiacol molecule, i.e., C–O (methoxy group), CAr–O (methoxy group), and CAr–OH (hydroxyl group) have bond energies equal to 247, 356, and 414 kJ/mol, respectively, where CAr corresponds to the carbon of the aromatic ring [84]. By comparison of these values it would be expected that the rupture of the bond C–O from the methoxy group would be the preferred path with the catechol formation being the most favorable reaction compared to the direct formation of anisole or phenol [14,84]. The

thermodynamic results presented here are consistent with the previous explanation that the DMO of guaiacol producing phenol and methanol (R3) is not a thermodynamically favorable path compared to DME (R1) and DDO (R2 and R5). In MRS1, catechol was the predominant product up to 600 K, then from 600–1000 K anisole and cresol became the most abundant compounds.

The insertion of reaction R4 instead of R3 in the simulation of the case study 2 (MRS2) significantly changed the results in relation to MRS1. Products distribution was different between MRS2 and MRS1. Furthermore, guaiacol concentration in the feed had a strong influence in MRS2 results, while it produced no effect in MRS1 up to 50% molar fraction. For a diluted stream of guaiacol (molar fraction = 1%), phenol was the dominant product and reaction R4 reached a high level of equilibrium conversion ≥ 97% from 500 to 1000 K. The high formation of phenol in MRS2 compared to MRS1 showed that DME+DDO route (R4) was more thermodynamically favorable compared to DMO route (R3) for guaiacol decomposition. For a feed composed by 25% of guaiacol, equilibrium conversion for reaction R4 dropped and stayed in the range of 43–66%, but still prevailed compared to R1, R2, and R5. However, for a feed comprised by identical amounts of guaiacol and hydrogen, as well as for an excess of guaiacol in the feed (molar fraction = 75% and 99%), results from MRS1 and MRS2 were very close. It could be noticed that hydrogen in excess was essential to allow the occurrence of route R4. The more diluted the stream of guaiacol was the more favorable was reaction R4, and thus the formation of phenol became more selective in MRS2.

The results for MRS3 and MRS4 are shown in Table 3.4. Reaction R3 was not thermodynamically viable in MRS3, analogously to MRS1. Furthermore, reaction R4 was favored in MRS4, similarly to what occurred in MRS2. In both MRS3 and MRS4 the reactions R6 (formation of toluene) and R7 (formation of benzene) were significant when an excess of hydrogen was used. In MRS3, toluene and benzene were the most abundant product, while in MRS4 phenol and benzene were predominant, followed by toluene at a guaiacol molar fraction of 1% and 25%. For both MRS3 and MRS4, the increasing temperature had a positive effect on the formation of toluene in the entire temperature range, while it was positive for benzene only up to 700 K. The equilibrium conversion was very close for the case study MRS3 compared to MRS1 and also for MRS4 compared to MRS2 for a feed comprised by 50%, 75%, and 99% of guaiacol molar fraction. This result suggests that the presence of an excess of hydrogen in the HDO of guaiacol is important to achieve complete oxygen removal, represented in this study by formation of benzene and toluene incorporated in MRS3 and MRS4.

Table 3.4 – Simulated equilibrium conversion as a function of both temperature and guaiacol molar fraction in the feed for the multiple reactions simulations (MRS3 and MRS4)[a] performed at isothermal conditions.

%	Equilibrium conversion for MRS3 [c]							Equilibrium conversion for MRS4 [d]						
GUA[b]	Reaction	Temperature (K)						Reaction	Temperature (K)					
		500	600	700	800	900	1000		500	600	700	800	900	1000
1	R1	7.0	5.6	1.5	0.6	0.4	0.3	R1	0.5	0.3	0.0	0.0	0.0	0.0
1	R2	0.4	0.4	0.4	0.5	1.1	1.5	R2	0.2	0.2	0.2	0.2	0.3	0.4
1	R3	0.0	0.0	0.0	0.0	0.0	0.0	R4	41.8	41.9	42.1	44.5	56.8	62.0
1	R5	0.4	0.4	0.4	0.5	0.2	0.0	R5	0.2	0.2	0.2	0.2	0.0	0.0
1	R6	30.6	31.1	32.4	37.1	66.5	82.5	R6	15.3	15.4	15.4	16.9	25.7	29.6
1	R7	61.6	62.5	65.2	61.2	31.7	15.7	R7	42.0	42.1	42.1	38.2	17.1	7.9
25	R1	28.5	24.1	7.8	3.1	2.1	1.3	R1	17.2	12.5	1.2	0.2	0.0	0.0
25	R2	9.3	10.4	14.6	17.3	34.9	43.2	R2	7.7	8.3	9.8	10.7	18.1	21.1
25	R3	0.1	0.0	0.0	0.0	0.0	0.0	R4	24.5	27.1	33.9	35.9	46.7	50.7
25	R5	9.3	10.4	14.6	17.3	4.9	1.2	R5	7.7	8.3	9.8	10.7	2.6	0.6
25	R6	15.8	16.3	18.2	20.3	36.8	44.1	R6	10.9	10.9	10.8	11.6	18.5	21.2
25	R7	37.1	38.8	44.8	42.0	21.3	10.1	R7	32.0	32.8	34.5	31.0	14.1	6.5
50	R1	40.3	35.2	12.0	4.6	2.8	1.6	R1	41.3	35.5	12.0	4.6	2.8	1.6
50	R2	28.6	31.9	43.7	47.5	84.9	95.4	R2	29.3	32.2	43.9	47.6	85.1	95.6
50	R3	2.6	1.0	0.6	0.4	0.3	0.2	R4	0.0	0.0	0.0	0.0	0.0	0.0
50	R5	28.6	31.9	43.7	47.5	12.0	2.7	R5	29.3	32.2	43.9	47.6	12.0	2.7
50	R6	0.0	0.0	0.0	0.0	0.0	0.0	R6	0.0	0.0	0.0	0.0	0.0	0.0
50	R7	0.0	0.0	0.0	0.0	0.0	0.0	R7	0.0	0.1	0.1	0.1	0.0	0.0
75	R1	13.4	11.7	4.0	1.5	0.9	0.5	R1	13.8	11.8	4.0	1.5	0.9	0.5
75	R2	9.5	10.6	14.6	15.8	28.3	31.8	R2	9.8	10.7	14.7	15.9	28.4	31.9
75	R3	0.9	0.3	0.2	0.1	0.1	0.1	R4	0.0	0.0	0.0	0.0	0.0	0.0
75	R5	9.5	10.6	14.6	15.8	4.0	0.9	R5	9.8	10.7	14.7	15.9	4.0	0.9
75	R6	0.0	0.0	0.0	0.0	0.0	0.0	R6	0.0	0.0	0.0	0.0	0.0	0.0
75	R7	0.0	0.0	0.0	0.0	0.0	0.0	R7	0.0	0.0	0.0	0.0	0.0	0.0
99	R1	0.4	0.4	0.1	0.0	0.0	0.0	R1	0.4	0.4	0.1	0.0	0.0	0.0
99	R2	0.3	0.3	0.4	0.5	0.9	1.0	R2	0.3	0.3	0.4	0.5	0.9	1.0
99	R3	0.0	0.0	0.0	0.0	0.0	0.0	R4	0.0	0.0	0.0	0.0	0.0	0.0
99	R5	0.3	0.3	0.4	0.5	0.1	0.0	R5	0.3	0.3	0.4	0.5	0.1	0.0
99	R6	0.0	0.0	0.0	0.0	0.0	0.0	R6	0.0	0.0	0.0	0.0	0.0	0.0
99	R7	0.0	0.0	0.0	0.0	0.0	0.0	R7	0.0	0.0	0.0	0.0	0.0	0.0

[a] MRS (multiple reactions simulations) was performed by inserting together a group of independent reactions in the "Equilibrium Reactor" (UniSim terminology); [b] Guaiacol molar fraction in the feed stream (guaiacol + H_2); [c] MRS3 was comprised by reactions R1 (guaiacol + H_2 ⇄ catechol + CH_4), R2 (guaiacol + H_2 ⇄ anisole + H_2O), R3 (guaiacol + H_2 ⇄ phenol + CH_3OH), R5 (guaiacol + H_2 ⇄ o-cresol + H_2O); R6 (guaiacol + $2H_2$ ⇄ toluene + $2H_2O$); R7 (guaiacol + $2H_2$ ⇄ benzene + H_2O + CH_3OH); [d] MRS4 was comprised by reactions R1, R2, R4 (guaiacol + $2H_2$ ⇄ phenol + H_2O + CH_4), R5, R6, and R7.

The multiple reactions analysis showed that complete deoxygenation was possible by the formation of toluene and benzene through reactions R6 and R7, respectively. It appeared as a stable thermodynamic state in both MRS3 and MRS4 when an excess of hydrogen was used. However, the equilibrium was not directed for the formation of only one oxygen-free product with high selectivity, but for a mixture of possible products. It is worth to mention that phenol and benzene are commonly reported as predominant products when oxygen removal is achieved, while catechol is observed when oxygen removal do not occur in experimental studies of the catalytic HDO of guaiacol [17,18,23,59,71,79,81].

3.2.2 Chemical equilibrium analysis: minimization of the Gibbs free energy

Unlike the analysis through the equilibrium constants method in which specific reactions were inserted in the "Equilibrium Reactor", the minimization of the Gibbs free energy method provides the most thermodynamically stable molecules, not reactions. This type of analysis can be considered, then, more wide-ranging, although the study of specific reactions can provide more details to propose a reaction network for a catalytic system.

The products distribution in the equilibrium as a function of temperature, determined by the minimization of the Gibbs free energy for different hydrogen to guaiacol molar ratio values can be seen in Figure 3.2. For all simulation cases analyzed, even in the absence of hydrogen (Figure 3.2f), guaiacol conversion was 100%. This meant that the possible products selected were molecules more thermodynamically stable than guaiacol, i.e., they showed lower values of the Gibbs free energy. This result clearly revealed that thermodynamic did not appear to be a constraint for the HDO of guaiacol process, as noted by other authors [11], [85]. The absence of hydrogen in the feed did not avoid guaiacol conversion in the "Gibbs Reactor" but prevented the occurrence of reactions of the MRS in the "Equilibrium Reactor" (Table 3.3 and Table 3.4). This is expected, since the reaction was stoichiometrically set up in the case of the "Equilibrium Reactor".

Once the "Gibbs Reactor" operated without any specified reaction, only some hypothesis can be made on how each product at the equilibrium state might have been formed. The molecules cyclohexane, cyclohexene, cyclohexanol, cyclohexanone, methanol, and o-cresol were not present in the results, what suggest that they were intermediates of reactions or not stable final products. It is worth to mention that the increasing pressure can provide a different result. As reported by the simulation of Moon et al. [58], at 8 atm the hydrogenated product cyclohexane was the most stable molecule.

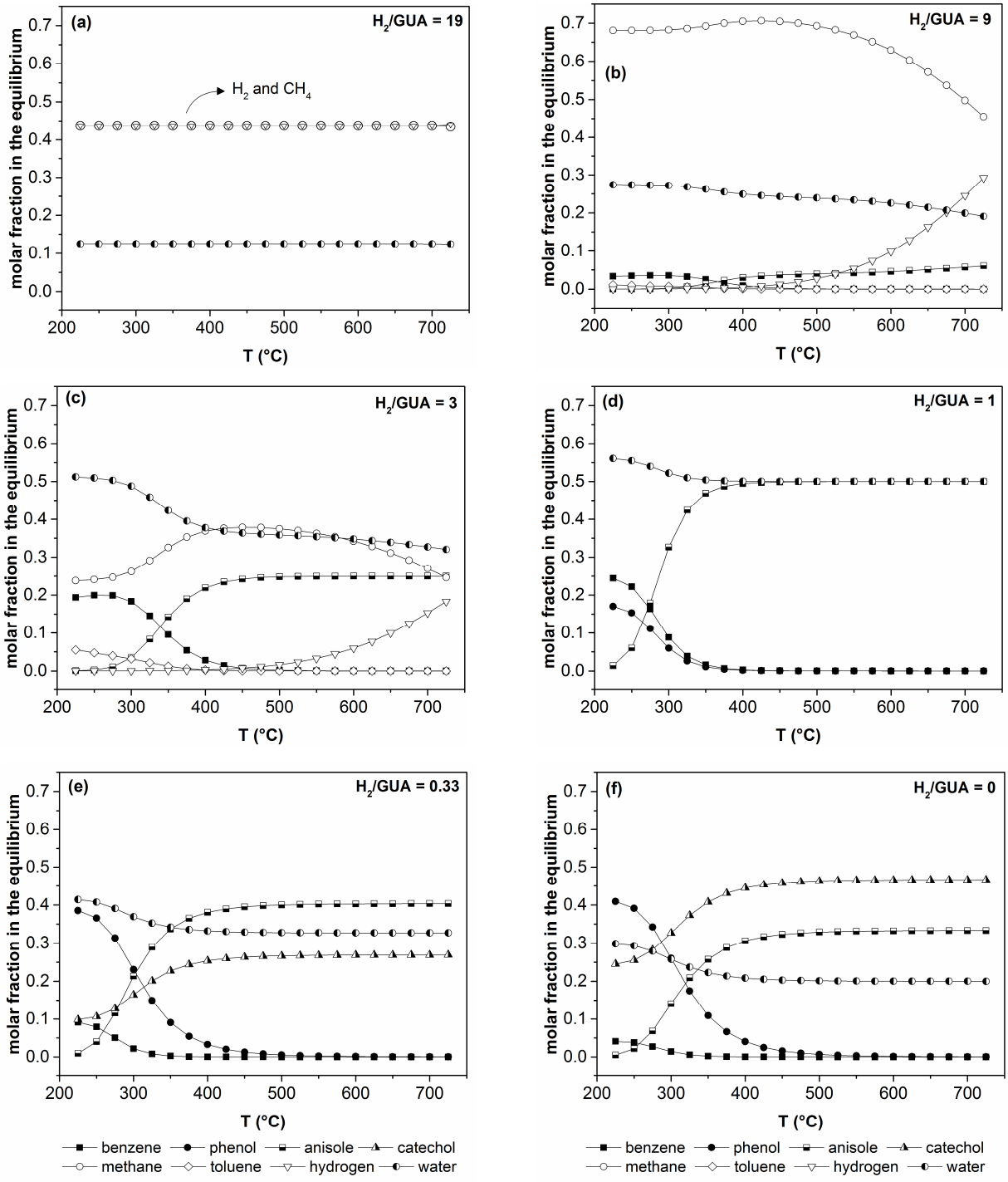

Figure 3.2 – Chemical composition at the equilibrium as a function of temperature. Simulation conditions: 1 atm, isothermal "Gibbs Reactor", guaiacol molar fraction in the feed (H_2 + guaiacol) equal to (a) 5% (H_2/GUA = 19); (b) 10% (H_2/GUA = 9); (c) 25% (H_2/GUA = 3); (d) 50% (H_2/GUA = 1); (e) 75% (H_2/GUA = 0.33); (f) 100% (H_2/GUA = 0). Guaiacol conversion was 100% for all cases, even in the absence of hydrogen as co-reactant.

For a feed stream comprised by 5% of guaiacol in hydrogen (H_2/GUA = 19 mol/mol), methane, water, and unreacted hydrogen were the only compounds present in the product stream for the entire temperature range (Figure 3.2a). Methane and water were

produced in the molar proportion of CH_4/H_2O = 3.5, which is represented by the complete DDO of guaiacol (reaction R8 from Table 3.1). The decomposition of guaiacol into CH_4 and H_2O showed a high equilibrium conversion value of 87% (Table 3.2). This finding is in accordance with the work of Olcease et al. [18], who also found methane as the final product if the thermodynamic equilibrium is achieved. The authors determined the equilibrium composition by the simulation of 31 possible compounds using a stream composed by 1% guaiacol, 90% hydrogen, and 9% argon at 1 atm and 673 K. However, differently from the present work, ref. [18] did not study the influence of H_2/guaiacol molar ratio that strongly interferes in the equilibrium result (Figure 3.2).

As the feed became more concentrated in guaiacol (Figure 3.2b–c), besides methane and water, benzene, toluene, and anisole were also formed. For a feed stream comprised by 10% of guaiacol (H_2/GUA = 9), the product distribution resemble the result for H_2/GUA = 19. The molar fraction of methane (0.68–0.45) and water (0.27–0.19) remained predominant from 225–725 °C, yet benzene (0.03–0.00), anisole (0.00–0.06), and toluene (0.01–0.00) have been minor products. At the condition of 25% guaiacol in the feed (H_2/GUA = 3) from 225–400 °C, benzene (0.19–0.03), water (0.51–0.38), methane (0.23–0.37), and toluene (0.05–0.00) were abundant. After approximately 400 °C, the molar fraction of products changed and anisole (0.22–0.25), water (0.38–0.32), and methane (0.37–0.25) were abundant from 400–725 °C for H_2/GUA = 3.

For a stoichiometric feed of guaiacol and hydrogen (H_2/GUA = 1) (Figure 3.2d), at lower temperatures (< 400 °C), water (0.56–0.50), benzene (0.24–0.00), phenol (0.17–0.00), and anisole (0.02–0.49) were produced from 225 to 400 °C. Above 400 °C until 725 °C, the molar fraction was 0.5 for both anisole and water. This result indicates that only reaction R2 (Table 3.1) occurred in this condition. The increasing temperature had a negative influence on benzene and phenol formation, but it was positive for anisole.

When an excess of guaiacol was used in the feed (Figure 3.2e–f), the behavior of benzene, phenol, water, and anisole in relation to temperature resemble the curves for H_2/GUA = 1. However, there was the appearance of a new product, catechol, whose molar fraction increased from 225 °C until around 400 °C then remained constant from 400–700 °C. Catechol molar fraction at higher temperatures was 27% and 47% for H_2/GUA = 0.33 and H_2/GUA = 0, respectively. It could be noted that oxygen removal became impaired with a concentrated stream of guaiacol by favoring catechol formation instead of less oxygenated compounds. These findings indicate the important role of hydrogen as co-reactant to produce oxygen-free compounds. This evidence was also observed by experimental studies from

literature [18,60]. The conversion of guaiacol catalyzed by Fe/SiO_2 at atmospheric pressure increased from 30% in the absence of hydrogen to 70% for a hydrogen partial pressure of 0.2 bar. However, when the pressure was further raised from 0.2 to 0.9 bar, the H_2 pressure effect became irrelevant [18]. Moreover, when the H_2 to guaiacol molar ratio increased from 10 to 33, phenol selectivity increased almost 70% while catechol selectivity decreased around 80%, in the conversion catalyzed by Pt/Al_2O_3 at 573 K and 1.4 bar [60].

The fluidization-dilution gas is typically present in pyrolysis vapor from a fluidized bed. Then, a simulation was carried out inserting N_2 as reagent as well, in order to analyze its effect in the HDO of guaiacol at 573 K. Figure 3.3 shows the molar fraction of products as a function of the molar fraction of H_2 in the feed gas stream comprised by H_2+N_2 for different guaiacol concentration in the total feed stream.

For a stream diluted in guaiacol (5% molar fraction, Figure 3.3a), the addition of the increasing quantity from 40% to 90% of nitrogen in hydrogen produced a beneficial effect of reducing the formation of methane (0.44–0.01) and increasing benzene (0.00–0.05). Without nitrogen, only methane and water were formed in this condition, as previously showed in Figure 3.2a. Olcease et al. [18] also observed methane as the most stable product at 1 atm, 673 K, 1% guaiacol, and 9% inert gas. A stream comprised by 90% N_2/H_2 produced the highest quantity of benzene (5%). A similar behavior of nitrogen addition to a stream comprised by 10% guaiacol was observed, with the difference that 80% N_2/H_2 lead to a 9% molar fraction of benzene. Both methane and benzene are hydrocarbons, but benzene is more interesting for the HDO purpose, thus the presence of nitrogen appeared to be promising.

For 25%, 50%, and 75% of guaiacol molar fraction in the feed (Figure 3.3c–e) the addition of nitrogen decreased the formation of benzene and increased the undesired catechol. This finding suggests that nitrogen might be beneficial only for diluted streams of guaiacol. Experimental studies have showed that a lower content of guaiacol in the feed increased the conversion levels, as would be expected, and allowed the formation of more compounds with one oxygen atom in the reaction catalyzed by $CoO\text{-}MoO_3/\gamma\text{-}Al_2O_3$ [86]. For the concentrated stream containing 75% of guaiacol (Figure 3.3e) the influence of the inert presence was softer, but still alike the behavior of the 50% guaiacol stream.

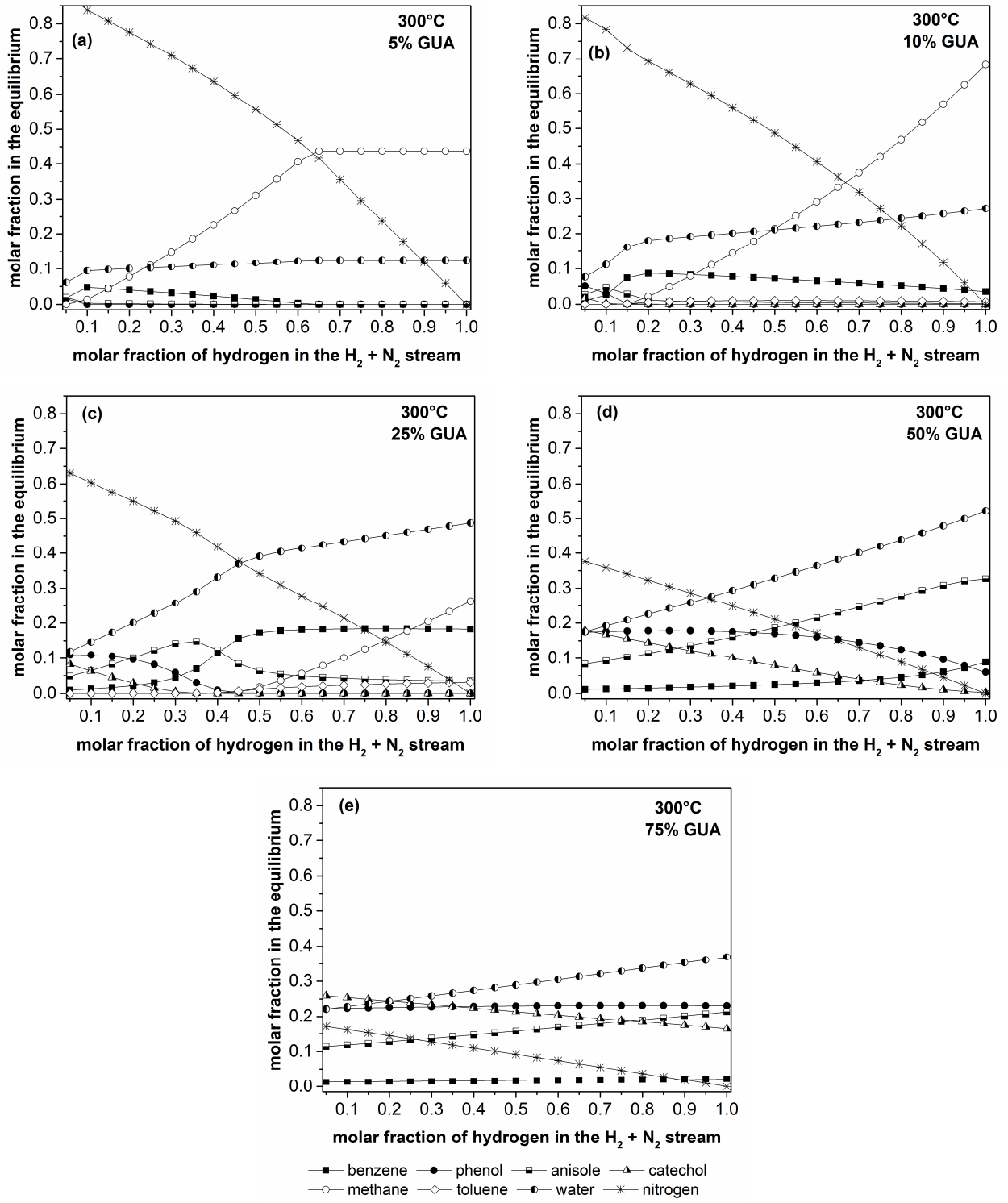

Figure 3.3 – Chemical composition at the equilibrium as a function of the molar fraction of hydrogen in the stream $H_2 + N_2$. Simulation conditions: 1 atm, 573 K, isothermal "Gibbs Reactor" (UniSim terminology), guaiacol molar fraction in the total feed stream ($H_2 + N_2$ + guaiacol) equal to (a) 5%; (b) 10%; (c) 25%; (d) 50%; (e) 75%. Guaiacol conversion was 100% for all cases, even in the absence of hydrogen as co-reactant.

3.3 Conclusions

A thermodynamic analysis comprising the chemical equilibrium of the atmospheric HDO of guaiacol system has been conducted using UniSim Design R400. Both the equilibrium constants method and the minimization of the Gibbs free energy method showed that this conversion does not have a thermodynamic restriction to occur. Besides, the reactions studied were mostly exothermic. The equilibrium conversion of the reactions along with the equilibrium constants values presented here may help on the definition of reaction pathways of the catalytic HDO of guaiacol. The simulation through the minimization of the Gibbs free energy method showed that the most thermodynamically stable molecules (with the lowest values of the Gibbs free energy) were dependent on both temperature and guaiacol concentration. The presence of an excess of inert gas in the hydrogen stream for a diluted concentration of guaiacol was crucial to the formation of benzene, instead of only methane. The desirable direct deoxygenation (DDO) reactions, which remove oxygen trough the release of water preserving the C–C bonds, were thermodynamically favored under the studied conditions.

CHAPTER 4 – PROMOTING EFFECT OF Nb_2O_5 ADDITION TO Al_2O_3 ON SUPPORTED Pt CATALYSTS APPLIED ON THE ATMOSPHERIC HYDRODEOXYGENATION OF GUAIACOL

Different catalysts were evaluated for the HDO of biomass-related compounds. Bifunctional catalysts are believed to be a suitable option for the HDO process because the existence of two different active sites can allow more elementary reaction steps to occur [21]. Some works tested the catalytic system comprised by a noble metal supported on a reducible oxide, which presented promising results [19,23–28]. Ru/TiO_2 showed superior performance in terms of activity and stability compared to Ru supported on Al_2O_3, SiO_2, or C on the atmospheric HDO of guaiacol at 400 °C. The reduction of titania contributed for the enhanced activity [19,23].

The use of niobia as a support was promising to either achieve high activity or to promote the cleavage of C–O bounds [24–28]. Pt/Nb_2O_5 was effective for producing high yields (88–100%) of linear alkanes on the hydrodeoxygenation of lauric, capric, palmitic, myristic, oleic, and stearic acids [24]. The Ru/Nb_2O_5 catalyst was effective for the cleavage of C–O–C bonds in the raw lignin and it was also selective for the cleavage of the $C_{aromatic}$–OH bond in 4-methylphenol [27]. The $Pt/20\%Nb_2O_5–Al_2O_3$ catalyst was more stable than Pt/Al_2O_3 on the HDO of diphenyl ether (lignin model compound) [26]. The Pd/Nb_2O_5 catalyst showed higher reaction rate and superior selectivity for benzene compared to Pd/SiO_2 on the HDO of phenol at atmospheric pressure [28]. However, it was not found a work about the atmospheric HDO of guaiacol over platinum supported in niobia or niobia-alumina.

In this work it was evaluated the performance of the catalyst comprised by Pt supported on xNb_2O_5/Al_2O_3 (x = 0, 5, 20, 100, wt.%) on the HDO of guaiacol at atmospheric pressure. The influence of H_2 partial pressure, temperature, space velocity, and pure support behavior on activity and selectivity was investigated. A reaction pathway for Pt/Nb_2O_5 was proposed.

4.1 Experimental

4.1.1 Synthesis of supports

Ammonium niobium oxalate, $NH_4[NbO(C_2O_4)_2(H_2O)_2](H_2O)_n$ (ANO/CBMM AD/2956), was calcined at 773 K during 4 h, at a heating rate of 10 K/min, to produce the support Nb_2O_5. Pseudoboehmite (AlO(OH) – G-250/BASF) was calcined at the same conditions to produce the support γ-Al_2O_3.

The Nb_2O_5/Al_2O_3 mixed supports were prepared by wet impregnation of the γ-Al_2O_3 (15 g) with an aqueous solution (300 mL) of ammonium niobium oxalate (ANO). To establish the amount of ANO used to prepare the aqueous solution it was considered the weight loss to form Nb_2O_5 during the calcination, in such a way that the niobia nominal loading was 5% or 20% (weight basis). The impregnation was done at 333 K and 170 rpm for 16 h in a rotary evaporator. Then the excess of water was removed from the material by setting the temperature to 353 K and turning on the vaccum pump attached to the rotary evaporator. This was followed by drying at an oven at 393 K during 12–16 h. The sample was calcined at 773 K during 4 h (10 K/min). All calcinations were done with a muffle furnace in static air. It is worth to mention that the monolayer coverage on alumina (γ-Al_2O_3 = 180 m^2/g) was reached at around 19 wt.% of Nb_2O_5 prepared using niobium oxalate [30].

4.1.2 Synthesis of catalysts

Catalysts were prepared by incipient wetness impregnation of the supports with an aqueous solution of chloroplatinic acid hexahydrate ($H_2PtCl_6.6H_2O$, Sigma Aldrich, $\geq$ 37.50% Pt). It was used a Pt nominal loading of 1 wt.% for all catalysts, except for Pt/Nb_2O_5, whose nominal platinum loading was 0.5 wt.%. A lower metal loading (0.5 wt.%) was used for the Pt/Nb_2O_5 catalyst to avoid agglomeration of Pt in the niobia calcined with low surface area. Incipient wetness was determined to be: 1.14 mL H_2O/g Al_2O_3; 0.68 mL H_2O/g 5%Nb_2O_5/Al_2O_3; 0.63 mL H_2O/g 20%Nb_2O_5/Al_2O_3; 0.29 mL H_2O/g Nb_2O_5. The impregnation was done with a mortar and pestle. Then the impregnated support was dried at 393 K for 12–15 h, followed by calcination at 10 K/min to 573 K during 4 h (except for the Pt/Al_2O_3 catalyst, which was calcined at 773 K). All calcinations were done with a muffle furnace in static air. The catalysts were pelletized with a press, then crushed and sieved to a size of 60–100 mesh (0.15 < d# < 0.25 mm, d# was the sieve size).

4.1.3 Catalysts characterization

X-ray diffraction (XRD) measurements were conducted on powder with a Shimadzu Lab X – XRD-6000 diffractometer operated at 40 kV and 45 mA with CuKα radiation (λ = 0.154 nm). Data were collected with steps of 0.02° (2θ) and scan speed of 2°/min aiming to determine the phases and crystalline structure of the materials.

Specific surface areas and pore volumes were determined by the sorption isotherms of nitrogen at 77 K with a Micromeritics ASAP 2010. The samples (0.5 g) were previously degassed at 363 K during 4 h, at a heating rate of 1 K/min under vacuum (10 μmHg). The specific surface areas were determined using the Brunauer-Emmett-Teller (BET) method. The total pore volume was calculated at a relative pressure of P/P_0 = 0.98. The average pore diameter was determined by the Barrett-Joyner-Halenda (BJH) method with desorption isotherm branches.

CO chemisorption was measured by the static volumetric method in a Micromeritics ASAP 2010 automated gas sorption analyzer in order to titrate the surface Pt atoms. The pretreatment of the samples (0.5 g) consisted of drying in He (30 mL/min) at 393 K for 30 min, cooling to room temperature under He flow, followed by reduction *in situ* in flowing pure H_2 (30 mL/min). The catalysts were reduced from room temperature to 573 K for 10 h, then hold at 573 K during 2 h, except the Pt/Al_2O_3 catalyst, which was reduced at 773 K at the same 12 h period of total activation. Pt/Nb_2O_5 reduced at 573 K is primarily comprised by metallic Pt partially covered with NbO_x species, derived from the partial reduction of niobia [24]. Nb_2O_5 is known as a reducible transition metal oxide which exhibits strong metal-support interaction (SMSI) properties [87]. Literature [88] reported that the TPR profile of $Pt/Nb_2O_5–Al_2O_3$ had a peak at around 560 K related to the complex PtO_xCl_y, derived from the H_2PtCl_6 solution. After reduction, the samples were evacuated for 30 min at the reduction temperature to remove any residual H_2, before cooling to 308 K under vacuum (10 μmHg) for analysis. The CO monolayer uptake was determined by the difference between the total and the reversible CO adsorptions, assuming that each active site adsorbs one CO molecule. The particle size was calculated considering the nominal loading of Pt according to the equation: $d = (P/100)\times[6/(A_m\rho)]$, 6 is the shape factor for a spherical particle, A_m is the surface area of Pt, P is the percent loading of Pt, ρ is the Pt density [89].

The Brønsted acid sites (BAS) and the Lewis acid sites (LAS) were quantified by temperature-programmed desorption of isopropylamine (IPA-TPD), carried out in a multipurpose unit for catalyst characterization, which lines were kept heated at 323 K. After

the activation *in situ* of the catalyst, whose conditions were the same described for CO chemisorption, the sample (0.75 g) was cooled to 318 K in argon flow (100 mL/min). Then isopropylamine (C_3H_9N), kept inside a saturator at 287 K, was dosed for 20 min at the reactor, kept at 318 K. The reactor was purged with argon (100 mL/min) prior to TPD measurements in order to remove the excess of isopropylamine until the baseline become stable. The desorption profile was recorded at 10 K/min until 873 K. Masses 44, 41, and 17 were monitored by a mass spectrometer, since isopropylamine (m/e = 44) is decomposed into ammonia (m/e = 17) and propylene (m/e = 41) over Brønsted acid sites through a Hoffman-elimination reaction [90]. The amount of desorbed propylene was calibrated with 1 mL pulses of a gas mixture comprised by 10% propylene in argon.

4.1.4 Catalytic tests: HDO of guaiacol

Catalytic tests were performed in a continuous down-flow glass reactor with sintered plate at atmospheric pressure. Liquid guaiacol (Sigma Aldrich, ≥ 99%) was pumped (Shimadzu LC-20AT HPLC pump) and combined inside the reactor with a gas stream of pure H_2 (for H_2/Guaiacol = 8, mol/mol) or in a mixture of 13% H_2 in Ar (for H_2/Guaiacol = 1, mol/mol), whose flow rate were controlled by a MKS Type 247. The total molar flow was the same for all runs, in such a way that guaiacol molar fraction in the feed remained constant and equal to 11%. The reaction temperature was measured by a thermocouple placed to the outside wall of the reactor, which was heated by an electrical furnace. After the reactor there was a glass condenser kept at 278 K. The liquid product stored in the gas-liquid separator was drained periodically for immediate analysis of the composition.

Before each run, all catalysts were reduced *in situ* at the conditions previously described in the procedure for CO chemisorption. The catalyst loading (0.16–0.47 g, 60–100 mesh), the H_2 flow rate (5–38 mL/min), the Ar flow rate (0–33 mL/min), and the guaiacol flow rate (0.017–0.019 mL/min) were adjusted in certain conditions which resulted in guaiacol conversions below 40% at the stationary state, which avoid mass transfer limitations. The influence of H_2/Guaiacol (molar ratio), temperature, weight hourly space velocity (WHSV = g guaiacol/(h × g catalyst)), and pure catalytic support performance was analyzed. The data presented in this work correspond to long periods of time on stream (~ 60 h), unless otherwise mentioned. The carbon balance was greater than 95%.

Internal and external mass transfer limitations were found to be negligible according to the tests carried out with the Pt/Nb_2O_5 catalyst at 573 K. Internal mass transfer limitation

was verified by using two particle sizes: 60–100 and 100–200 meshes. Guaiacol conversion and products selectivity did not change with the particle size, indicating that internal mass transfer limitation was negligible. The external diffusion resistance test was carried out with the ratio of guaiacol flow rate to catalyst mass constant and equal to 2.7 g guaiacol/(h × g catalyst. The catalytic tests of this work were conducted in the region where guaiacol conversion remained constant with increasing flow rate, which indicates the elimination of external resistance. These information are important because if the kinetic regime is guaranteed the overall reaction rate will be connected with the reaction mechanism, not with physical processes. More information about the external mass transfer test can be found in Appendix A (Fig. A).

The gas product stream was comprised by unreacted hydrogen and CH_4. The gases were analyzed on-line with a gas chromatograph (Shimadzu, GC-17A) equipped with a thermal conductivity detector (TCD) followed by a flame ionization detector (FID) and a HayeSep D 100/120 packed column (6 m × 3.2 mm). The heating program was 313 K for 5 min, 10 K/min to 543 K then hold 25 min, and a column flow rate of 20 mL/min argon. Quantification was performed by the external standard method using a base mixture of 10% CH_4 in argon, which was diluted at an inert flow to give different compositions and hence a calibration curve.

The condensable product was initially identified off-line by gas chromatography-mass spectrometry (Shimadzu, GC-2010 MS). The liquid samples were collected in intervals around 90–120 min and were quantified off-line with a gas chromatograph (Shimadzu, GC-2010 FID) equipped with a FID detector and coupled to an auto sampler (AOC-20i). The GC was equipped with a RTX-VMS capillary column (30 m × 0.25 mm × 1.40 μm). The oven temperature regime was as follow: from 343 K to 443 K at 6 K/min, 1 K/min to 466 K, 6 K/min to 503 K then hold 15 min. The carrier gas (He) linear velocity was 12 cm/s, the split ratio 1/100, and the injection volume was 1 μL. The external standard method was used for quantification, with ethanol as solvent to prepare the standard mixtures. The liquid products analyzed were anisole (C_7H_8O), benzene (C_6H_6), catechol ($C_6H_6O_2$), cyclohexane (C_6H_{12}), cyclohexanone ($C_6H_{10}O$), methanol (CH_4O), o-cresol (C_7H_8O), phenol (C_6H_6O), toluene (C_7H_8), and veratrole ($C_8H_{10}O_2$).

Guaiacol conversion (X_{GUA}), the selectivity to product i (S_i), the degree of deoxygenation (DOD) [11], and the reaction rate (r) were calculated according to the following equations:

$$X_{GUA} = \frac{F_{GUA}^{in} - F_{GUA}^{out}}{F_{GUA}^{in}}$$

$$S_i = \frac{n_C^i \cdot F_i}{n_C^{GUA} \cdot \left(F_{GUA}^{in} - F_{GUA}^{out}\right)}$$

$$DOD = 1 - \frac{wt.\%O_{products}}{wt.\%O_{guaiacol}}$$

$$r = \frac{F_{GUA}^{in} \cdot X_{GUA}}{w_{cat}}$$

where F = molar flow rate, n_c = number of carbons in the molecule, w = mass, $wt.\%O$ = weight percent of oxygen.

The conversion was determined as an average over a given time interval, since it was based on the guaiacol injected and the product collected over that corresponding period. The selectivity to products from the gas stream and liquid stream was calculated separately for each phase. The partially oxygenated products (e.g., phenol and anisole) were included in the determination of the DOD. The reaction rate was determined considering the hypothesis of differential reactor (operation at low conversion values < 25%).

4.2 Results and discussion

4.2.1 X-ray diffraction (XRD)

XRD patterns of the xNb_2O_5/Al_2O_3 (x = 0, 5, 20, 100, wt.%) supports are shown in Figure 4.1. The XRD experiment was not carried out for the catalysts because the platinum nominal loading in the support was low (0.5 or 1 wt.%) and the Pt particles were small to be detected. Pure Al_2O_3 support was on the γ crystalline phase as indicated by the position of the diffraction patterns at 37°, 46°, and 67° [26,91]. For pure niobium pentoxide the peaks at 23°, 28°, 37°, 46°, 51°, and 55° were compatible with the hexagonal TT phase [26,92]. It is worth to mention that ammonium niobium oxalate is not completely anhydrous after calcination at 773 K, but there is still the form $Nb_2O_5 \cdot H_2O$. About 833 K anhydrous Nb_2O_5 is formed [93].

The Nb_2O_5/Al_2O_3 supports (5 and 20 wt.% of niobia loading) synthesized by wet impregnation had a similar pattern of pure alumina and no lines of crystalline niobia were observed. This result is coherent with literature [94]. However, bulk Nb_2O_5 particles were identified in the XRD patterns of the physical mixture comprised by 20% of Nb_2O_5 in Al_2O_3 (Fig. B). It can be deduced that niobium oxide was well dispersed in a two-dimensional layer (amorphous) on Al_2O_3 [30,95]. The high interaction between niobia and alumina is interesting for the stability in thermal treatments [95].

4.2.2 Nitrogen physisorption

The textural properties for both the supports and catalysts are reported in Table 4.1. The materials BET specific surface areas were distributed over a broad range. Niobium oxide showed the lowest specific surface (42 m^2/g) after calcination at 773 K while alumina had the highest value (244 m^2/g). The mixed support displayed a lower area compared to the pure alumina. The Nb_2O_5/Al_2O_3 support had a specific area 19% and 6% lower than Al_2O_3 for a niobia content equal to 20 wt.% and 5 wt.%, respectively. There was a small decrease of 9% on specific area for the Nb_2O_5 and 20% Nb_2O_5/Al_2O_3 supports after the Pt impregnation. No significant difference was observed for the area of both Al_2O_3 and 5%Nb_2O_5/Al_2O_3 supports compared with the Pt corresponding catalysts.

The Pt/Al_2O_3 catalyst had a 4.2 times higher pore volume than Pt/Nb_2O_5, which had the lowest value (0.16 cm^3/g) among all catalysts. On the other hand, Pt/Nb_2O_5 exhibited the highest average pore diameter (11.48 nm). Fig. C depicts N_2 sorption isotherms for all catalysts, which exhibited hysteresis, typical of mesoporous materials.

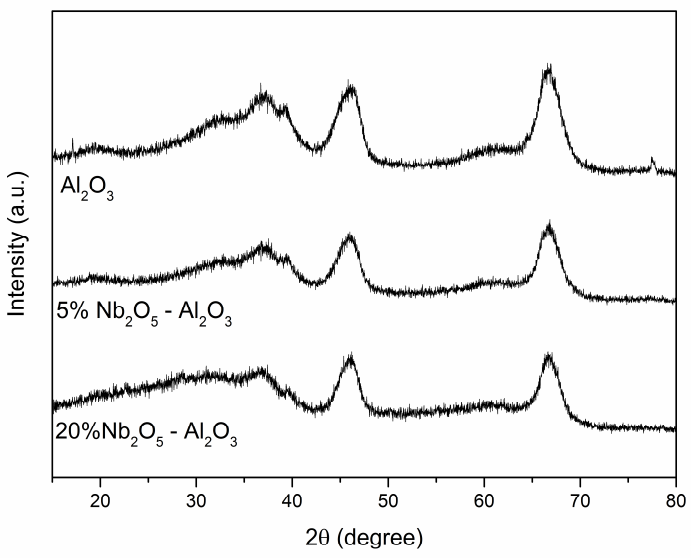

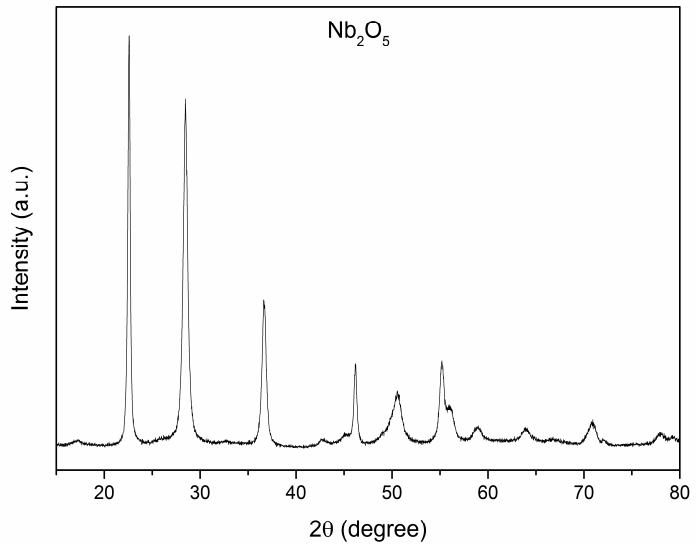

Figure 4.1 – XRD patterns of the xNb_2O_5/Al_2O_3 (x = 0, 5, 20, 100, wt.%) supports.

Table 4.1 – Textural properties of xNb_2O_5/Al_2O_3 (x = 0, 5, 20, 100 wt.%) supports and Pt supported catalysts.

Support/Catalyst	BET specific surface area (m^2/g)	Pore volume (cm^3/g)	Average pore diameter (nm)
Al_2O_3[a]	244	0.67	8.31
5% Nb_2O_5–Al_2O_3[a]	229	0.63	8.14
20% Nb_2O_5–Al_2O_3[a]	197	0.54	8.22
Nb_2O_5[a]	42	0.16	10.87
1% Pt/Al_2O_3[a]	239	0.58	7.63
1% Pt/5%Nb_2O_5–Al_2O_3[b]	229	0.62	8.24
1% Pt/20%Nb_2O_5–Al_2O_3[b]	180	0.47	7.91
0.5% Pt/Nb_2O_5[b]	38	0.16	11.48

[a] Calcination at 773 K; [b] Calcination at 573 K.

4.2.3 CO chemisorption

Table 4.2 reports the CO uptakes at 308 K for the catalysts. Dispersion of metal sites was determined using a nominal loading of Pt. The order of dispersion was Pt/5%Nb_2O_5–Al_2O_3 (85.4%) > Pt/20%Nb_2O_5–Al_2O_3 (73.7%) > Pt/Al_2O_3 (55.4%) > Pt/Nb_2O_5 (39.4%). Pt impregnated on the mixed support was better dispersed than on the pure supports. The superior reduction temperature of 773 K used for the activation of Pt/Al_2O_3 might be the cause of low dispersion due to the metal sinterization. The Nb_2O_5 specific area was 83%

lower than the alumina area but sufficient to provide almost three-quarter of the Pt dispersion achieved on Al_2O_3.

Table 4.2 – CO chemisorption results for $Pt/xNb_2O_5/(100-x)Al_2O_3$ (x = 0, 5, 20, 100, wt.%) catalysts.

Catalyst	CO uptake (µmol/g)	Dispersion (%)	Average crystallite size (nm)
1% Pt/Al_2O_3	28.4	55.4	2.0
1% $Pt/5\%Nb_2O_5–Al_2O_3$	43.8	85.4	1.3
1% $Pt/20\%Nb_2O_5–Al_2O_3$	37.7	73.7	1.5
0.5% Pt/Nb_2O_5	10.1	39.4	2.9

4.2.4 Temperature-programmed desorption of isopropylamine (IPA-TPD)

The IPA-TPD profiles of the catalysts are shown in Fig. D and are explained on the Appendix section D. Table 4.3 summarizes the IPA-TPD measurements. The amount of Brønsted acid sites (BAS) of the catalysts was in the same order of magnitude on a per mass basis (µmol/g). As well as alumina (27 µmol/g), niobia showed low BAS density (20 µmol/g). Nb_2O_5 strongly loses both its Lewis and Brønsted sites after calcination at 773 K [96,97]. However, the amount of propylene formed on a per area basis was at least 4 times higher for Pt/Nb_2O_5 (0.57 µmol/m²) compared to the other catalysts.

Table 4.3 –Summary of isopropylamine TPD results for the $Pt/xNb_2O_5/(100-x)Al_2O_3$ (x = 0, 5, 20, 100, wt.%) catalytic system.

Sample	Propene desorbed (Brønsted acid sites, BAS)		Isopropylamine desorbed (Lewis acid sites, LAS)		LAS/ LAS+BAS
	(µmol/g)	(µmol/m²)	(µmol/g)	(µmol/m²)	
γ-Al_2O_3	27	0.11	672	2.76	0.96
Nb_2O_5	20	0.47	65	1.54	0.76
1% Pt/Al_2O_3	35	0.15	968	4.05	0.96
1% $Pt/5\%\ Nb_2O_5 – Al_2O_3$	17	0.07	1101	4.80	0.98
1% $Pt/20\%\ Nb_2O_5 – Al_2O_3$	23	0.13	1121	6.23	0.98
0.5% Pt/Nb_2O_5	22	0.57	125	3.25	0.85

The alumina support had small amounts of BAS compared to the significant Lewis acid sites (LAS) density. Tittensor et al. [98] observed 29 µmol/g of propylene desorbed in

the IPA-TPD for γ-Al_2O_3 (180 m²/g). But the coating of alumina with niobia changes the LAS features and creates new BAS in Al_2O_3 with increasing Nb_2O_5 loadings, according to previous works [88,94,97]. However, in the present work the formation of BAS on the Pt/Nb_2O_5–Al_2O_3 catalysts did not occur. Pt/Nb_2O_5–Al_2O_3 displayed BAS amounts close to the value obtained for Pt/Nb_2O_5. This result may be associated with the catalysts precursors and also with the preparation method used in this work, which somehow differs from literature [88,99]. Passos et al. [88] used an oxalic acid solution of niobium oxalate while ammonium niobium oxalate [94] was used in this work to prepare the Nb_2O_5/Al_2O_3 support.

The amount of isopropylamine desorbed increased 44% and 92% for the Pt/Al_2O_3 and Pt/Nb_2O_5 catalysts, respectively, in relation to the pure supports. It was suggested that most of the unreacted isopropylamine on alumina interacts with Lewis acid sites (LAS) [98]. Based on this assumption it can be inferred that the impregnation of Pt increased the LAS of the catalysts compared to the pure supports. Pt/Nb_2O_5 showed the lowest LAS density (125 µmol/g) and Pt/20%Nb_2O_5–Al_2O the highest (1121 µmol/g).

It was reported that the acidity of acid supports (USY zeolite embedded in a silica-alumina matrix, zeolite ZSM-5, and amorphous silica-alumina) was crucial for controlling the selectivity for phenol and catechol on the HDO of guaiacol over nickel phosphide supported catalysts [64]. On the other hand, no correlation was found between the density of acid sites and the selectivity to deoxygenated products on the HDO of phenol over the Pd/Nb_2O_5 catalyst [28]. Considering the low values of both BAS and LAS (Table 4.3) it was suggested that the acid sites density was not the central agent which determined the performance of Pt/Nb_2O_5.

4.2.5 HDO of guaiacol over Pt/xNb_2O_5/(100-x)Al_2O_3 catalysts

4.2.5 a) Results at low hydrogen supply

The catalytic activity of the catalysts studied in terms of guaiacol conversion as a function of time on stream (TOS) is shown in Figure 4.2. The test was carried out for around 60 h TOS at 573 K using a diluted stream of hydrogen (13% H_2 in argon, H_2/Guaiacol = 1 mol/mol) to represent a gas saving condition.

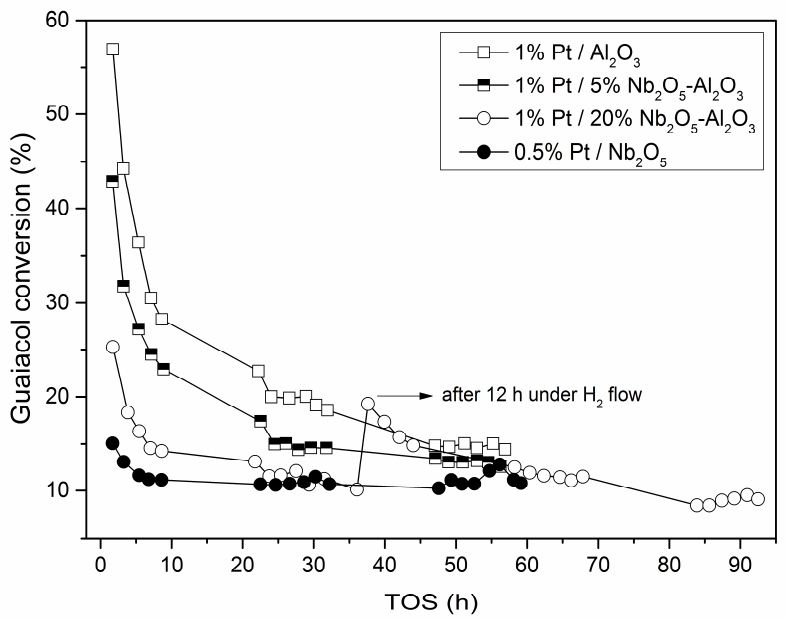

Figure 4.2 – Guaiacol conversion as a function of time on stream (TOS) for $Pt/xNb_2O_5/(100-x)Al_2O_3$ (x = 0, 5, 20, 100, wt.%) catalysts. Reaction conditions: atmospheric pressure, 573 K, WHSV = $2.7h^{-1}$, H_2/Guaiacol = 1 (mol/mol). The catalyst $Pt/20\%Nb_2O_5–Al_2O_3$ was regenerated after 35 h TOS by flowing H_2 at 573 K during 12 h, then the reaction was retaken for more 60 h.

It was observed that all catalysts deactivated since guaiacol conversion decreased from the first sample collected (~100 min TOS) to the last (~60 h TOS). Catalyst deactivation occurs in the HDO of guaiacol generally due to thermal degradation (i.e., sintering) and coking [23,62]. A previous work [61] reported that there was no evidence of changing in the platinum diameter cluster but carbonaceous deposits were observed after guaiacol conversion over Pt/Al_2O_3. An infrared (IR) spectroscopy study showed that guaiacol strongly interacts with alumina Lewis acid sites by the formation of doubly anchored phenates, which could be a source of severe catalyst deactivation [100]. For noble metals supported in carbon, coke was the main cause of deactivation due to the deposition of polyaromatics in the catalysts [62]. A catalytic system similar to the investigated in the present work, comprised by a noble metal supported on reducible oxide, Ru/TiO_2, displayed a decreasing selectivity for BTX over the first 2 h TOS. The loss of oxygen removal did not follow the same extent of change in guaiacol conversion, which remained practically constant with the time advance. This behavior was attributed to the likely coke formation that inhibited hydrogenolysis or to the SMSI effect arising from TiO_2 covering of the Ru metal [23].

It was speculated that coking was the main cause of catalyst deactivation in the catalytic system tested in this work. To support this assumption, the reusability of $Pt/20\%Nb_2O_5–Al_2O_3$ was checked after 35 h TOS by flowing H_2 at 573 K during 12 h, then

the reaction was retaken for more 60 h. The first sample conversion was 25% for the first run. After the catalyst regeneration the conversion dropped to 19%. This represented a reduction equal to 24%, indicating that the activity was partially recovered. The partial recovery of the first sample conversion seems to indicate that coking mainly caused catalyst deactivation, but sintering also occurred.

Table 4.4 reports the reaction rates for all catalysts, which followed the sequence: Pt/Al_2O_3 > $Pt/5\%Nb_2O_5–Al_2O_3$ > Pt/Nb_2O_5 > $Pt/20\%Nb_2O_5–Al_2O_3$. Pt/Al_2O_3 displayed a reaction rate 33% higher than Pt/Nb_2O_5, yet Pt/Nb_2O_5 with 0.5 wt.% Pt loading had a reaction rate (0.67 $\mu mol_{GUA}/(s.g_{cat})$) superior than 1% $Pt/20\%Nb_2O_5–Al_2O_3$ (0.55 $\mu mol_{GUA}/(s.g_{cat})$). The inferior Pt loading over Pt/Nb_2O_5 might have contributed for its lower activity compared to the catalysts predominantly comprised by alumina as support. It is noteworthy that the catalytic system containing niobia is complex. The active sites are not comprised by only the Pt metal, but also by the interface between Pt and the reducible support. The degree of deoxygenation (DOD) increased with the increasing niobia loading. Oxygen removal was the highest for Pt/Nb_2O_5 (DOD = 33%).

Table 4.4 – Reaction rate and degree of deoxygenation (DOD) of guaiacol conversion over Pt supported on $xNb_2O_5/(100-x)Al_2O_3$ (x = 0, 5, 20, 100, wt.%). Reaction conditions: atmospheric pressure, 573 K, WHSV = 2.7 h^{-1}, and H_2/Guaiacol = 1 (mol/mol).

Catalyst	Guaiacol conversion (%)	Reaction rate ($\mu mol_{GUA}/(s.g_{cat})$)	DOD (%)
1% Pt/Al_2O_3	14.4	0.89	0
1% $Pt/5\%Nb_2O_5–Al_2O_3$	12.6	0.77	10
1% $Pt/20\%Nb_2O_5–Al_2O_3$	9.1	0.55	22
0.5% Pt/Nb_2O_5	10.8	0.67	33

The selectivity to the main products (phenol, catechol, anisole, o-cresol, veratrole, benzene) for all catalysts had a smooth variation with the reaction time (Fig. E). The products distribution at the same low conversion level for all catalysts is depicted in Figure 4.3. Catechol or phenol were by far the major products of guaiacol conversion catalyzed by the $Pt/xNb_2O_5/(100-x)Al_2O_3$ system, but anisole, o-cresol, benzene, and veratrole were also formed in small amounts. The reaction network for the HDO of guaiacol catalyzed by Pt/γ-Al_2O_3 was proposed by literature [101].

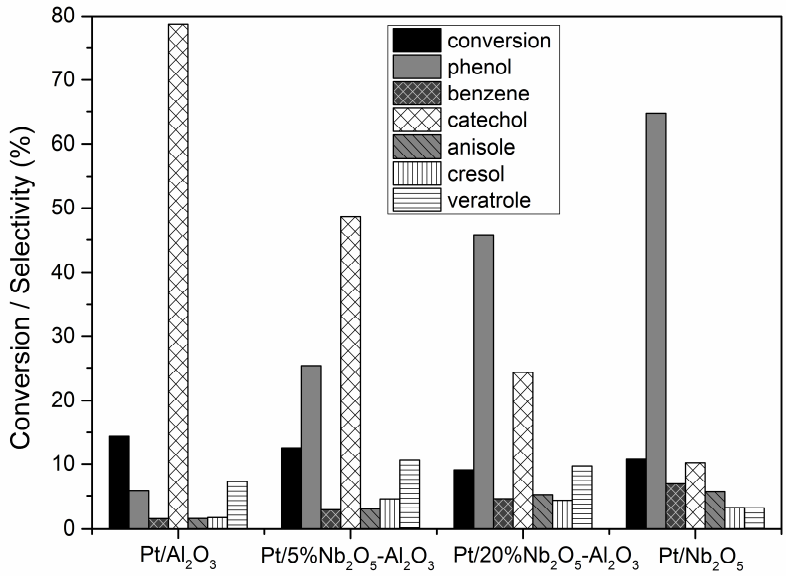

Figure 4.3 – Conversion and selectivity of the main products for the HDO of guaiacol over Pt supported on $xNb_2O_5/(100\text{-}x)Al_2O_3$ (x = 0, 5, 20, 100, wt.%) catalysts. Selectivity values bellow 2% were omitted for clarity. Reaction conditions: atmospheric pressure, 573 K, WHSV = 2.7 h^{-1}, H_2/Guaiacol = 1 (mol/mol).

The support plays a crucial role in determining the product distribution in the HDO of guaiacol [23,28,61,64,76,100]. While Pt/Al_2O_3 droves the production mainly to catechol (79%), Pt/Nb_2O_5 formed phenol as the main product (65%). Phenol selectivity increased and catechol formation decreased with increasing niobium content in the catalyst. The degree of deoxygenation (DOD) of the guaiacol molecule decreased in the following order (Table 4.4): Pt/Nb_2O_5 (33%) > $Pt/20\%Nb_2O_5–Al_2O_3$ (22%) > $Pt/5\%Nb_2O_5–Al_2O_3$ (10%) > Pt/Al_2O_3 (0%). These data revealed that Pt/Nb_2O_5 showed good activity and the best oxygen removal ability compared to the other samples.

The interaction between Pt and niobia was likely the central cause of improved oxygen removal ability for the catalytic system tested in this work. The Pt supported in niobia was better than the catalyst supported in niobia-alumina probably because more active sites were created by the cooperation between Pt and niobia compared with the catalysts containing alumina. Previous works analyzed the good performance of niobium oxide as support on the HDO of biomass derived compounds. Kon et al. [24] observed higher activity for Pt/Nb_2O_5 on the HDO of fatty acids and triglycerides compared to both pure Nb_2O_5 and other Pt-loaded catalysts. They explained that a synergy occurred between platinum and niobia. Shao et al. [27] reported high mass yields and unusual selectivities to aromatic hydrocarbons over Ru/Nb_2O_5 on the upgrading of raw lignin. The authors attributed the high formation of arenes to a combination of effects which were strong adsorption, selective cleavage of $C_{aromatic}$–OH

bounds, and the synergistic effect between the Ru and NbO_x species. Barrios et al. [28] obtained a reaction rate 90-fold higher and selectivity for benzene 40-fold superior for Pd/Nb_2O_5 compared to Pd/SiO_2 on the HDO of phenol. According to the authors the better performance of Pd/Nb_2O_5 likely came from the strong interaction between the Nb^{5+}/Nb^{4+} cations (oxophilic sites) and the oxygen from phenol. In the case of the analogous Ru/TiO_2 catalyst the high activity was explained by the defect sites derived from hydrogen spillover on the Ru to the TiO_2 support [19].

4.2.5 b) Influence of H_2 partial pressure

The influence of H_2/Guaiacol molar ratio on conversion and products distribution was evaluated at 573 K and WHSV = 2.7 h^{-1}, as can be seen in Table 4.5. The conversion reduced with decreasing H_2 partial pressure for all catalysts but with different extension for each one. The conversion was 3.3 times higher for H_2/Guaiacol = 8 than for H_2/Guaiacol = 1 in the case of Pt/Nb_2O_5. The Pt supported on 5 and 20 wt.% niobia-alumina had conversion almost 3 times higher for the superior H_2 partial pressure. But for Pt/Al_2O_3 the conversion was only 1.4 times superior for the higher molar ratio compared to the lowest mol/mol value. These results showed that the influence of hydrogen amounts on conversion was stronger for the niobia based catalysts. It is remarkable the effect of hydrogen on the HDO activity. Nimmanwudipong et al. [101] reported that the conversion decreased 92% when the HDO of guaiacol catalyzed by Pt/Al_2O_3 was carried out in the absence of hydrogen, compared to the reaction with the H_2 partial pressure equal to 95 kPa or 127 kPa (conversion around 8%). Fe/SiO_2 displayed a conversion of 30% for the reaction without H_2 and this value rose to 70% for 0.2–0.9 bar of H_2 [18].

The selectivity values were also dependent on the hydrogen initial concentration for Pt/Al_2O_3, which was at a condition near to isoconversion. Selectivity to phenol was 3 times higher at the highest H_2/Guaiacol molar ratio compared to the lowest, while the selectivity to catechol was 24% lower with the increase of H_2 partial pressure from 0.1 bar to 0.8 bar. The decreasing catechol selectivity with increasing H_2 partial pressure over $Pt/\gamma\text{-}Al_2O_3$ was already reported [101]. The increase in cyclohexanone amounts with the increasing H_2 partial pressure was expected since it is a product from a hydrogenation (of phenol) reaction [101]. Cyclohexane, a complete hydrogenation product, was formed as trace indicating that the complete hydrogenation pathway was not favored at the operating conditions used. This is a positive result because avoiding the saturation of the aromatic ring minimizes hydrogen

consumption. The crucial role of H_2 to promote deoxygenation in the HDO of guaiacol was reported in previous works [18,101].

Table 4.5 – Guaiacol conversion and selectivity of products as a function of H_2/Guaiacol (molar ratio) for the atmospheric HDO of guaiacol over $Pt/xNb_2O_5/(100\text{-}x)Al_2O_3$ (x = 0, 5, 20, 100, wt.%) catalysts at 573 K, WHSV = 2.7 h^{-1}.

Catalyst	Pt/Al_2O_3		Pt/5NbAl*		Pt/20NbAl*		Pt/Nb_2O_5	
H_2/Guaiacol	1	8	1	8	1	8	1	8
Conversion	14.4	19.8	12.6	35.4	9.1	26.9	10.8	35.5
Selectivity (%)								
Phenol	5.8	16.9	25.3	42.0	45.8	52.8	64.7	53.7
Benzene	1.5	2.1	2.9	6.0	4.6	5.8	6.9	15.5
Catechol	78.7	59.4	48.6	15.7	24.3	9.6	10.2	1.1
Anisole	1.5	2.4	3.0	6.4	5.2	6.4	5.7	8.3
o-cresol	1.7	2.7	4.5	8.6	4.3	4.3	3.2	1.6
Cyclohexanone	0.4	4.2	0.5	4.9	0.5	2.7	0.6	5.4
Veratrole	7.3	6.5	10.6	7.5	9.7	6.7	3.1	2.1
Toluene	0.7	0.7	1.0	1.1	1.0	0.7	0.8	0.5
Cyclohexane	1.9	1.7	2.1	1.2	1.8	1.5	1.5	1.8
CH_3OH	0.3	0.6	0.7	1.5	1.1	2.3	0.9	0.7
CH_4	0.1	2.7	0.7	5.2	1.7	7.3	2.3	9.9
C identified (%)	98.4	95.0	98.9	102.0	104.2	107.8	104.4	105.0
DOD (%)	0	6	10	29	22	32	33	47

* NbAl refers to Nb_2O_5/Al_2O_3 and the number refers to the niobia loading (wt.%) in alumina.

4.2.5 c) Influence of temperature

The influence of temperature was analyzed at WHSV = 2.7 h^{-1} and H_2/Guaiacol = 8 (mol/mol). Data illustrating the temperature dependence on conversion and selectivity are shown in Figure 4.4. The catalysts had expected responses with higher conversions at higher temperatures.

Temperature effect on selectivity was much stronger for Pt/Al_2O_3: while at 573 K catechol was the main product (62%), at 523 K phenol was the most abundant compound (30%). The increasing selectivity to catechol and the decreasing formation of phenol with

increasing temperature in the range of 523 to 573 K is in accordance with literature [101]. On the other hand increases in temperature were positive for phenol formation on the niobia-based catalysts. The selectivity for cyclohexanone was higher at lower temperatures regardless the catalyst, indicating that hydrogenation was favored at reduced temperatures, as expected. The DOD increased 17% for Pt/Nb_2O_5 and decreased 74% for Pt/Al_2O_3 with the temperature rise from 523 to 573 K. In the case of the catalyst comprised by the mixed support, the DOD remained around 30% in all temperatures.

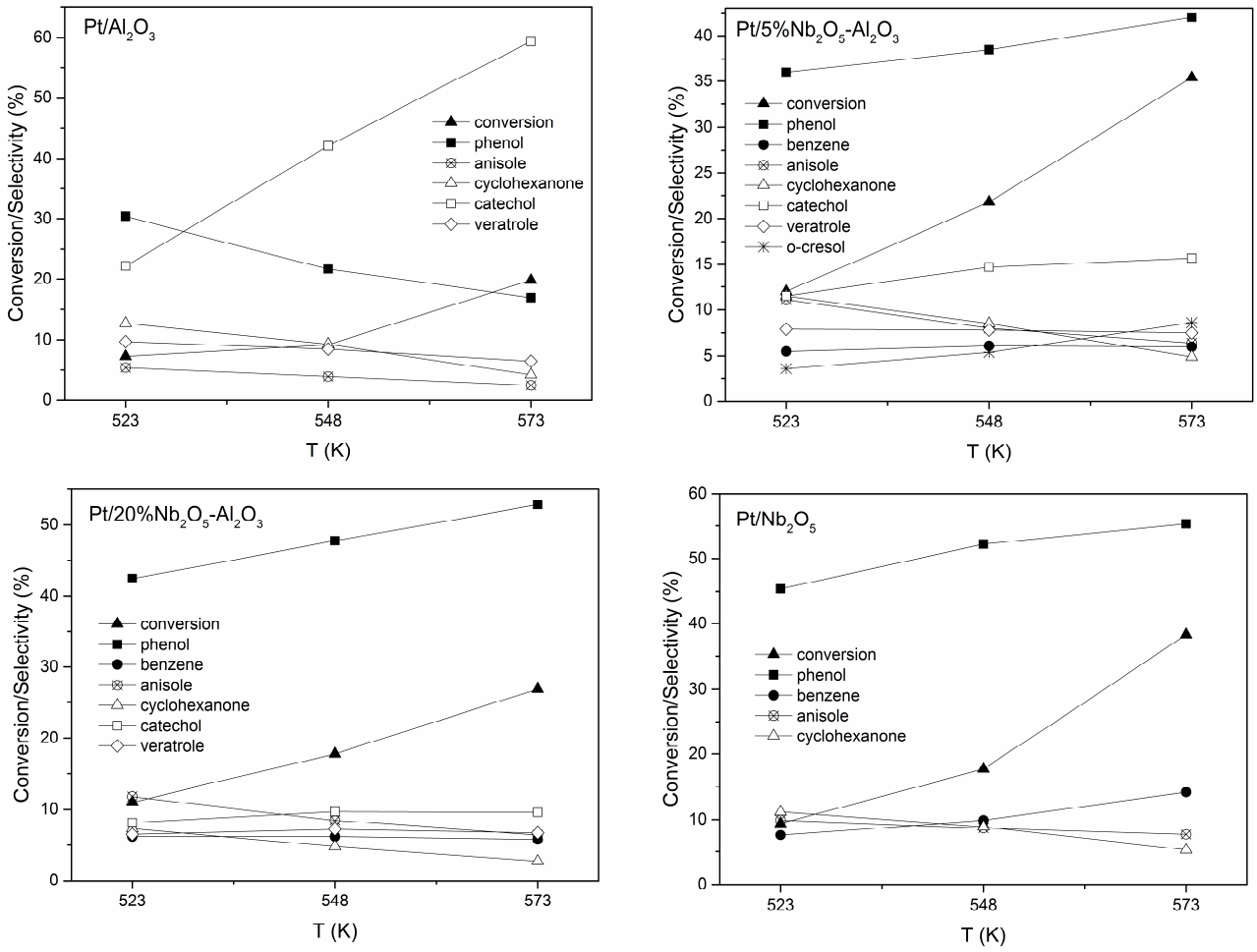

Figure 4.4 – Guaiacol conversion and products selectivity as a function of temperature for the HDO of guaiacol over Pt supported on $xNb_2O_5/(100\text{-}x)Al_2O_3$ (x = 0, 5, 20, 100, wt.%) catalysts. Selectivity values bellow 5% were omitted for clarity. Reaction conditions: atmospheric pressure, WHSV = 2.7 h^{-1}, H_2/Guaiacol = 8 (mol/mol), and temperatures equal to 523, 548, and 573 K.

4.2.5 d) Influence of the catalytic supports

Experiments were carried out with the supports alone in order to analyze their influence on the HDO of guaiacol at 573 K, WHSV = 2.7 h^{-1}, and H_2/Guaiacol = 8 (mol/mol). Figure 4.5 shows the first hours of reaction for both the supports and catalysts. The first

sample conversion of the supports varied in a broad range of 27–2%, in which Al_2O_3 showed the highest conversion at stationary state (5%) and Nb_2O_5 the lowest (1%). The increasing niobium oxide loading in alumina lowered the conversion values at the initial times of reaction. At around 30 h TOS the conversion remained constant and below 6% for all supports. Niobia conversion remained below 2% during the course of reaction.

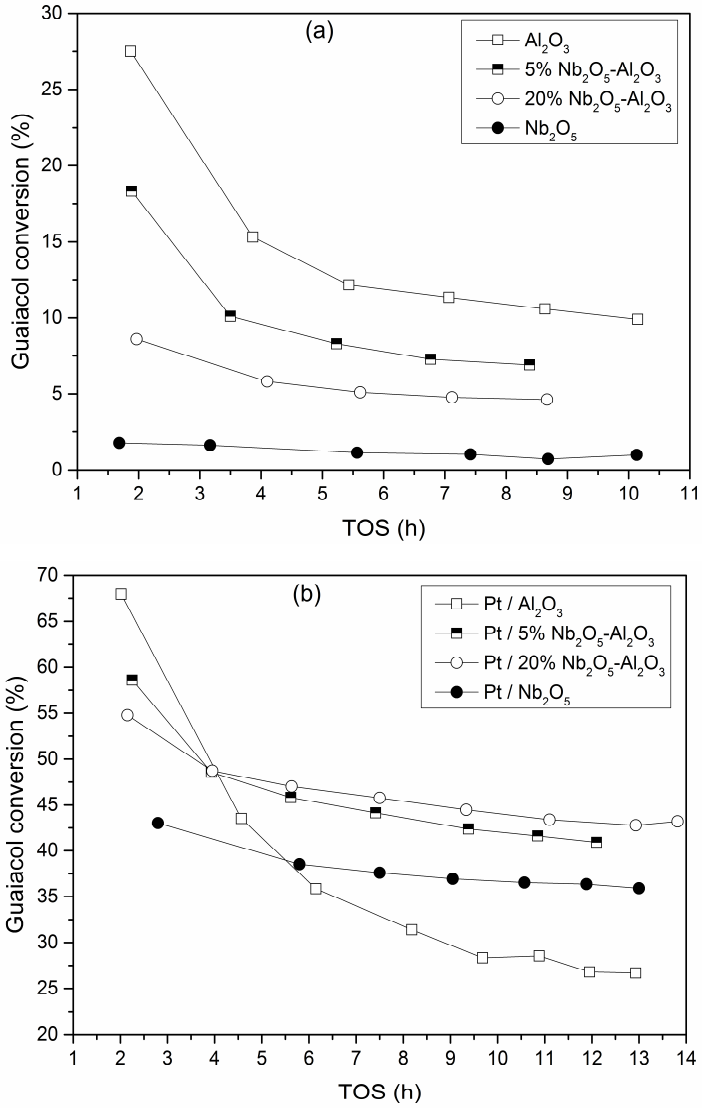

Figure 4.5 – Guaiacol conversion as a function of time on stream (TOS) for: (a) $xNb_2O_5/(100\text{-}x)Al_2O_3$ (x = 0, 5, 20, 100, wt.%) supports; (b) Pt supported catalysts. Reaction conditions: atmospheric pressure, 573 K, WHSV = 2.7 h^{-1}, H_2/Guaiacol = 8 (mol/mol).

The support with the higher first sample conversion (Figure 4.5a) resulted in the catalyst with the superior first sample conversion (Figure 4.5b). The specific rate ($\mu mol_{GUA}/(s \cdot g_{support})$) of the supports followed the sequence: $5\%Nb_2O_5/Al_2O_3$ (0.33) > Al_2O_3 (0.29) > 20% Nb_2O_5/Al_2O_3 (0.11) > Nb_2O_5 (0.06). Al_2O_3 and $5\%Nb_2O_5/Al_2O_3$ supports

displayed a reaction rate around 5 times higher than niobia rate. The high catalytic activity for pure alumina compared with titania and zirconia, which are also reducible supports, was reported [76]. Lewis acidity of Al_2O_3 may provide the high activity [23] but may also be responsible by the formation of precursors of coke products (e.g., methylphenols) [76].

The products distribution of both the supports and corresponding catalysts are compared in Figure 4.6. Phenol, catechol, veratrole, and o-cresol were the products formed on the reaction catalyzed by the pure supports. Catechol was the most abundant product for all supports with selectivity in the range of 33–63%. Al_2O_3 had the highest selectivity to catechol (63%) while niobia had the lowest (33%). Moreover, Nb_2O_5 had the highest selectivity for phenol (21%). In the case of the Pt supported catalysts, Pt/Al_2O_3 also showed the highest selectivity for catechol (60%) and Pt/Nb_2O_5 displayed the superior formation of phenol (54%). These findings suggest that the pure supports had an important function for giving direction for the products distribution of the Pt supported catalysts.

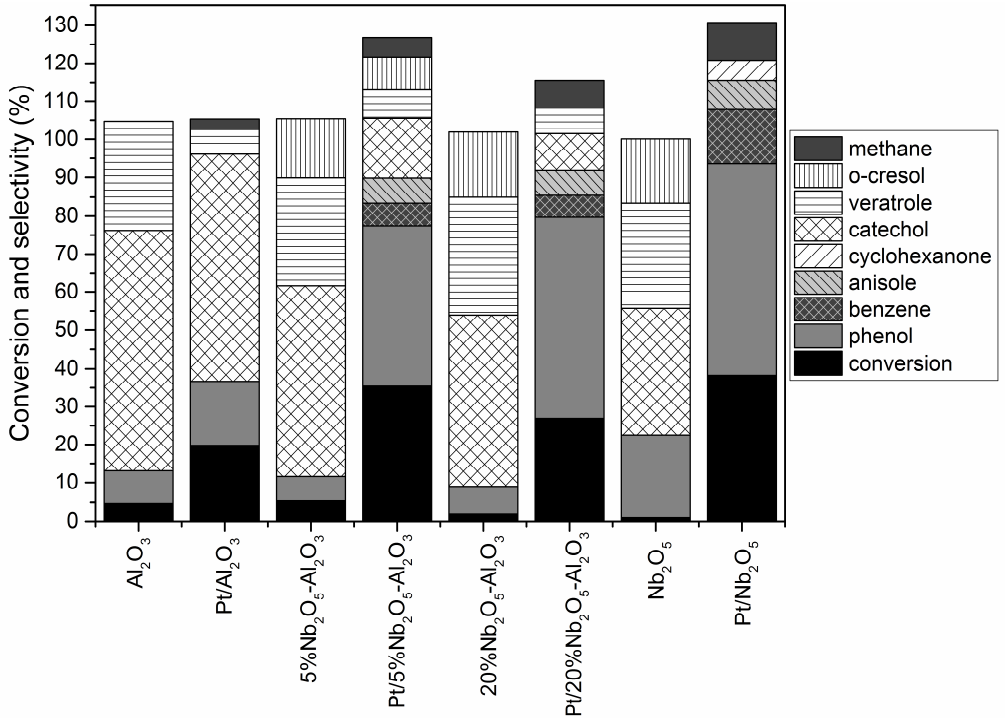

Figure 4.6 – Comparison of guaiacol conversion and product distribution between the xNb_2O_5/Al_2O_3 (x = 0, 5, 20, 100, wt.%) supports and the Pt supported catalysts. Selectivity values bellow 5% were omitted for clarity. Reaction conditions: atmospheric pressure, 573 K, WHSV = 2.7 h^{-1}, H_2/Guaiacol = 8 (mol/mol), and around 30 h and 80 h TOS for the supports and catalysts reaction, respectively.

The platinum crucial role on the catalyst performance was evidenced by the increase on both guaiacol conversion and selectivity for deoxygenated products (i.e., phenol, benzene) compared with the values for the corresponding pure support, which conforms to literature

[76,101]. Probably Pt contributed by splitting the H_2 molecule [24,27]. It was reported that the acidic function represented by the zeolite HY was not active for oxygen removal reactions but catalyzed only transalkylation reactions, indicating that the metal function Pt/Al_2O_3 was primordial for oxygen removal from guaiacol [101]. Transalkylation is a methyl-group transfer reaction typical of acid catalysts that can happen through an intramolecular rearrangement or it can involve two molecules (intermolecular transalkylation) [17,76,101]. Besides the methyl group transfer reactions, demethylation of guaiacol to produce catechol and partial transformation of catechol to phenol seemed to happen in all the pure supports. Hydrocarbons (benzene, toluene, cyclohexane) were not formed in the reaction catalyzed by the supports alone, as observed by other authors [76].

4.2.5 e) Influence of space velocity (WHSV)

The operating conditions used to verify the influence of WHSV were 573 K, H_2/Guaiacol = 8 (mol/mol), and around 12 h TOS (the stationary state was not established). Higher space velocity values demand a smaller reactor thus reduce the capital investment, but the contact time may be insufficient for the reactant to be converted. As can be observed in Table 4.6 the conversion reduced with increasing WHSV for all catalysts, as expected.

Table 4.6 – Activity of Pt supported on xNb_2O_5/Al_2O_3 (x = 0, 5, 20, 100, wt.%) at WHSV equal to 2.7 h^{-1} and 7 h^{-1}. Reaction conditions: atmospheric pressure, 573 K, H_2/Guaiacol = 8 (mol/mol), and around 12 h TOS.

Catalyst	Reaction rate ($\mu mol_{GUA}/(s.g_{cat})$)	Conversion (%)	
	At WHSV = 7 h^{-1}	WHSV = 7 h^{-1}	WHSV = 2.7 h^{-1}
1% Pt/Al_2O_3	2.21	13.8	26.7
1% $Pt/5\%Nb_2O_5–Al_2O_3$	3.75	24.3	40.9
1% $Pt/20\%Nb_2O_5–Al_2O_3$	3.05	19.6	43.2
0.5% Pt/Nb_2O_5	1.97	12.5	35.5

Guaiacol conversion fell approximately by half when WHSV was doubled from 2.7 h^{-1} to 7 h^{-1}. On the other hand product distribution little changed with this variation of space velocity. At the highest WHSV the reaction rate decreased with increasing niobia content at alumina (Table 4.6). The reaction rate for Pt/Nb_2O_5 (1.97 $\mu mol_{GUA}/(s.g_{cat})$) was a little lower than the value for Pt/Al_2O_3 (2.21 $\mu mol_{GUA}/(s.g_{cat})$).

4.2.5 f) Reaction pathway for Pt/Nb_2O_5

The influence of the inverse space velocity (1/WHSV) was analyzed for the most effective catalyst, Pt/Nb_2O_5, as shown in Figure 4.7. The reaction network was deduced based on the fact that a high initial selectivity is expected for primary products, while increasing selectivity with increasing conversion is expected for final products [62,64].

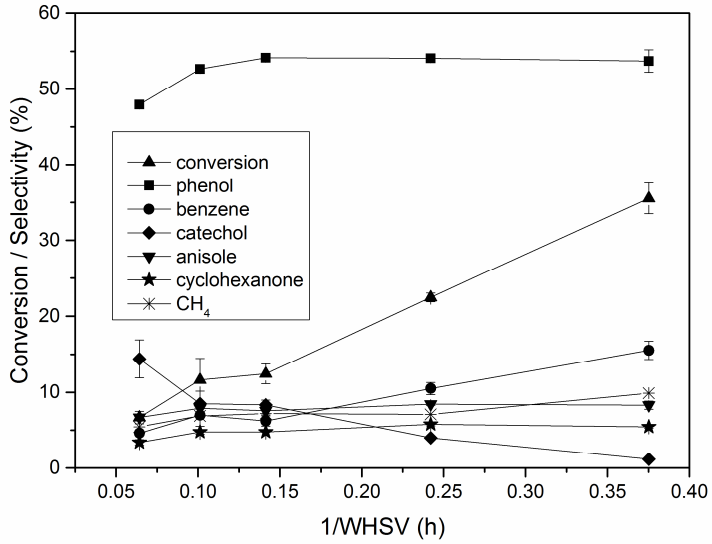

Figure 4.7 – Conversion and selectivities of the major products as a function of the inverse space velocity (1/WHSV) for the Pt/Nb_2O_5 catalyst. Selectivities which remained below 6% in the entire range of 1/WHSV were omitted for clarity. The error bars represent standard deviations determined in duplicate experiments. Reaction conditions: atmospheric pressure, 573 K, H_2/Guaiacol = 8 (mol/mol), and around 30 h TOS.

Guaiacol conversion increased with increasing inverse space velocity, an expected result from the increase of contact time of the reagent with the catalyst. Phenol was the most prominent product in the entire range of 1/WHSV. The second most abundant product was catechol at low values of contact time and benzene at high conversions. When 1/WHSV increased from 0.06 h to 0.37 h the selectivity of phenol increased from 48% to 54%, meanwhile the selectivity of benzene increased from 5% to 15% and the selectivity of catechol decreased from 15% to 1%. These results suggest that catechol was an intermediate product while phenol was both intermediate and final product and benzene was a final product. The selectivity for anisole was around 8% in the range of 1/WHSV tested, which indicates it was both primary and final product. The selectivity for methane increased from 5% to 10% when the contact time increased from the lowest to the highest value along with increasing benzene. Cyclohexanone (6–3%), o-cresol (6–2%), veratrole (5–2%), cyclohexane (3–2%), methanol (3–1%), and toluene (≤ 1%) were minor products. Based on the major

products behavior the possible reaction pathway for the Pt/Nb_2O_5 catalyst was inferred, as shown in Figure 4.8.

Probably the selectivity for catechol was not high (15–1%) because it reacted rapidly with H_2 to produce phenol in the reaction over Pt/Nb_2O_5. But catechol is less reactive on acid catalysts [17], which may explain its high selectivity value for the more acid Pt/Al_2O_3 catalyst (Figure 4.3) compared to Pt/Nb_2O_5. Catechol can be formed either by metal-catalyzed demethylation or by acid-catalyzed transalkylation (e.g., along with veratrole through bimolecular transalkylation of guaiacol) [23,101]. Phenol is likely to derive from catechol through the release of water (dehydroxylation) or by the removal of methanol from guaiacol (demethoxylation) [62,76,84]. In this work, the methane selectivity was much higher than methanol formation. This result indicates that the removal of the methoxy group from guaiacol to form phenol occurred in less extent than the removal of water from catechol.

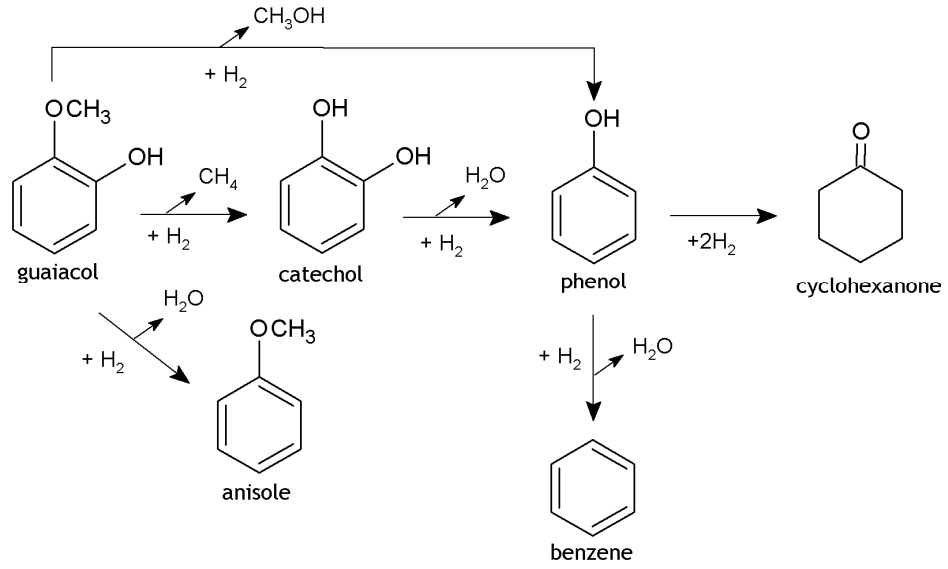

Figure 4.8 – Proposed reaction network for the HDO of guaiacol catalyzed by Pt/Nb_2O_5 considering the major products.

Comparing the oxygen–carbon bond energies of the guaiacol molecule the preferred path would be the demethylation to form catechol (247 kJ/mol), followed by the demethoxylation to form phenol (356 kJ/mol) and the most difficult rupture of bond would be the dehydroxylation to produce anisole (414 kJ/mol) [84]. The higher production of phenol compared to anisole on Pt/Nb_2O_5 is in accordance with this thermodynamic point of view. The superior selectivity for phenol in relation to anisole indicates that the demethoxylation was more favorable than dehydroxylation of guaiacol, as previously reported [18,101].

However, selectivity for anisole was superior for niobia-based catalysts compared to Pt/Al_2O_3 (Table 4.5). Shao et al. [27] showed that Ru/Nb_2O_5 was able to form toluene through the $C_{aromatic}$–OH bond cleavage of 4-methylphenol (dehydroxylation). This interesting result was explained by the niobia ability to reduce the disassociation energy of $C_{aromatic}$–OH bond and present a unique catalytic activity compared to alumina, zirconia, and titania.

The oxygen-free compound formed in the final reaction stage, benzene, may have derived from the direct deoxygenation of phenol. Cyclohexanone was also likely produced from phenol through hydrogenation. Barrios et al. [28] observed cyclohexanone and benzene as products on the HDO of phenol over Pd/Nb_2O_5 and discussed the reaction pathways. The sum of deoxygenated products in this work increased with increasing 1/WHSV, which is in agreement with literature [18].

4.3 Conclusions

The HDO of guaiacol over the catalytic system comprised by Pt supported in Nb_2O_5/Al_2O_3 revealed that the niobia loading (0, 5, 20, 100, wt.%) in the support strongly interfered on the catalyst behavior. The higher the niobia content the higher was the selectivity for phenol. Pt/Nb_2O_5 was superior in terms of oxygen removal. The cooperation between Pt and NbO_x species was attributed as the reason of the improved catalytic performance of Pt/Nb_2O_5. The pure supports behavior appeared not to be negligible and they might have given direction for the corresponding catalyst performance.

CHAPTER 5 – HYDRODEOXYGENATION OF GUAIACOL OVER Pt/Nb_2O_5 AND $Pt/NbOPO_4$

Niobia was used as a support for the hydrodeoxygenation of model compounds different from guaiacol, as discussed in Chapter 4. Niobium phosphate was also used as catalytic support on biomass-derived products upgrading reactions with hydrogen carried out on liquid phase. The $Pd/NbOPO_4$ catalyst showed high activity and stability in the HDO of furan-derived adduct, aiming at the production of liquid alkanes. The Pd metal was the active center for hydrogenation, the NbO_x species helped on the C–O bond cleavage, and the acid function catalyzed dehydration [102]. The water-stable and bifunctional catalyst comprised by the acid $NbPO_5$ and the metal Pt was used on dehydration followed by hydrogenation of hydrogenated aldol adducts into pure alkanes. The $Pt/NbPO_5$ catalyst did not deactivated nor developed a pressure drop with the reaction extent, unlike Pt supported in SiO_2/Al_2O_3 or zeolites [103]. The $Pt/NbOPO_4$ catalyst was effective for producing methylcyclopentane (gasoline additive) through hydrogenation of 3-methylcyclopent-2-enone (representative of the carbohydrate portion of lignocellulosic biomass) [104]. Moreover, $Pt/NbOPO_4$ was used in the HDO of raw woods into liquid alkanes through the simultaneous conversion of cellulose, hemicellulose, and lignin fractions. The superior performance of this catalyst was explained by the synergistic effect between Pt, NbO_x species, and acidic sites [65].

This study aimed to evaluate the performance of niobium-based catalysts comprised by Pt supported on niobia and niobium phosphate on the HDO of guaiacol at atmospheric pressure. Two different precursors of niobia were used for comparison, niobic acid and ammonium niobium oxalate. Moreover, the effect of operating conditions (H_2 partial pressure, temperature, space velocity, and pure support behavior) on activity and selectivity was investigated. The strong metal-support interaction (SMSI) [87] for the best performance catalyst, Pt/Nb_2O_5–ANO, was analyzed.

5.1 Experimental

5.1.1 Synthesis and characterization of catalysts

Two different precursors of hydrated niobium pentoxide were used to produce the support Nb_2O_5. The first one was niobic acid, $Nb_2O_5 \cdot nH_2O$ (HY-340/CBMM) and the second was ammonium niobium oxalate, $NH_4[NbO(C_2O_4)_2(H_2O)_2](H_2O)_n$ (ANO/CBMM). Both precursors were calcined at 773 K during 4 h, at a heating rate of 10 K/min. Niobium phosphate ($NbOPO_4 \cdot nH_2O$/CBMM) was calcined at 623 K during 4 h (10 K/min) to produce the support $NbOPO_4$ (or $NbPO_5$).

Catalysts were prepared by incipient wetness impregnation of the supports with an aqueous solution of chloroplatinic acid hexahydrate ($H_2PtCl_6.6H_2O$, Sigma Aldrich, ≥ 37.50% Pt). It was used a Pt nominal loading of 0.5 wt.% for Pt/Nb_2O_5 and 1 wt.% for $Pt/NbOPO_4$. Incipient wetness was determined to be: 0.29 mL H_2O/g Nb_2O_5 and 0.34 mL H_2O/g $NbOPO_4$. The impregnation was done with a mortar and pestle. Then the impregnated support was dried at 393 K for 12–15 h, followed by calcination at 10 K/min to 573 K during 4 h. All calcinations were done with a muffle furnace in static air. The catalysts were pelletized with a press, then crushed and sieved to a size of 60–100 mesh ($0.15 < d\# < 0.25$ mm, d# was the sieve size).

The catalysts were characterized by the following techniques, described in details in section 4.1.3: X-ray diffraction, nitrogen physisorption, CO chemisorption, and temperature-programmed desorption of isopropylamine.

5.1.2 Catalytic tests: HDO of guaiacol

The catalytic testes were carried out in a similar manner as described in section 4.1.4. The reduction for all catalysts occurred *in situ* from room temperature to 573 K for 10 h, then hold at 573 K during 2 h at a hydrogen flow of 30 mL/min.

5.2 Results and discussion

5.2.1 Characterization of catalyst results

Figure 5.1 shows the XRD patterns of the niobia and niobium phosphate supports. The position of the diffraction peaks at 23°, 28°, 37°, 46°, 51°, and 55° was identical for

Nb_2O_5 from ANO and from HY-340, indicating that they were in the hexagonal TT crystalline phase [26,92]. Nonetheless, the intensity (amplitude) of the lines was very different. The superior intensity of the lines for Nb_2O_5–ANO indicates that this support was more crystalline than Nb_2O_5–HY-340. In the case of niobium phosphate, no diffraction peaks were detected indicating that it was amorphous [105].

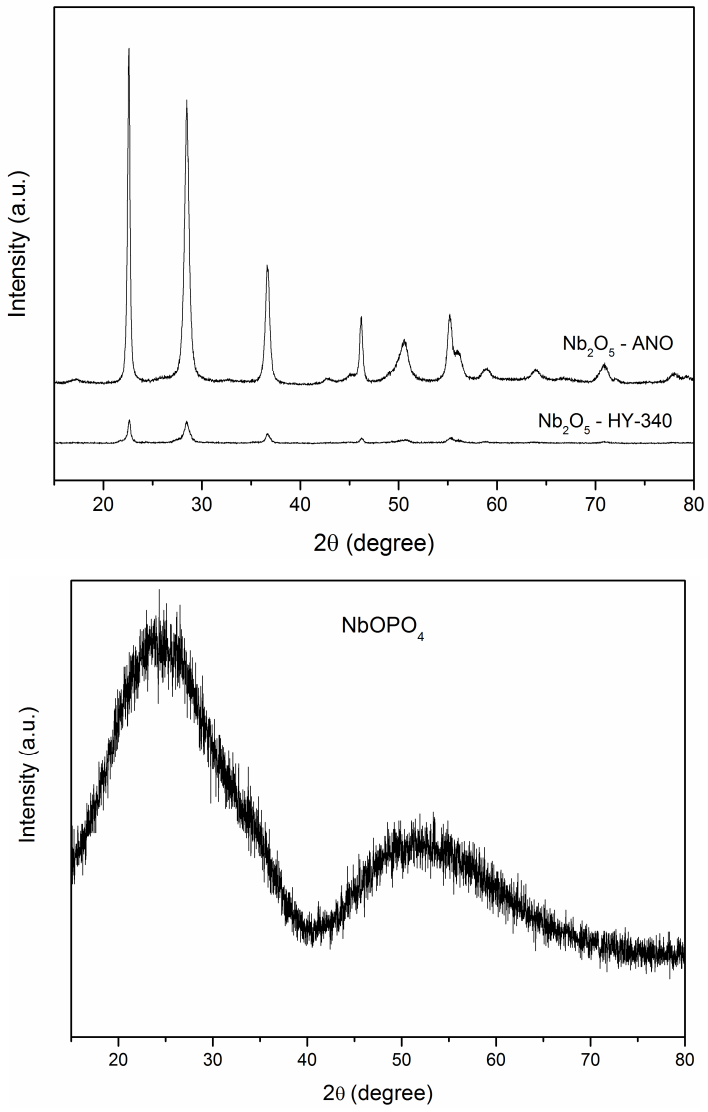

Figure 5.1 – XRD patterns of the Nb_2O_5 and $NbOPO_4$ supports.

Niobia from HY-340 had a surface area (16 m^2/g) 62% lower than the area from niobia originated from ANO (42 m^2/g) for the same calcination temperature of 773 K, as can be seen in Table 5.1. Niobium phosphate calcined at 623 K showed a superior surface area of 179 m^2/g. There was a decrease on the support surface area after the Pt impregnation in the following sequence: $NbOPO_4$ (31%) > Nb_2O_5–HY-340 (12%) > Nb_2O_5–ANO (9%). The highest pore volume was 0.28 cm^3/g for Pt/$NbOPO_4$. The superior pore volume of niobium

phosphate compared to niobium oxide is associated with its lamelar structure, as explained by literature [105]. The N_2 sorption isotherms for the catalysts are shown in Fig. F and they were classified as Type IV, whose characteristic feature is its hysteresis loop [105,106].

Table 5.1 – Textural properties of Nb_2O_5 and $NbOPO_4$ supports and Pt supported catalysts.

Support/Catalyst	BET surface area (m^2/g)	Pore volume (cm^3/g)	Average pore diameter (nm)
Nb_2O_5 (ANO)	42	0.16	10.87
Nb_2O_5 (HY-340)	16	0.07	11.16
$NbOPO_4$	179	0.29	4.44
0.5% Pt/Nb_2O_5 (ANO)	38	0.16	11.48
0.5% Pt/Nb_2O_5 (HY-340)	14	0.07	11.04
0.5% Pt/$NbOPO_4$	124	0.28	6.13

The uptakes of CO at 308 K for the catalysts are shown in Table 5.2, determined using Pt nominal loading. The niobia supported catalysts exhibited dispersion around 40%, regardless the precursor used. Pt/$NbOPO_4$ showed a lower Pt dispersion (25%) and had a crystallite size (4.6 nm) 59% higher than the value for Pt/Nb_2O_5.

Table 5.2 – CO chemisorption results for Pt/Nb_2O_5 and Pt/$NbOPO_4$ catalysts.

Catalyst	CO uptake (µmol/g)	Dispersion (%)	Crystallite size (nm)
0.5% Pt/Nb_2O_5 (ANO)	10.1	39.4	2.9
0.5% Pt/Nb_2O_5 (HY-340)	9.9	39.0	2.9
1% Pt/$NbOPO_4$	12.7	24.8	4.6

The acidity measurements by temperature-programmed desorption of isopropylamine are summarized in Table 5.3. The amount of Brønsted acid sites (BAS) for $NbOPO_4$ support (273 µmol/g) was almost 11 times higher than that for the Nb_2O_5 support, regardless the precursor used. The incorporation of platinum in $NbOPO_4$ reduced the Brønsted acidity, since the propylene desorbed was 3 times higher for the support compared to Pt/$NbOPO_4$ (89 µmol/g). The catalyst synthesis method through incipient wetness impregnation using $H_2PtCl_6.6H_2O$ may explain this reduction of acidity. The preparation method of the active phase can also affect catalyst performance and deactivation. The positive effect of chloride

anion reported by some authors is that it enhances the catalyst activity [20]. The Ru/C catalyst prepared using $RuCl_3$ as precursor had the highest activity for the hydrotreatment of fast pyrolysis oil at 350 °C and 200 bar. The precursors $Ru(NO)(NO_3)_3$ and $Ru(acac)_3$ (acac = acetylacetonate) were also tested, and the catalyst prepared using the nitrate salt had low activity attributed to the poor Ru distribution [20,107].

It was desorbed 22 μmol/g of propylene in the TPD of Pt/Nb_2O_5–ANO, which was an amount 2.7 times higher than the obtained for Pt/Nb_2O_5–HY-340. However, the propylene formed on a per area basis was approximately 0.60 μmol/g for Pt/Nb_2O_5, regardless the precursor of niobia used. The Brønsted acid sites (BAS) concentration in a per mass basis was 4 and 11 times higher for $Pt/NbOPO_4$ than for Pt/Nb_2O_5–ANO and Pt/Nb_2O_5–HY-340, respectively.

Table 5.3 – Summary of isopropylamine TPD results for the Pt/Nb_2O_5 and $Pt/NbOPO_4$ catalysts.

Sample	Propene desorbed (Brønsted acid sites)		Isopropylamine desorbed	
	(μmol/g)	(μmol/m^2)	(μmol/g)	(μmol/m^2)
Nb_2O_5 (ANO)	25	0.60	65	1.54
$NbOPO_4$	273	1.52	596	3.32
0.5% Pt/Nb_2O_5 (ANO)	22	0.57	125	3.25
0.5% Pt/Nb_2O_5 (HY-340)	8	0.61	48	3.43
1% $Pt/NbOPO_4$	89	0.50	474	2.64

The amount of unreacted isopropylamine desorbed increased 92% and decreased 20% for the Pt/Nb_2O_5–ANO and $Pt/NbOPO_4$ catalysts, respectively, compared to the pure supports. This result may indicate that the Lewis acid sites (LAS) concentration increased for niobia after Pt impregnation, while Lewis acidity was reduced when Pt was incorporated in niobium phosphate. Among the catalysts studied, $Pt/NbOPO_4$ showed the highest amount of isopropylamine desorbed in a per mass basis (474 μmol/g). In the case of alumina, it was inferred that most of the isopropylamine interacts with Lewis acid sites [98]. In this work, the unreacted isopropylamine was quantified to give a notion of the LAS concentration and allow a comparison between catalysts.

Hydrated niobium pentoxide ($Nb_2O_5 \cdot nH_2O$) exhibits strong acid sites (70% H_2SO_4 solution) for low pretreatment temperatures. Unlike the majority of acid metal oxides, the acidity of niobium pentoxide decreases with increasing pretreatment temperature due to the

transformation of protonic sites to Lewis sites through water release. After calcination about 773 K, the surface of niobia become almost neutral. Niobium phosphate displays textural and acid properties similar to niobium oxide, yet its properties are preserved until higher pretreatment temperatures [108].

Pt supported on niobium-based catalysts (niobium phosphate, niobic acid, phosphated niobic acid) showed higher reactivity compared to the catalyst $Pt/SiO_2–Al_2O_3$ in the aqueous-phase dehydration and hydrogenation (APDH) of sorbitol to alkanes. The superior reactivity was not attributed to the concentration of acid sites but rather was supposed to be due to the interaction of reactive molecules with Nb=O and adjacent hydroxyl groups [29]. Moreover, the results from the HDO of phenol over the Pd/Nb_2O_5 revealed that there was no correlation between the density of acid sites and the selectivity to deoxygenated products [28]. Considering these information, it seems that the acidity of niobium-based catalysts was not the central agent that determined the catalysts performance. In the case of niobia-supported Pt of low acidity this observation may be more strongly applied than on niobium phosphate-supported Pt of higher acidity.

5.2.2 Catalytic results of the HDO of guaiacol

5.2.2 a) Results at low hydrogen supply

Figure 5.2 shows guaiacol conversion as a function of time on stream (TOS) for the Pt/Nb_2O_5 and $Pt/NbOPO_4$ catalysts. The experiment was conducted to evaluate the catalysts during approximately 60 h of reaction at 573 K with low supply of hydrogen (13% H_2 in argon, H_2/Guaiacol = 1 mol/mol). Catalyst deactivation on the HDO of guaiacol reactions is typically caused by coking and thermal degradation (sintering) [23,62].

The activity on a Pt mass basis for each catalyst is shown in Table 5.4. The reaction rate for $Pt/NbOPO_4$ (0.88 $\mu mol_{GUA}/(s.g_{cat})$) was around 26% higher than the specific rate for Pt/Nb_2O_5. Guaiacol conversion for all catalysts displayed close values (11–14%), which allows the comparison of selectivities at an isoconversion level.

Figure 5.3 illustrates the products distribution for the niobium-based catalysts. Phenol was the major product for Pt/Nb_2O_5 with selectivity of 64%, while catechol was the most abundant compound for $Pt/NbOPO_4$ (selectivity = 51%). The product distribution was similar for both Pt/Nb_2O_5 catalysts and independent of the precursor of niobia used. Phenol and catechol were prominent products for the catalytic system studied, but anisole, o-cresol,

benzene, and veratrole were also formed. The oxygen removal was superior for Pt supported in niobium oxide. The DOD was 4.7 times higher for Pt/Nb_2O_5 compared to $Pt/NbOPO_4$ (Table 5.4). It could be noted that Pt/Nb_2O_5 was more effective to produce less oxygenated compounds. The good performance of niobium oxide as support of a noble metal on the HDO of biomass-derived compounds was reported in other studies and was attributed to the cooperation between niobia and the noble metal [24,27,28]. In the case of $Pt/NbOPO_4$, the mechanism in which the catalyst works might be associated with a synergism between Pt, NbO_x species, and the acidity of the support (Brønsted acid sites on PO_4 and Lewis acid sites on NbO_x) [65].

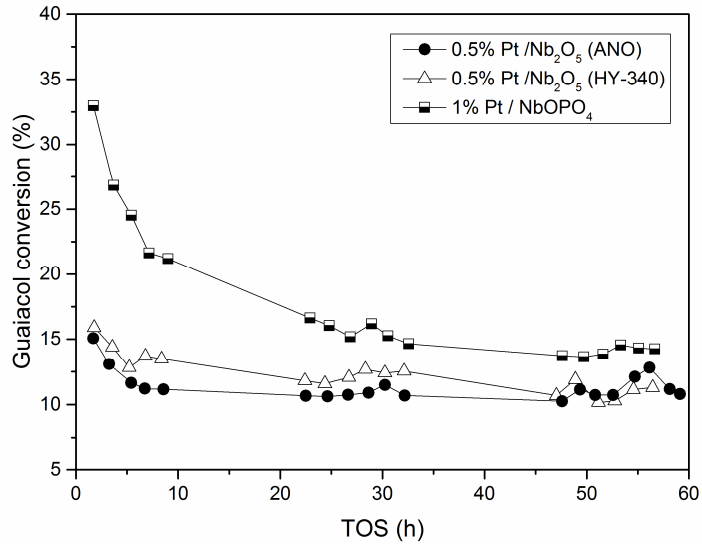

Figure 5.2 – Guaiacol conversion as a function of time on stream (TOS) for Pt/Nb_2O_5 and $Pt/NbOPO_4$ catalysts. Reaction conditions: atmospheric pressure, 573 K, WHSV = 2.7 h^{-1}, H_2/Guaiacol = 1 (mol/mol), and gas flow comprised by 13% H_2 in Ar.

Table 5.4 – Rates of reaction of guaiacol conversion over Pt supported on Nb_2O_5 and $NbOPO_4$. Reaction conditions: atmospheric pressure, 573 K, WHSV = 2.7 h^{-1}, H_2/Guaiacol = 1 (mol/mol), and gas flow comprised by 13% H_2 in Ar.

Catalyst	Guaiacol conversion (%)	Reaction rate ($\mu mol_{GUA}/(s.g_{cat})$)	DOD (%)
0.5% Pt/Nb_2O_5 (ANO)	10.8	0.67	33
0.5% Pt/Nb_2O_5 (HY-340)	11.3	0.70	33
1% $Pt/NbOPO_4$	14.3	0.88	7

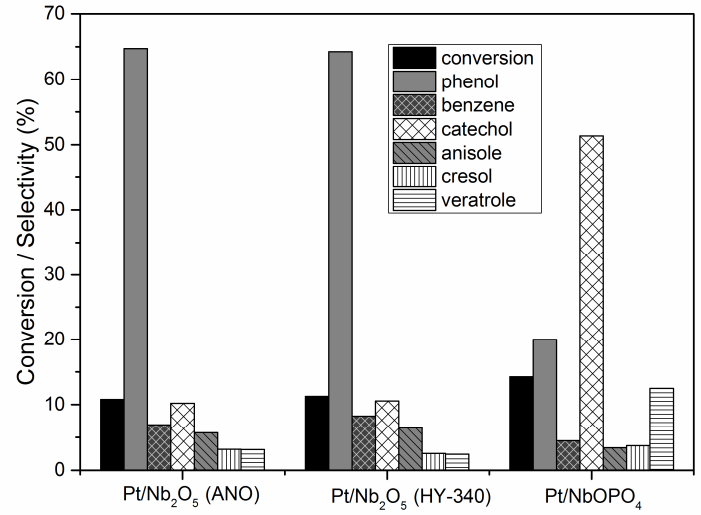

Figure 5.3 – Conversion and selectivity of the main products for the HDO of guaiacol over Pt supported on Nb_2O_5 and $NbOPO_4$ catalysts. Selectivity values bellow 2% were omitted for clarity. Reaction conditions: atmospheric pressure, 573 K, WHSV = 2.7 h^{-1}, H_2/Guaiacol = 1 (mol/mol), and gas flow comprised by 13% H_2 in Ar.

5.2.2 b) Influence of H_2 partial pressure

It can be seen in Table 5.5 the influence of the hydrogen partial pressure on the catalysts conversion at 573 K and WHSV = 2.7 h^{-1}. The tests were performed keeping fixed both the amount of guaiacol (11% molar fraction) and the total molar flow of feed. For a hydrogen partial pressure of 0.1 bar (H_2/Guaiacol = 1) a gas mixture comprised by 13% hydrogen in argon was used, while for a hydrogen pressure equal to 0.8 bar (H_2/Guaiacol = 8) it was used a pure hydrogen stream.

The increase on H_2/Guaiacol molar ratio from 1 to 8 practically did not altered the conversion for Pt/Nb_2O_5–HY-340, which remained around 10–11%. On the other hand, the conversion was 3.3 and 2.4 times higher for Pt/Nb_2O_5–ANO and Pt/$NbOPO_4$, respectively, when the H_2 partial pressure increased from 0.1 to 0.8 bar. While for H_2/Guaiacol = 1 the precursor of niobia had no influence on Pt/Nb_2O_5 performance (as previously noticed in Figure 5.3), in the presence of hydrogen in excess Pt/Nb_2O_5–ANO was more active compared to Pt/Nb_2O_5–HY-340. Pt/Nb_2O_5–ANO displayed a conversion (35%) 3.5 times higher than the value for Pt/Nb_2O_5–HY-340 at a H_2/Guaiacol = 8.

The hydrogen concentration at feed influenced on products distribution in the case of Pt/Nb_2O_5–HY-340, which was at the same conversion level. There was an increase in catechol and veratrole selectivities with the increase of the H_2 partial pressure, while there was a decrease in benzene formation and in oxygen removal (DOD) for Pt/Nb_2O_5–HY-340. There was an increase in cyclohexanone and CH_4 with increasing hydrogen supply. The superior

formation of cyclohexanone, which is a hydrogenation product, occurred according the expected at the highest H_2/Guaiacol value [101]. Complete hydrogenation of the aromatic ring through the formation of cyclohexane was not significant at the conditions tested, which reduces the consumption of H_2. The important role of hydrogen either in HDO activity or for oxygen removal in the HDO of guaiacol was observed by other authors [18,101].

Table 5.5 – Guaiacol conversion and selectivity of products as a function of H_2/Guaiacol (molar ratio) for the atmospheric HDO of guaiacol over Pt/Nb_2O_5 and $Pt/NbOPO_4$ catalysts at 573 K, WHSV = 2.7 h^{-1}.

Catalyst	Pt/Nb_2O_5 (ANO)		Pt/Nb_2O_5 (HY-340)		$Pt/NbOPO_4$	
H_2/Guaiacol	1	8	1	8	1	8
Conversion	10.8	35.5	11.3	10.2	14.3	34.9
Selectivity (%)						
Phenol	64.7	53.7	64.3	53.0	20.0	36.8
Benzene	6.9	15.5	8.2	4.3	4.5	6.1
Catechol	10.2	1.1	10.6	14.1	51.4	33.7
Anisole	5.7	8.3	6.4	6.3	3.4	3.5
o-cresol	3.2	1.6	2.5	6.3	3.7	4.4
Cyclohexanone	0.6	5.4	0.7	3.1	0.3	2.3
Veratrole	3.1	2.1	2.4	4.1	12.5	7.6
Toluene	0.8	0.5	0.9	1.0	0.8	0.7
Cyclohexane	1.5	1.8	1.8	2.9	1.5	1.0
CH_3OH	0.9	0.7	1.0	2.8	1.2	1.5
CH_4	2.3	9.9	1.3	2.1	0.7	2.4
C identified (%)	104.4	105.0	102.2	99.7	101.8	98.9
DOD (%)	33	47	33	25	7	17

5.2.2 c) Influence of temperature

Figure 5.4 shows the conversion and selectivity as a function of temperature for the niobium-based catalysts. It was observed higher conversion values at higher temperatures for all catalysts, as expected.

The influence of temperature, evaluated at the condition of excess of hydrogen (H_2/Guaiacol = 8), was different for each Pt/Nb_2O_5 catalyst from ANO or HY-340. While the

conversion values were between 35% and 9% for Pt/Nb_2O_5–ANO, it stayed in the lower range of 10–5% for Pt/Nb_2O_5–HY-340 from 523 K to 573 K. For Pt/$NbOPO_4$ the variation of conversion with temperature was 35–11% from 523–573 K, close to the observed for Pt/Nb_2O_5–ANO. The increasing temperature was positive for phenol formation over all catalysts. Catechol selectivity was lower at higher temperatures. The degree of deoxygenation increased with increasing temperature for Pt/Nb_2O_5–ANO (40%–47%), while it smoothly decrease with the temperature raise for Pt/Nb_2O_5–HY-340 (27%–24%) and Pt/$NbOPO_4$ (18%–17%). Pt supported on niobia produced more oxygen-free compounds than Pt supported on niobium phosphate.

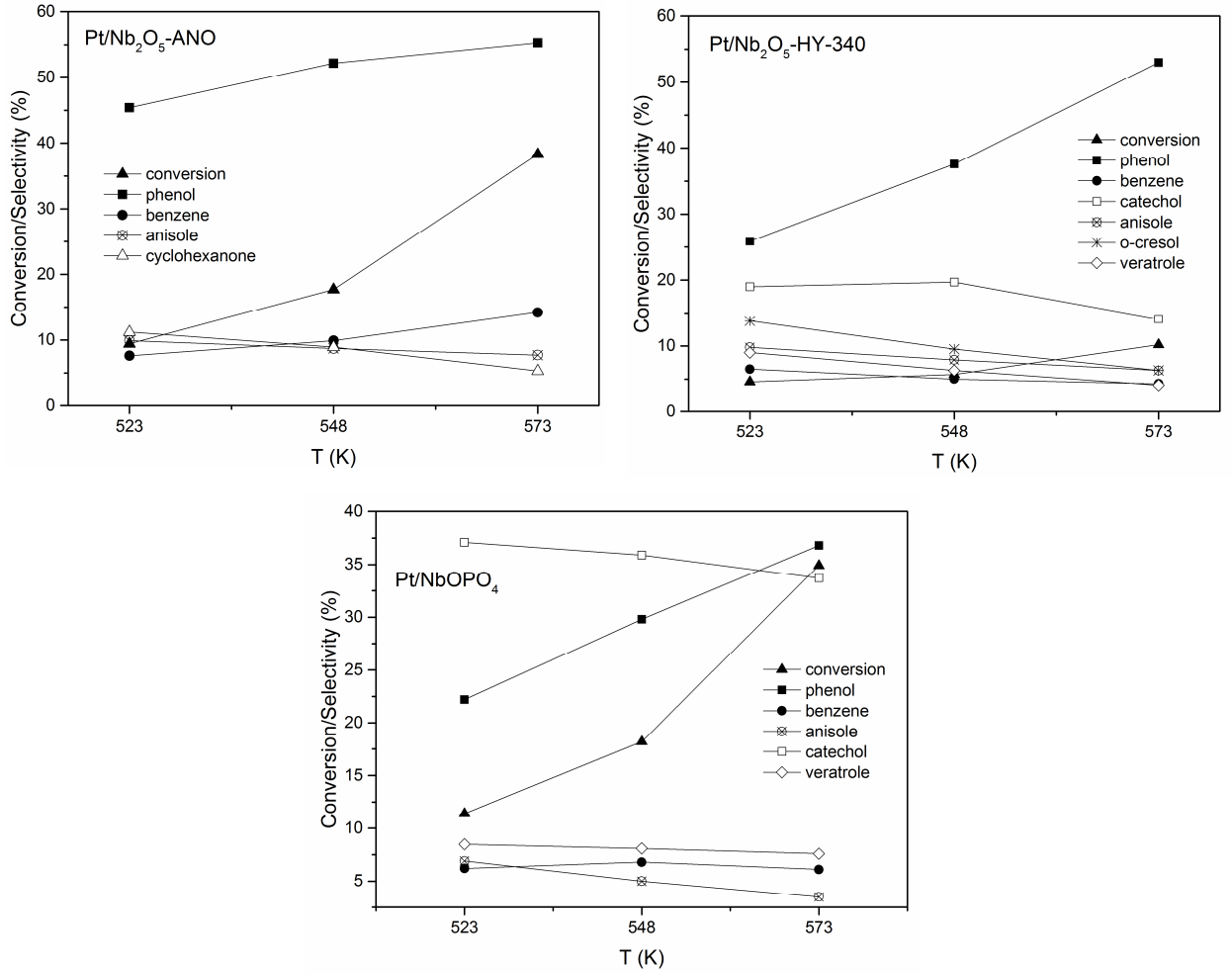

Figure 5.4 – Guaiacol conversion and products selectivity as a function of temperature for the HDO of guaiacol over Pt supported on Nb_2O_5 and $NbOPO_4$ catalysts. Selectivity values bellow 5% were omitted for clarity. Reaction conditions: atmospheric pressure, WHSV = 2.7 h^{-1}, H_2/Guaiacol = 8 (mol/mol), and temperatures equal to 523, 548, and 573 K.

5.2.2 d) Influence of the catalytic supports

The comparison between the pure supports behavior and the Pt supported catalysts can be seen in Figure 5.5. Niobia displayed a conversion of 1%, regardless the precursor used, while the niobium phosphate conversion was 6%. The products formed on the reactions with the supports alone were catechol, phenol, veratrole, and o-cresol. Phenol selectivity was 22% for Nb_2O_5 either from ANO or from HY-340, while its selectivity was 6% for $NbOPO_4$. The selectivity for catechol followed the order: $NbOPO_4$ (57%) > Nb_2O_5–ANO (33%) > Nb_2O_5–HY-340 (12%). It can be noted that the formation of more deoxygenated compounds occurred with the Nb_2O_5–HY-340 support. Oxygen-free compounds (hydrocarbons) were not produced in the reaction with pure supports, as previously noticed [76]. Methyl group transfer reactions (transalkylation), demethylation of guaiacol to produce catechol, and direct deoxygenation of catechol to form phenol were probably the main reactions that occurred over the supports alone.

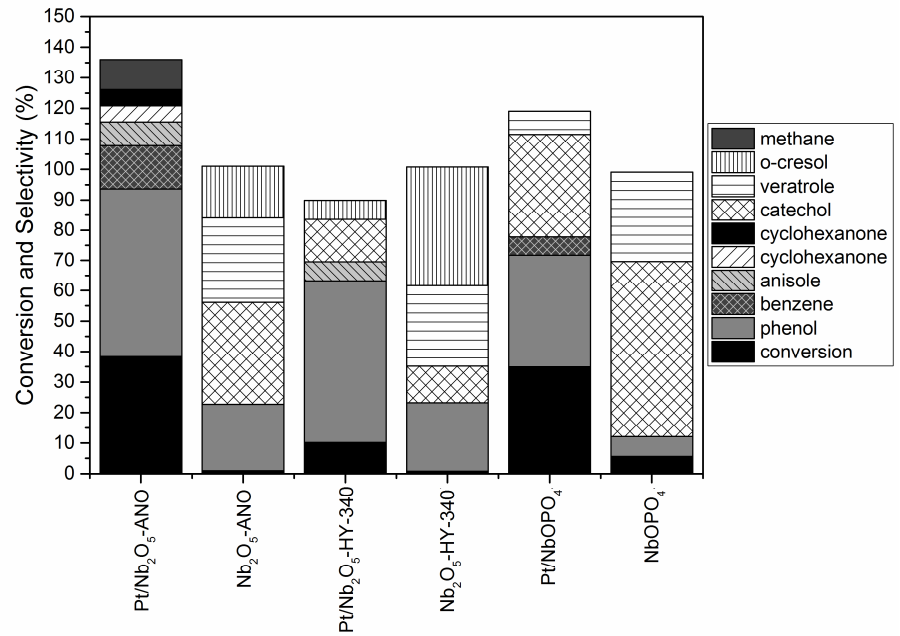

Figure 5.5 – Comparison of guaiacol conversion and product distribution between the Nb_2O_5 and $NbOPO_4$ supports and the Pt supported catalysts. Selectivity values bellow 5% were omitted for clarity. Reaction conditions: atmospheric pressure, 573 K, WHSV = 2.7 h^{-1}, H_2/Guaiacol = 8 (mol/mol), and around 10 h and 80 h TOS for the supports and catalysts reaction, respectively.

After the impregnation of Pt in the supports, there was a raise in both the conversion and production of deoxygenated products. The Pt metal may have contributed by splitting the molecule of hydrogen [24,27,65]. The selectivity for catechol decreased while phenol increased for each catalyst compared with its corresponding support. The increase in phenol

selectivity formed on the pure support compared to the Pt supported catalyst was 2.5, 2.4, and 5.7 times for Nb_2O_5–ANO, Nb_2O_5–HY-340, $NbOPO_4$, respectively.

5.2.2 e) Influence of space velocity (WHSV)

Table 5.6 shows the reaction rate at the higher value of space velocity (7 h^{-1}) and the comparison of conversion for WHSV equal to 2.7 h^{-1} and 7 h^{-1} for around 12 h TOS (the stationary state was not established). Conversion decreased with increasing space velocity, according to the expected, but with different extent for each catalyst. The reduction on conversion with the increasing space velocity occurred in the following sequence: Pt/$NbOPO_4$ (75.6%) > Pt/Nb_2O_5–ANO (64.8%) > Pt/Nb_2O_5–HY-340 (36.5%). The reaction rate ($\mu mol_{GUA}/(s.g_{cat})$) at 7 h^{-1} followed the order: Pt/Nb_2O_5–ANO (1.97) > Pt/$NbOPO_4$ (1.89) > Pt/Nb_2O_5–HY-340 (1.59).

Table 5.6 – Activity of Pt supported on Nb_2O_5 and $NbOPO_4$ at WHSV equal to 2.7 h^{-1} and 7 h^{-1}. Reaction conditions: atmospheric pressure, 573 K, H_2/Guaiacol = 8 (mol/mol), and around 12 h TOS.

Catalyst	Reaction rate ($\mu mol_{GUA}/(s.g_{cat})$) at WHSV = 7 h^{-1}	Conversion (%)	
		WHSV = 7 h^{-1}	WHSV = 2.7 h^{-1}
0.5% Pt/Nb_2O_5-ANO	1.97	12.5	35.5
0.5% Pt/Nb_2O_5-HY-340	1.59	9.9	15.6
1% Pt/$NbOPO_4$	1.89	11.7	48.0

5.2.2 f) SMSI effect for Pt/Nb_2O_5–ANO

Pt/Nb_2O_5–ANO was the best performance catalyst considering the formation of deoxygenated products. It was exposed that it might exhibit SMSI behavior already after reduction at 573 K, since the partial coverage of Pt by NbO_x species was observed at this temperature [24], although water formation may destroy the SMSI effect. The effect of an even higher reduction temperature of Pt/Nb_2O_5–ANO was investigated through a comparison by activating the catalyst at 573 K or 773 K, as can be seen in Table 5.7. The reaction rate reduced 82% when the reduction temperature increased from 573 K to 773 K. Product distribution when reduction was carried out at 773 K reminds that of the pure Nb_2O_5 shown in Figure 5.5, which is in agreement with the hypothesis of the platinum metal coverage by NbO_x species. The reduction in activity indicates that there was a strong suppression of the

hydrogen adsorption capacity of the Pt/Nb_2O_5–ANO catalyst. This finding is in agreement with the SMSI behavior [109]. On the HDO of phenol over Pt/Nb_2O_5 the specific rate (mmol/(min×g_{cat})) diminished 95% when the reduction temperature increased from 573 K to 773 K, yet product distribution was not affected. The authors suggested that Nb^{4+} sites and the oxygen vacances created during the catalyst activation were not responsible for the high formation of less oxygenated products [28].

5.2.2 g) Activation energy for Pt/Nb_2O_5–ANO

The determination of the activation energy for guaiacol HDO over Pt/Nb_2O_5–ANO is presented in Figure 5.6.

Table 5.7 – Guaiacol conversion and product distribution for Pt/Nb_2O_5–ANO catalyst at different reduction temperatures (573 K and 773 K). Reaction conditions: atmospheric pressure, 573 K, WHSV = 7 h^{-1}, H_2/Guaiacol = 8 (mol/mol), and around 30 h TOS.

Catalyst	Reduction at 573 K	Reduction at 773 K
X_{GUA} (%)	12.5	2.4
Reaction rate (µmol_{GUA}/(s.g_{cat}))	2.12	0.39
Selectivity (%)		
Phenol	54.1	24.5
Benzene	6.2	8.8
Catechol	8.3	18.7
Anisole	7.6	9.0
o-cresol	3.5	21.2
Cyclohexanone	4.8	0.0
Veratrole	2.8	16.7
Toluene	0.7	0.0
Cyclohexane	2.2	0.0
Methanol	2.6	1.1
CH_4	7.2	0.0
C identified (%)	105.9	100.0
DOD (%)	33	24

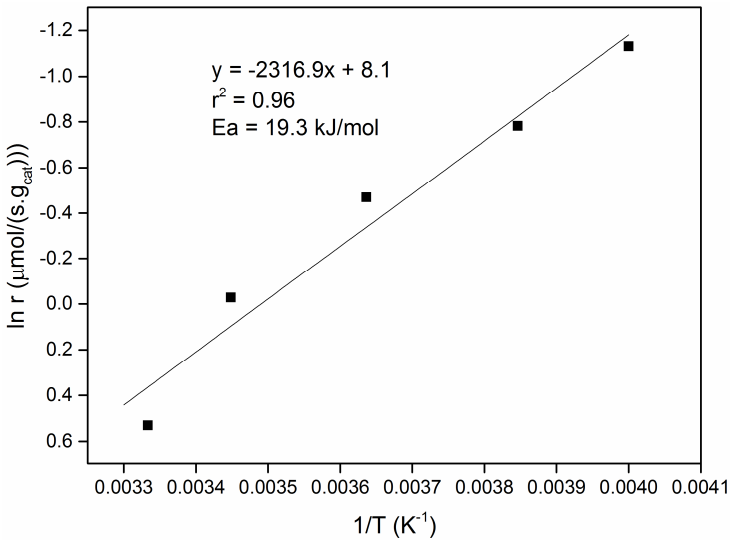

Figure 5.6 – Activation energy for guaiacol HDO over Pt/Nb_2O_5-ANO catalyst. Reaction conditions: atmospheric pressure, 523–573 K, WHSV = 4 h^{-1}, H_2/Guaiacol = 8 (mol/mol).

The activation energy for the HDO of guaiacol over transition metal phosphide catalysts supported on SiO_2 resulted in activation energies in the range of 23–63 kJ/mol, the lowest value corresponded to WP/SiO_2 [79]. The low value of the activation energy (19.3 kJ/mol) explains the high activity of the Pt/Nb_2O_5–ANO catalyst [110]. It is worth to mention that the activation energy for the HDO of phenol using the Pd/Nb_2O_5 catalyst prepared using niobic acid calcined at 623 K was 65 kJ/mol [28].

5.3 Conclusions

The HDO of guaiacol over Pt/Nb_2O_5 catalyst revealed that the precursor of niobia used changed both the catalyst properties and catalytic behavior at high hydrogen partial pressures. Pt/Nb_2O_5 prepared from ammonium niobium oxalate source was superior to the catalyst prepared using niobic acid in terms of activity and oxygen removal. It was inferred that the cooperation between Pt and the NbO_x species was the reason of the improved catalytic performance of Pt/Nb_2O_5, whose main product was phenol. The $Pt/NbOPO_4$ catalyst produced less deoxygenated compounds than Pt/Nb_2O_5.

CHAPTER 6 – GENERAL CONCLUSIONS AND SUGGESTIONS FOR FUTURE WORKS

6.1 Conclusions

The main findings of this work were the following:

- The HDO of guaiacol processes did not appear as being limited by the thermodynamic. The majority of the reactions from the studied reaction pathways behaved exothermically.
- The influence of the catalytic support was not negligible on the guaiacol conversion under the operating conditions tested.
- The higher the niobia content of Pt supported in xNb_2O_5/Al_2O_3 (x = 0, 5, 20, 100, wt.%) the higher was the selectivity for phenol and the degree of deoxygenation. Niobia had a promoting effect in the alumina deoxygenation ability.
- The $Pt/NbOPO_4$ catalyst produced less deoxygenated compounds than Pt/Nb_2O_5.
- The best performance catalyst was Pt/Nb_2O_5, which showed better oxygen removal ability compared to the other catalysts. The cooperation between Pt and NbO_x species was attributed as the reason of the improved catalytic performance.
- Pt/Nb_2O_5 prepared using ammonium niobium oxalate as the precursor of niobia was superior to the catalyst prepared using niobic acid in terms of activity and oxygen removal.
- High temperature, low space velocity, and excess of hydrogen in the feed were favorable for the guaiacol conversion and for the formation of deoxygenated products over Pt/Nb_2O_5.

6.2 Suggestions for future works

Characterization of the spent catalysts was not carried out, although it can reveal rich information. For example, a thermogravimetric analysis (TGA test) of the post-reaction catalyst may quantify the solid residue (coke).

It would be interesting to use another precursor of Pt for impregnation on the supports not based in chlorine, for example $Pt(NH_3)_4(NO_3)_2$, to see the effect on the acid sites density of the catalytic system studied and also the localization of the Pt metal in the support.

The best performance catalyst, Pt/Nb_2O_5, could be applied on the HDO reaction using other model compounds (e.g., phenol, anisole, catechol, syringol, eugenol) or pure lignin as feed.

The niobia support could be impregnated with different metals (e.g., Ni-Fe).

REFERENCES

[1] H. Ritchie and M. Roser, "Fossil fuels," *OurWorldInData.org*, 2018. [Online]. Available: https://ourworldindata.org/fossil-fuels.

[2] J. C. Serrano-Ruiz and J. A. Dumesic, "Catalytic production of liquid hydrocarbon transportation fuels," in *Catalysis for alternative energy generation*, New York: Springer Science+Business Media, 2012. https://doi.org/10.1007/978-1-4614-0344-9_2

[3] "Climate Change 2014: Synthesis Report. Contribution of Working Groups I, II and III to the Fifth Assessment Report of the Intergovernmental Panel on Climate Change," IPCC, 2014.

[4] "UNDP (United Nations Development Programme)," *UN Web Services Section*. [Online]. Available: http://www.un.org/sustainabledevelopment/. [Accessed: 03-Dec-2017].

[5] G. W. Huber, S. Iborra, and A. Corma, "Synthesis of transportation fuels from biomass: chemistry, catalysts, and engineering," *Chemical Reviews*, vol. 106, no. 9, pp. 4044–4098, 2006. https://doi.org/10.1021/cr068360d

[6] Y.-C. Lin and G. W. Huber, "The critical role of heterogeneous catalysis in lignocellulosic biomass conversion," *Energy & Environmental Science*, vol. 2, no. 1, pp. 68–80, 2009. https://doi.org/10.1039/b814955k

[7] A. V. Bridgwater, "Review of fast pyrolysis of biomass and product upgrading," *Biomass and Bioenergy*, vol. 38, pp. 68–94, 2012. https://doi.org/10.1016/j.biombioe.2011.01.048

[8] A. Oasmaa and S. Czernik, "Fuel oil quality of biomass pyrolysis oils state of the art for the end users," *Energy & Fuels*, vol. 13, no. 4, pp. 914–921, 1999. https://doi.org/10.1021/ef980272b

[9] S. Czernik and A. V. Bridgwater, "Overview of applications of biomass fast pyrolysis oil," *Energy & Fuels*, vol. 18, no. 2, pp. 590–598, 2004. https://doi.org/10.1021/ef034067u

[10] D. A. Bulushev and J. R. H. Ross, "Catalysis for conversion of biomass to fuels via pyrolysis and gasification: a review," *Catalysis Today*, vol. 171, no. 1, pp. 1–13, 2011. https://doi.org/10.1016/j.cattod.2011.02.005

[11] P. M. Mortensen, J.-D. Grunwaldt, P. A. Jensen, K. G. Knudsen, and A. D. Jensen, "A review of catalytic upgrading of bio-oil to engine fuels," *Applied Catalysis A: General*, vol. 407, no. 1, pp. 1–19, 2011. https://doi.org/10.1016/j.apcata.2011.08.046

[12] B. Kamm and M. Kamm, "Principles of biorefineries," *Applied Microbiology and Biotechnology*, vol. 64, no. 2, pp. 137–145, 2004. https://doi.org/10.1007/s00253-003-1537-7

[13] S. Fernando, S. Adhikari, C. Chandrapal, and N. Murali, "Biorefineries: current status, challenges, and future direction," *Energy & Fuels*, vol. 20, no. 4, pp. 1727–1737, 2006. https://doi.org/10.1021/ef060097w

[14] E. Furimsky, "Catalytic hydrodeoxygenation," *Applied Catalysis A: General*, vol. 199, no. 2, pp. 147–190, 2000. https://doi.org/10.1016/S0926-860X(99)00555-4

[15] I. Graça, J. M. Lopes, H. S. Cerqueira, and M. F. Ribeiro, "Bio-oils upgrading for second generation biofuels," *Industrial & Engineering Chemistry Research*, vol. 52, no. 1, pp. 275–287, 2013. https://doi.org/10.1021/ie301714x

[16] Q. Bu *et al.*, "A review of catalytic hydrodeoxygenation of lignin-derived phenols from biomass pyrolysis," *Bioresource Technology*, vol. 124, pp. 470–477, 2012. https://doi.org/10.1016/j.biortech.2012.08.089

[17] M. Á. González-Borja and D. E. Resasco, "Anisole and guaiacol hydrodeoxygenation over monolithic Pt–Sn catalysts," *Energy & Fuels*, vol. 25, no. 9, pp. 4155–4162, 2011. https://doi.org/10.1021/ef200728r

[18] R. N. Olcese, M. Bettahar, D. Petitjean, B. Malaman, F. Giovanella, and A. Dufour, "Gas-phase hydrodeoxygenation of guaiacol over Fe/SiO_2 catalyst," *Applied Catalysis B: Environmental*, vol. 115–116, pp. 63–73, 2012. https://doi.org/10.1016/j.apcatb.2011.12.005

[19] T. Omotoso, S. Boonyasuwat, and S. P. Crossley, "Understanding the role of TiO_2 crystal structure on the enhanced activity and stability of Ru/TiO_2 catalysts for the conversion of lignin-derived oxygenates," *Green Chemistry*, vol. 16, no. 2, pp. 645–652, 2014. https://doi.org/10.1039/c3gc41377b

[20] D. A. Ruddy, J. A. Schaidle, J. R. Ferrell III, J. Wang, L. Moens, and J. E. Hensley, "Recent advances in heterogeneous catalysts for bio-oil upgrading via 'ex situ catalytic fast pyrolysis': catalyst development through the study of model compounds," *Green Chemistry*, vol. 16, no. 2, pp. 454–490, 2014. https://doi.org/10.1039/c3gc41354c

[21] A. M. Robinson, J. E. Hensley, and J. W. Medlin, "Bifunctional catalysts for upgrading of biomass-derived oxygenates: a review," *ACS Catalysis*, vol. 6, no. 8, pp. 5026–5043, 2016. https://doi.org/10.1021/acscatal.6b00923

[22] D. E. Resasco and S. P. Crossley, “Implementation of concepts derived from model compound studies in the separation and conversion of bio-oil to fuel,” *Catalysis Today*, vol. 257, pp. 185–199, 2015. https://doi.org/10.1016/j.cattod.2014.06.037

[23] S. Boonyasuwat, T. Omotoso, D. E. Resasco, and S. P. Crossley, “Conversion of guaiacol over supported Ru catalysts,” *Catalysis Letters*, vol. 143, no. 8, pp. 783–791, 2013. https://doi.org/10.1007/s10562-013-1033-3

[24] K. Kon, W. Onodera, S. Takakusagi, and K. Shimizu, “Hydrodeoxygenation of fatty acids and triglycerides by Pt-loaded Nb_2O_5 catalysts,” *Catalysis Science & Technology*, vol. 4, no. 10, pp. 3705–3712, 2014. https://doi.org/10.1039/c4cy00757c

[25] Shao Yi, Xia Qineng, Liu Xiaohui, Lu Guanzhong, and Wang Yanqin, “$Pd/Nb_2O_5/SiO_2$ catalyst for the direct hydrodeoxygenation of biomass-related compounds to liquid alkanes under mild conditions,” *ChemSusChem*, vol. 8, no. 10, pp. 1761–1767, 2015. https://doi.org/10.1002/cssc.201500053

[26] W. Guan, X. Chen, S. Jin, C. Li, C.-W. Tsang, and C. Liang, “Highly stable Nb_2O_5–Al_2O_3 composites supported Pt catalysts for hydrodeoxygenation of diphenyl ether,” *Industrial & Engineering Chemistry Research*, vol. 56, no. 47, pp. 14034–14042, 2017. https://doi.org/10.1021/acs.iecr.7b03736

[27] Y. Shao *et al.*, “Selective production of arenes via direct lignin upgrading over a niobium-based catalyst,” *Nature Communications*, vol. 8, p. 16104, 2017. https://doi.org/10.1038/ncomms16104

[28] A. M. Barrios *et al.*, “Hydrodeoxygenation of phenol over niobia supported Pd catalyst,” *Catalysis Today*, vol. 302, pp. 115–124, 2018. https://doi.org/10.1016/j.cattod.2017.03.034

[29] R. M. West, M. H. Tucker, D. J. Braden, and J. A. Dumesic, “Production of alkanes from biomass derived carbohydrates on bi-functional catalysts employing niobium-based supports,” *Catalysis Communications*, vol. 10, no. 13, pp. 1743–1746, 2009. https://doi.org/10.1016/j.catcom.2009.05.021

[30] J.-M. Jehng and I. E. Wachs, “Molecular structures of supported niobium oxide catalysts under ambient conditions,” *Journal of Molecular Catalysis*, vol. 67, no. 3, pp. 369–387, 1991. https://doi.org/10.1016/0304-5102(91)80050-D

[31] “BP Statistical Review of World Energy,” British Petroleum, 66th edition, Jun. 2017.

[32] “BIG - Banco de Informações de Geração,” *ANEEL – Agência Nacional de Energia Elétrica*. [Online]. Available: http://www2.aneel.gov.br/aplicacoes/capacidadebrasil/OperacaoCapacidadeBrasil.cfm. [Accessed: 14-Jul-2017].

[33] D. L. Klass, “Biomass for Renewable Energy and Fuels,” in *Encyclopedia of Energy*, New York: Elsevier, 2004, pp. 193–212.

[34] “Conceituando biomassa,” *CENBIO (Centro Nacional de Referência em Biomassa do Instituto de Energia e Ambiente da Universidade de São Paulo – CENBIO/IEE/USP)*. [Online]. Available: http://www.iee.usp.br/gbio/?q=livro/conceituando-biomassa. [Accessed: 07-Jul-2017].

[35] D. L. Klass, *Biomass for renewable energy, fuels, and chemicals*. San Diego: Academic Press, 1998.

[36] Z. He and X. Wang, “Hydrodeoxygenation of model compounds and catalytic systems for pyrolysis bio-oils upgrading,” *Catalysis for Sustainable Energy*, vol. 1, pp. 28–52, 2012. https://doi.org/10.2478/cse-2012-0004

[37] M. Saidi, F. Samimi, D. Karimipourfard, T. Nimmanwudipong, B. C. Gates, and M. R. Rahimpour, “Upgrading of lignin-derived bio-oils by catalytic hydrodeoxygenation,” *Energy & Environmental Science*, vol. 7, no. 1, pp. 103–129, 2014. https://doi.org/10.1039/c3ee43081b

[38] P. Azadi, O. R. Inderwildi, R. Farnood, and D. A. King, “Liquid fuels, hydrogen and chemicals from lignin: a critical review,” *Renewable and Sustainable Energy Reviews*, vol. 21, pp. 506–523, 2013. https://doi.org/10.1016/j.rser.2012.12.022

[39] J. Zakzeski, P. C. A. Bruijnincx, A. L. Jongerius, and B. M. Weckhuysen, “The catalytic valorization of lignin for the production of renewable chemicals,” *Chemical Reviews*, vol. 110, no. 6, pp. 3552–3599, 2010. https://doi.org/10.1021/cr900354u

[40] A. . Bridgwater and G. V. . Peacocke, “Fast pyrolysis processes for biomass,” *Renewable and Sustainable Energy Reviews*, vol. 4, no. 1, pp. 1–73, 2000. https://doi.org/10.1016/S1364-0321(99)00007-6

[41] R. Maggi and B. Delmon, “Comparison between ‘slow’ and ‘flash’ pyrolysis oils from biomass,” *Fuel*, vol. 73, no. 5, pp. 671–677, 1994. https://doi.org/10.1016/0016-2361(94)90007-8

[42] P. Grange, E. Laurent, R. Maggi, A. Centeno, and B. Delmon, “Hydrotreatment of pyrolysis oils from biomass: reactivity of the various categories of oxygenated compounds and preliminary techno-economical study,” *Catalysis Today*, vol. 29, no. 1, pp. 297–301, 1996. https://doi.org/10.1016/0920-5861(95)00295-2

[43] M. Graglia, N. Kanna, and D. Esposito, “Lignin refinery: towards the preparation of renewable aromatic building blocks,” *ChemBioEng Reviews*, vol. 2, no. 6, pp. 377–392, 2015. https://doi.org/10.1002/cben.201500019

[44] R. J. Angelici, “An overview of modeling studies in HDS, HDN and HDO catalysis,” *Polyhedron*, vol. 16, no. 18, pp. 3073–3088, 1997. https://doi.org/10.1016/S0277-5387(96)00581-5

[45] D. C. Elliott, “Historical developments in hydroprocessing bio-oils,” *Energy & Fuels*, vol. 21, no. 3, pp. 1792–1815, 2007. https://doi.org/10.1021/ef070044u

[46] M. J. Girgis and B. C. Gates, “Reactivities, reaction networks, and kinetics in high-pressure catalytic hydroprocessing,” *Industrial & Engineering Chemistry Research*, vol. 30, no. 9, pp. 2021–2058, 1991. https://doi.org/10.1021/ie00057a001

[47] V. N. Bui, G. Toussaint, D. Laurenti, C. Mirodatos, and C. Geantet, “Co-processing of pyrolisis bio oils and gas oil for new generation of bio-fuels: hydrodeoxygenation of guaiacol and SRGO mixed feed,” *Catalysis Today*, vol. 143, no. 1, pp. 172–178, 2009. https://doi.org/10.1016/j.cattod.2008.11.024

[48] R. Sotelo-Boyás, F. Trejo-Zárraga, and F. de J. Hernández-Loyo, “Hydroconversion of triglycerides into green liquid fuels,” in *Hydrogenation*, InTech: Iyad Karamé, 2012. https://doi.org/10.5772/48710

[49] Honeywell UOP, “Honeywell Green Diesel.” [Online]. Available: https://www.uop.com/processing-solutions/renewables/green-diesel. [Accessed: 16-Mar-2018].

[50] “Neste - Who we are.” [Online]. Available: https://www.neste.com/en/corporate-info/who-we-are/production. [Accessed: 16-Mar-2018].

[51] M. J. Mccall, R. J. Allen, and D. E. Mackowiak, “Conversion of lignocellulosic biomass to chemicals and fuels,” WO/2008/157165 A1.

[52] T. da S. Veras, T. S. Mozer, D. da C. R. M. dos Santos, and A. da S. César, “Hydrogen: trends, production and characterization of the main process worldwide,” *International Journal of Hydrogen Energy*, vol. 42, no. 4, pp. 2018–2033, 2017. https://doi.org/10.1016/j.ijhydene.2016.08.219

[53] H. Balat and E. Kırtay, “Hydrogen from biomass – present scenario and future prospects,” *International Journal of Hydrogen Energy*, vol. 35, no. 14, pp. 7416–7426, 2010. https://doi.org/10.1016/j.ijhydene.2010.04.137

[54] R. D. Cortright, R. R. Davda, and J. A. Dumesic, “Hydrogen from catalytic reforming of biomass-derived hydrocarbons in liquid water,” *Nature*, vol. 418, p. 964, 2002. https://doi.org/10.1038/nature01009

[55] J. H. Marsman, J. Wildschut, P. Evers, S. de Koning, and H. J. Heeres, “Identification and classification of components in flash pyrolysis oil and hydrodeoxygenated oils by

two-dimensional gas chromatography and time-of-flight mass spectrometry," *Journal of Chromatography A*, vol. 1188, pp. 17–25, 2008. https://doi.org/10.1016/j.chroma.2008.02.034

[56] T. V. Choudhary and C. B. Phillips, "Renewable fuels via catalytic hydrodeoxygenation," *Applied Catalysis A: General*, vol. 397, no. 1, pp. 1–12, 2011. https://doi.org/10.1016/j.apcata.2011.02.025

[57] Chheda Juben N., Huber George W., and Dumesic James A., "Liquid-phase catalytic processing of biomass-derived oxygenated hydrocarbons to fuels and chemicals," *Angewandte Chemie International Edition*, vol. 46, no. 38, pp. 7164–7183, 2007. https://doi.org/10.1002/anie.200604274

[58] J.-S. Moon, E.-G. Kim, and Y.-K. Lee, "Active sites of Ni_2P/SiO_2 catalyst for hydrodeoxygenation of guaiacol: a joint XAFS and DFT study," *Journal of Catalysis*, vol. 311, pp. 144–152, 2014. https://doi.org/10.1016/j.jcat.2013.11.023

[59] T. Nimmanwudipong, R. C. Runnebaum, D. E. Block, and B. C. Gates, "Catalytic reactions of guaiacol: reaction network and evidence of oxygen removal in reactions with hydrogen," *Catalysis Letters*, vol. 141, no. 6, pp. 779–783, 2011. https://doi.org/10.1007/s10562-011-0576-4

[60] R. C. Runnebaum, T. Nimmanwudipong, D. E. Block, and B. C. Gates, "Catalytic conversion of compounds representative of lignin-derived bio-oils: a reaction network for guaiacol, anisole, 4-methylanisole, and cyclohexanone conversion catalysed by Pt/[gamma]-Al_2O_3," *Catalysis Science & Technology*, vol. 2, no. 1, pp. 113–118, 2012. https://doi.org/10.1039/C1CY00169H

[61] T. Nimmanwudipong *et al.*, "Selective hydrodeoxygenation of guaiacol catalyzed by platinum supported on magnesium oxide," *Catalysis Letters*, vol. 142, no. 10, pp. 1190–1196, 2012. https://doi.org/10.1007/s10562-012-0884-3

[62] D. Gao, C. Schweitzer, H. T. Hwang, and A. Varma, "Conversion of guaiacol on noble metal catalysts: reaction performance and deactivation studies," *Industrial & Engineering Chemistry Research*, vol. 53, no. 49, pp. 18658–18667, 2014. https://doi.org/10.1021/ie500495z

[63] S.-K. Wu, P.-C. Lai, and Y.-C. Lin, "Atmospheric hydrodeoxygenation of guaiacol over nickel phosphide catalysts: effect of phosphorus composition," *Catalysis Letters*, vol. 144, no. 5, pp. 878–889, 2014. https://doi.org/10.1007/s10562-014-1231-7

[64] S. Ted Oyama *et al.*, "Production of phenol and cresol from guaiacol on nickel phosphide catalysts supported on acidic supports," *Topics in Catalysis*, vol. 58, no. 4, pp. 201–210, 2015. https://doi.org/10.1007/s11244-015-0361-5

[65] Q. Xia *et al.*, "Direct hydrodeoxygenation of raw woody biomass into liquid alkanes," *Nature Communications*, vol. 7, p. 11162, 2016. https://doi.org/10.1038/ncomms11162

[66] M. V. Bykova *et al.*, "Ni-based sol–gel catalysts as promising systems for crude bio-oil upgrading: guaiacol hydrodeoxygenation study," *Applied Catalysis B: Environmental*, vol. 113–114, pp. 296–307, 2012. https://doi.org/10.1016/j.apcatb.2011.11.051

[67] C. Liu, Y. Zhang, and X. Huang, "Study of guaiacol pyrolysis mechanism based on density function theory," *Fuel Processing Technology*, vol. 123, pp. 159–165, 2014. https://doi.org/10.1016/j.fuproc.2014.01.002

[68] A. M. Verma and N. Kishore, "DFT study on gas-phase hydrodeoxygenation of guaiacol by various reaction schemes," *Molecular Simulation*, vol. 43, no. 2, pp. 141–153, 2017. https://doi.org/10.1080/08927022.2016.1239825

[69] Honeywell International Inc., [Online]. Available: https://www.honeywell.com/.

[70] Honeywell, "UniSim® Design Simulation Basis Reference Guide," Canada, 2010.

[71] M. V. Bykova, S. G. Zavarukhin, L. I. Trusov, and V. A. Yakovlev, "Guaiacol hydrodeoxygenation kinetics with catalyst deactivation taken into consideration," *Kinetics and Catalysis*, vol. 54, no. 1, pp. 40–48, 2013. https://doi.org/10.1134/S0023158413010023

[72] S.-K. Wu, P.-C. Lai, Y.-C. Lin, H.-P. Wan, H.-T. Lee, and Y.-H. Chang, "Atmospheric hydrodeoxygenation of guaiacol over alumina-, zirconia-, and silica-supported nickel phosphide catalysts," *ACS Sustainable Chemistry & Engineering*, vol. 1, no. 3, pp. 349–358, 2013. https://doi.org/10.1021/sc300157d

[73] B. Güvenatam, O. Kurşun, E. H. J. Heeres, E. A. Pidko, and E. J. M. Hensen, "Hydrodeoxygenation of mono- and dimeric lignin model compounds on noble metal catalysts," *Catalysis Today*, vol. 233, pp. 83–91, 2014. https://doi.org/10.1016/j.cattod.2013.12.011

[74] C. R. Lee *et al.*, "Catalytic roles of metals and supports on hydrodeoxygenation of lignin monomer guaiacol," *Catalysis Communications*, vol. 17, pp. 54–58, 2012. https://doi.org/10.1016/j.catcom.2011.10.011

[75] R. N. Olcese, J. Francois, M. M. Bettahar, D. Petitjean, and A. Dufour, "Hydrodeoxygenation of guaiacol, a surrogate of lignin pyrolysis vapors, over iron based catalysts: kinetics and modeling of the lignin to aromatics integrated process," *Energy & Fuels*, vol. 27, no. 2, pp. 975–984, 2013. https://doi.org/10.1021/ef301971a

[76] V. N. Bui, D. Laurenti, P. Delichère, and C. Geantet, "Hydrodeoxygenation of guaiacol: Part II: support effect for CoMoS catalysts on HDO activity and selectivity,"

Applied Catalysis B: Environmental, vol. 101, no. 3, pp. 246–255, 2011. https://doi.org/10.1016/j.apcatb.2010.10.031

[77] C. Amen-Chen, H. Pakdel, and C. Roy, "Production of monomeric phenols by thermochemical conversion of biomass: a review," *Bioresource Technology*, vol. 79, no. 3, pp. 277–299, 2001. https://doi.org/10.1016/S0960-8524(00)00180-2

[78] D. J. Nowakowski, A. V. Bridgwater, D. C. Elliott, D. Meier, and P. de Wild, "Lignin fast pyrolysis: results from an international collaboration," *Journal of Analytical and Applied Pyrolysis*, vol. 88, no. 1, pp. 53–72, 2010. https://doi.org/10.1016/j.jaap.2010.02.009

[79] H. Y. Zhao, D. Li, P. Bui, and S. T. Oyama, "Hydrodeoxygenation of guaiacol as model compound for pyrolysis oil on transition metal phosphide hydroprocessing catalysts," *Applied Catalysis A: General*, vol. 391, no. 1, pp. 305–310, 2011. https://doi.org/10.1016/j.apcata.2010.07.039

[80] S. I. Sandler, *Chemical, biochemical, and engineering thermodynamics*. John Wiley & Sons, Inc., 2006.

[81] T. Prasomsri, M. Shetty, K. Murugappan, and Y. Roman-Leshkov, "Insights into the catalytic activity and surface modification of MoO3 during the hydrodeoxygenation of lignin-derived model compounds into aromatic hydrocarbons under low hydrogen pressures," *Energy & Environmental Science*, vol. 7, no. 8, pp. 2660–2669, 2014. https://doi.org/10.1039/C4EE00890A

[82] Schimming Sarah M. *et al.*, "Hydrodeoxygenation of guaiacol over ceria–zirconia catalysts," *ChemSusChem*, vol. 8, no. 12, pp. 2073–2083, 2015. https://doi.org/10.1002/cssc.201500317

[83] T. Nimmanwudipong, R. C. Runnebaum, K. Brodwater, J. Heelan, D. E. Block, and B. C. Gates, "Design of a high-pressure flow-reactor system for catalytic hydrodeoxygenation: guaiacol conversion catalyzed by platinum supported on MgO," *Energy & Fuels*, vol. 28, no. 2, pp. 1090–1096, 2014. https://doi.org/10.1021/ef4020026

[84] V. N. Bui, D. Laurenti, P. Afanasiev, and C. Geantet, "Hydrodeoxygenation of guaiacol with CoMo catalysts. Part I: promoting effect of cobalt on HDO selectivity and activity," *Applied Catalysis B: Environmental*, vol. 101, no. 3, pp. 239–245, 2011. https://doi.org/10.1016/j.apcatb.2010.10.025

[85] A. Gutierrez, R. K. Kaila, M. L. Honkela, R. Slioor, and A. O. I. Krause, "Hydrodeoxygenation of guaiacol on noble metal catalysts," *Catalysis Today*, vol. 147, no. 3, pp. 239–246, 2009. https://doi.org/10.1016/j.cattod.2008.10.037

[86] A. Vuori, A. Helenius, and J. B.-S. Bredenberg, “Influence of sulphur level on hydrodeoxygenation,” *Applied Catalysis*, vol. 52, no. 1, pp. 41–56, 1989. https://doi.org/10.1016/S0166-9834(00)83371-0

[87] S. J. Tauster and S. C. Fung, “Strong metal-support interactions: occurrence among the binary oxides of groups IIA–VB,” *Journal of Catalysis*, vol. 55, no. 1, pp. 29–35, 1978. https://doi.org/10.1016/0021-9517(78)90182-3

[88] F. B. Passos, D. A. . Aranda, R. R. Soares, and M. Schmal, “Effect of preparation method on the properties of Nb_2O_5 promoted platinum catalysts,” *Catalysis Today*, vol. 43, no. 1, pp. 3–9, 1998. https://doi.org/10.1016/S0920-5861(98)00131-X

[89] S. Lowell, J. E. Shields, M. A. Thomas, and M. Thommes, *Characterization of porous solids and powders: surface area, pore size and density*. New York: Springer Science+Business Media, 2004.

[90] O. Kresnawahjuesa, R. J. Gorte, D. de Oliveira, and L. Y. Lau, “A simple, inexpensive, and reliable method for measuring Brønsted-acid site densities in solid acids,” *Catalysis Letters*, vol. 82, no. 3, pp. 155–160, 2002. https://doi.org/10.1023/A:1020514911456

[91] A. Boumaza *et al.*, “Transition alumina phases induced by heat treatment of boehmite: An X-ray diffraction and infrared spectroscopy study,” *Journal of Solid State Chemistry*, vol. 182, no. 5, pp. 1171–1176, 2009. https://doi.org/10.1016/j.jssc.2009.02.006

[92] V. S. Braga, J. A. Dias, S. C. L. Dias, and J. L. de Macedo, “Catalyst materials based on Nb_2O_5 supported on SiO_2−Al_2O_3: preparation and structural characterization,” *Chemistry of Materials*, vol. 17, no. 3, pp. 690–695, 2005. https://doi.org/10.1021/cm048673u

[93] T. T. Su, Y. C. Zhai, H. Jiang, and H. Gong, “Studies on the thermal decomposition kinetics and mechanism of ammonium niobium oxalate,” *Journal of Thermal Analysis and Calorimetry*, vol. 98, no. 2, p. 449, 2009. https://doi.org/10.1007/s10973-009-0300-4

[94] F. M. . Mendes, C. . Perez, R. . Soares, F. . Noronha, and M. Schmal, “Ammonium complex of niobium as a precursor for the preparation of Nb_2O_5/Al_2O_3 catalysts,” *Catalysis Today*, vol. 78, no. 1, pp. 449–458, 2003. https://doi.org/10.1016/S0920-5861(02)00327-9

[95] R. Rodrigues, N. Isoda, M. Gonçalves, F. C. A. Figueiredo, D. Mandelli, and W. A. Carvalho, “Effect of niobia and alumina as support for Pt catalysts in the hydrogenolysis of glycerol,” *Chemical Engineering Journal*, vol. 198–199, pp. 457–467, 2012. https://doi.org/10.1016/j.cej.2012.06.002

[96] T. Iizuka, K. Ogasawara, and K. Tanabe, “Acidic and catalytic properties of niobium pentaoxide,” *Bulletin of the Chemical Society of Japan*, vol. 56, pp. 2927–2931, 1983.

[97] J. Datka, A. M. Turek, J. M. Jehng, and I. E. Wachs, "Acidic properties of supported niobium oxide catalysts: An infrared spectroscopy investigation," *Journal of Catalysis*, vol. 135, no. 1, pp. 186–199, 1992. https://doi.org/10.1016/0021-9517(92)90279-Q

[98] J. G. Tittensor, R. J. Gorte, and D. M. Chapman, "Isopropylamine adsorption for the characterization of acid sites in silica-alumina catalysts," *Journal of Catalysis*, vol. 138, no. 2, pp. 714–720, 1992. https://doi.org/10.1016/0021-9517(92)90318-C

[99] S. Guerrero, J. T. Miller, and E. E. Wolf, "Activity and selectivity control by niobium for the preferential oxidation of co on pt supported catalysts," *Applied Catalysis A: General*, vol. 328, no. 1, pp. 27–34, 2007. https://doi.org/10.1016/j.apcata.2007.04.010

[100] A. Popov *et al.*, "Bio-oils hydrodeoxygenation: adsorption of phenolic molecules on oxidic catalyst supports," *The Journal of Physical Chemistry C*, vol. 114, no. 37, pp. 15661–15670, 2010. https://doi.org/10.1021/jp101949j

[101] T. Nimmanwudipong, R. C. Runnebaum, D. E. Block, and B. C. Gates, "Catalytic conversion of guaiacol catalyzed by platinum supported on alumina: reaction network including hydrodeoxygenation reactions," *Energy & Fuels*, vol. 25, no. 8, pp. 3417–3427, 2011. https://doi.org/10.1021/ef200803d

[102] Xia Qi-Neng, Cuan Qian, Liu Xiao-Hui, Gong Xue-Qing, Lu Guan-Zhong, and Wang Yan-Qin, "Pd/$NbOPO_4$ multifunctional catalyst for the direct production of liquid alkanes from aldol adducts of furans," *Angewandte Chemie International Edition*, vol. 53, no. 37, pp. 9755–9760, 2014. https://doi.org/10.1002/anie.201403440

[103] West Ryan M., Liu Zhen Y., Peter Maximilian, and Dumesic James A., "Liquid alkanes with targeted molecular weights from biomass-derived carbohydrates," *ChemSusChem*, vol. 1, no. 5, pp. 417–424, 2008. https://doi.org/10.1002/cssc.200800001

[104] E. R. Sacia, M. H. Deaner, Y. "Lin" Louie, and A. T. Bell, "Synthesis of biomass-derived methylcyclopentane as a gasoline additive via aldol condensation/hydrodeoxygenation of 2,5-hexanedione," *Green Chemistry*, vol. 17, no. 4, pp. 2393–2397, 2015. https://doi.org/10.1039/C4GC02292K

[105] F. M. Reguera *et al.*, "The use of niobium based catalysts for liquid fuel production," *Materials Research*, vol. 7, no. 2, pp. 343–348, 2004. https://doi.org/10.1590/S1516-14392004000200021

[106] K. S. W. Sing *et al.*, "Reporting physisorption data for gas/solid systems with special reference to the determination of surface area and porosity (Recommendations 1984)," *Pure and Applied Chemistry*, vol. 57, no. 4, pp. 603–619, 1985. https://doi.org/10.1351/pac198557040603

[107] J. Wildschut, I. Melián-Cabrera, and H. J. Heeres, "Catalyst studies on the hydrotreatment of fast pyrolysis oil," *Applied Catalysis B: Environmental*, vol. 99, no. 1, pp. 298–306, 2010. https://doi.org/10.1016/j.apcatb.2010.06.036

[108] A. Florentino, P. Cartraud, P. Magnoux, and M. Guisnet, "Textural, acidic and catalytic properties of niobium phosphate and of niobium oxide: Influence of the pretreatment temperature," *Applied Catalysis A: General*, vol. 89, no. 2, pp. 143–153, 1992. https://doi.org/10.1016/0926-860X(92)80229-6

[109] M. Schmal, D. A. . Aranda, R. . Soares, F. . Noronha, and A. Frydman, "A study of the promoting effect of noble metal addition on niobia and niobia alumina catalysts," *Catalysis Today*, vol. 57, no. 3, pp. 169–176, 2000. https://doi.org/10.1016/S0920-5861(99)00323-5

[110] Y. Li, J. Fu, and B. Chen, "Highly selective hydrodeoxygenation of anisole, phenol and guaiacol to benzene over nickel phosphide," *RSC Adv.*, vol. 7, no. 25, pp. 15272–15277, 2017. https://doi.org/10.1039/C7RA00989E

[111] R. E. Hayes and J. P. Mmbaga, *Introduction to Chemical Reactor Analysis*, 2nd edition. CRC Press, 2013.

[112] R. J. Gorte, "What do we know about the acidity of solid acids?," *Catalysis Letters*, vol. 62, no. 1, pp. 1–13, 1999. https://doi.org/10.1023/A:1019010013989

[113] S. Jongpatiwut, Z. Li, D. E. Resasco, W. E. Alvarez, E. L. Sughrue, and G. W. Dodwell, "Competitive hydrogenation of poly-aromatic hydrocarbons on sulfur-resistant bimetallic Pt-Pd catalysts," *Applied Catalysis A: General*, vol. 262, no. 2, pp. 241–253, 2004. https://doi.org/10.1016/j.apcata.2003.11.032

APPENDIX I – SUPPLEMENTARY INFORMATION

A. External mass transfer limitation test

The intrinsic reaction rate – the rate in the absence of transport limitations – is achieved when the surface reaction is the slowest step, so it determines the overall reaction rate. In the kinetic regime, the overall reaction rate will be connected with the reaction mechanism and will not be determined by the rate of physical processes. The determination of the limiting step of a catalytic reaction is also important to make an extrapolation of experimental results to the industrial scale. Because of these facts, external mass transfer limitations tests were performed.

The experiments were conducted with the ratio of guaiacol flow rate at feed to catalyst mass constant and equal to WHSV = 2.7 h^{-1} [WHSV = g guaiacol/(h × g catalyst)]. The flow rate was changed, as the catalyst mass, in such a way to keep the ratio constant. The experiments were conducted according to ref. [111]. It was found that the external diffusion resistance vanished for a guaiacol flow rate around 1.3 g/h, as can be seen in Fig. A. As expected, guaiacol conversion increased with increasing flow rate, until it reached a plateau, which indicates the elimination of external resistance.

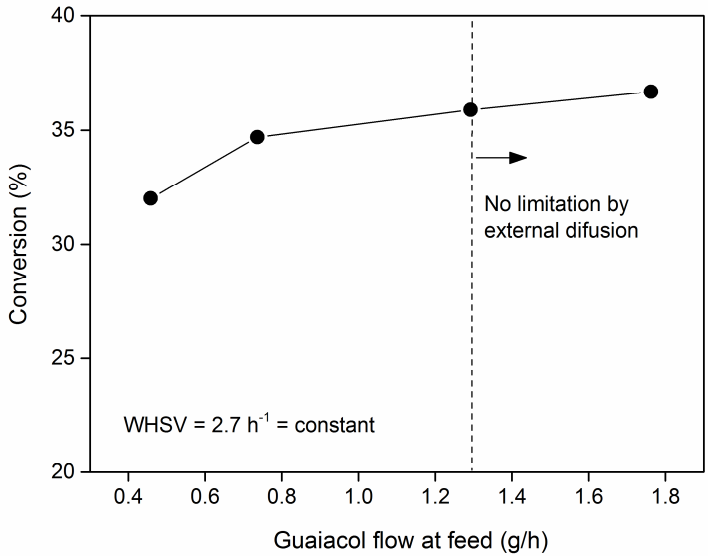

Fig. A – External diffusion resistance test at 300 °C and atmospheric pressure for 0.5% Pt/Nb_2O_5.

B. X-ray diffraction (Chapter 4)

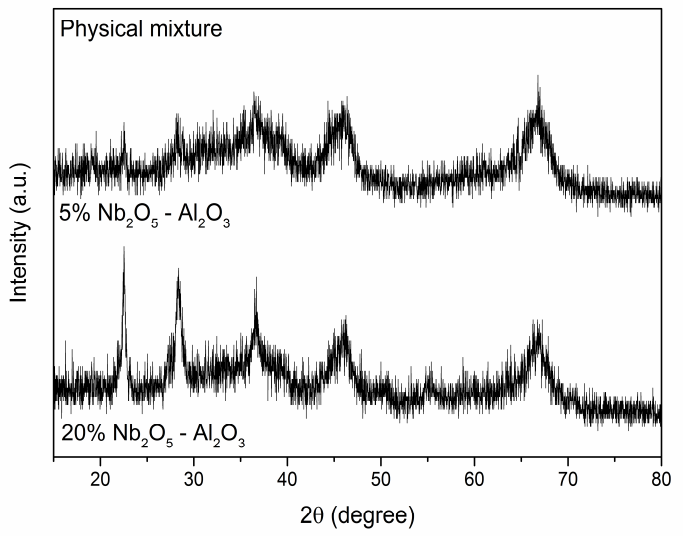

Fig. B – XRD patterns of the physical mixture comprised by the oxides Nb_2O_5 and Al_2O_3.

C. Nitrogen physisorption (Chapter 4)

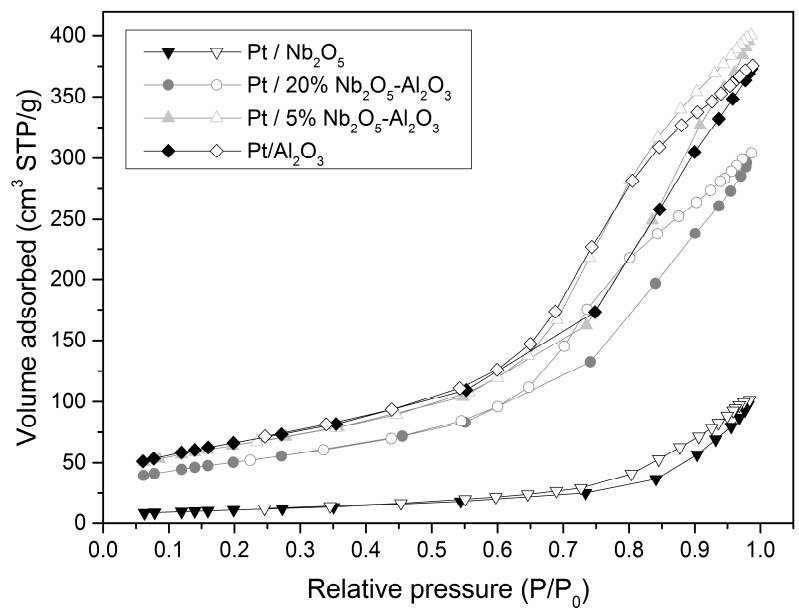

Fig. C – Nitrogen adsorption (filled points) and desorption (unfilled points) isotherms at 77 K for $Pt/xNb_2O_5/(100\text{-}x)Al_2O_3$ (x = 0, 5, 20, 100, wt.%) catalysts.

D. Temperature-programmed desorption of isopropylamine (Chapter 4)

The IPA-TPD profiles of the catalysts are shown in Fig. D. The desorbed species identified were propylene (m/e = 41), ammonia (m/e = 17), and unreacted isopropylamine (m/e = 44). Desorption of propylene and ammonia is related to protonated molecules at Brønsted acid sites (BAS). But the ammonia desorption is not recommended for quantification of the BAS, since isopropylamine possibly reacts in the heated stainless-steel tubing and forms ammonia [90]. Desorption of unreacted isopropylamine (physically adsorbed amine) at low temperature may refer to several species, such as Lewis acid sites (LAS), hydroxyl defects, and protonated amines at the Brønsted sites [112]. The m/e = 41 signal used to monitor propylene in the mass spectrometer can arises from either propylene or unreacted isopropylamine. To identify the m/e = 41 signal related to isopropylamine desorption a comparison with the m/e = 44 signal is needed [113].

It can be seen in the IPA-TPD profile for the γ-Al_2O_3 support that unreacted isopropylamine (m/e = 44) desorbed during all TPD experiment, but mostly before 400 °C. The peak with maximum at 509 °C refers to Brønsted acid sites. The amount of propylene desorbed at this temperature was 27 µmol/g, which conforms to literature [98,113]. The m/e= 44 signal of the Pt/Al_2O_3 and Pt/Nb_2O_5 catalysts was higher than the corresponding supports.

BAS: Brønsted acid sites

LAS: Lewis acid sites

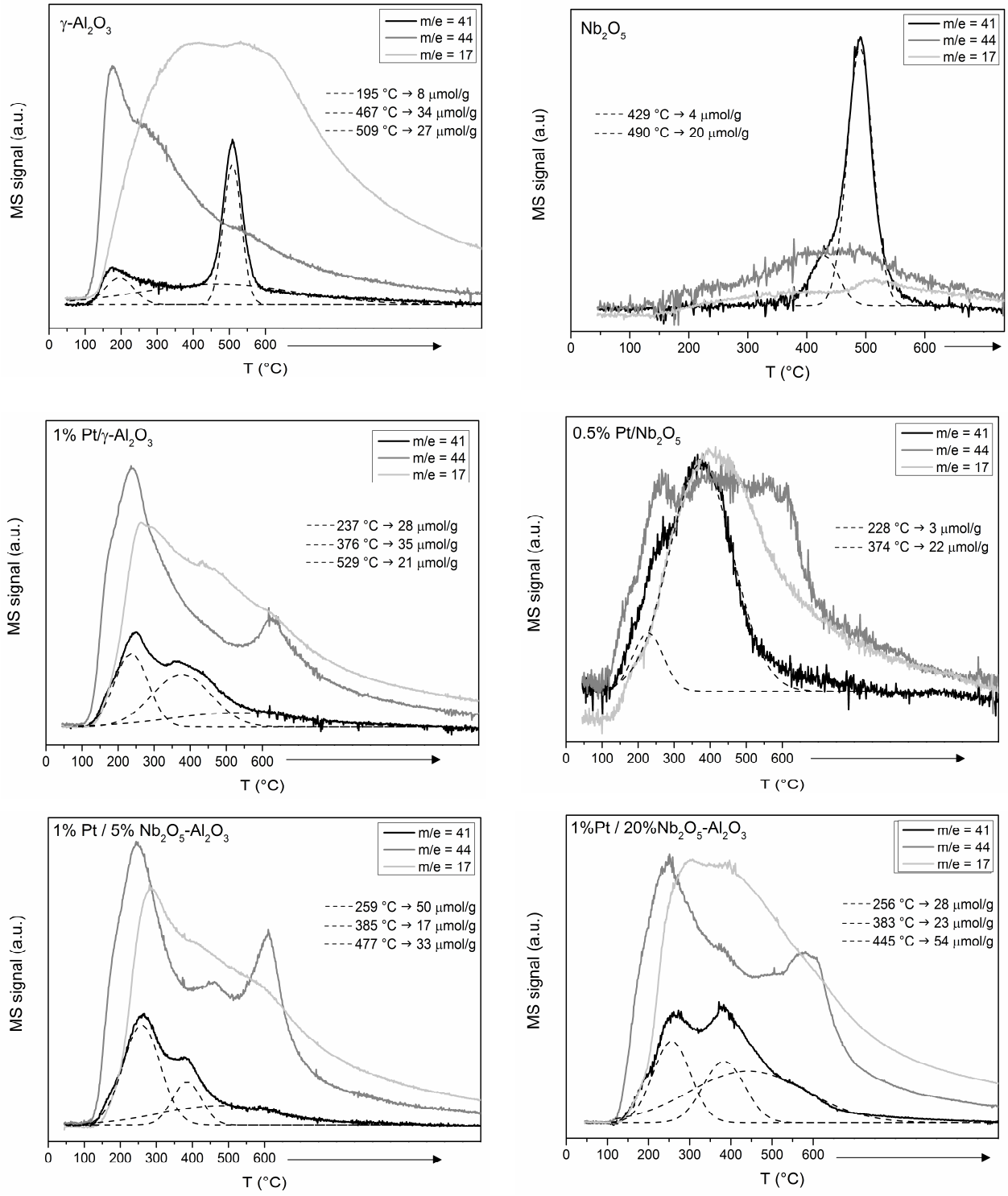

Fig. D – Isopropylamine TPD profiles for the $Pt/Nb_2O_5/Al_2O_3$ catalytic system corresponding to Brønsted acid site catalyzed decomposition of isopropylamine (m/e = 44) into propylene (m/e = 41) and ammonia (m/e = 17).

E. Selectivity as a function of time on stream (TOS) (Chapter 4)

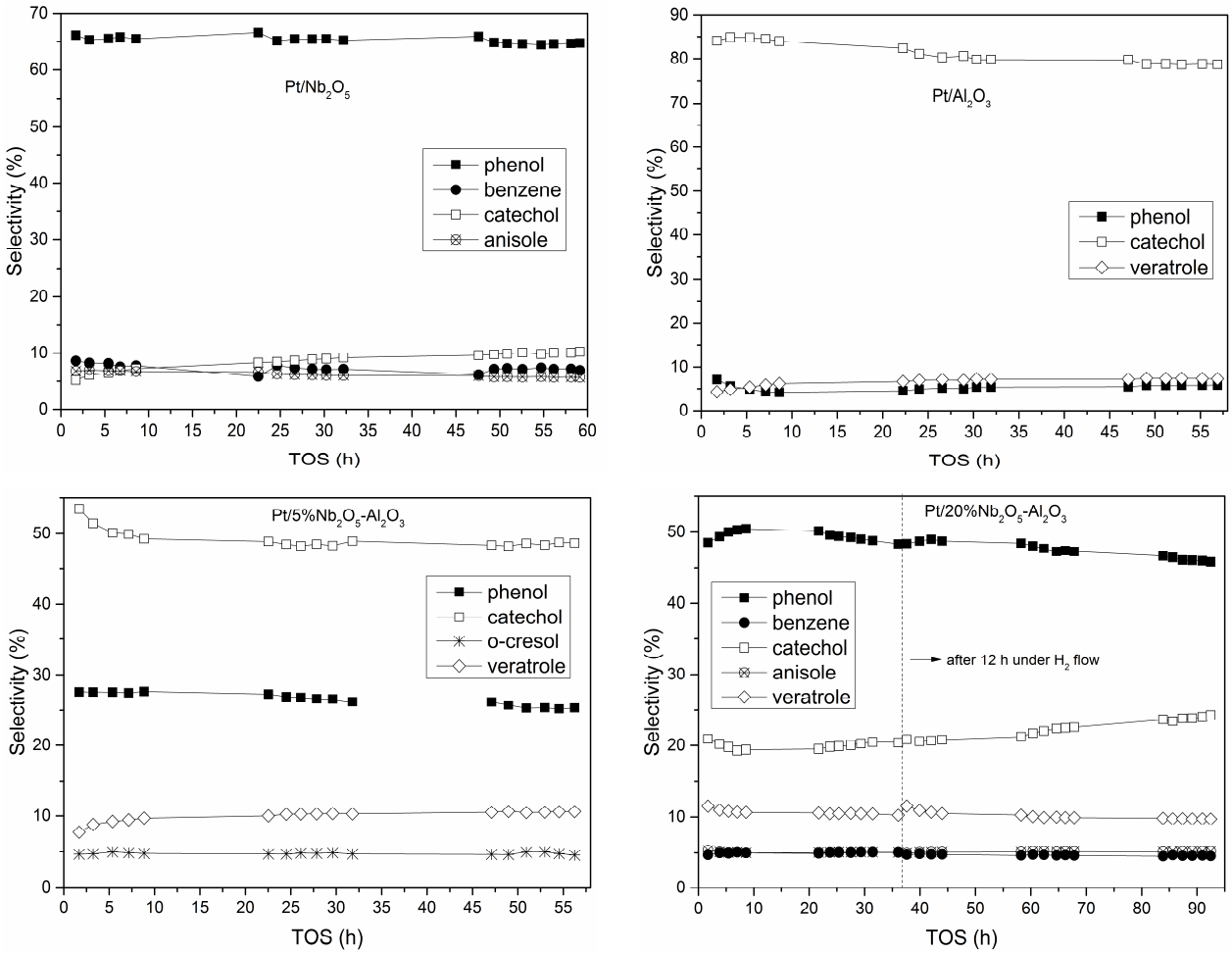

Fig. E – Selectivity of the main products as a function of time on stream (TOS) for the HDO of guaiacol over Pt supported on $xNb_2O_5/(100\text{-}x)Al_2O_3$ (x = 0, 5, 20, 100, wt.%). Selectivity values bellow 5% were omitted for clarity. Reaction conditions: atmospheric pressure, 573 K, WHSV = 2.7 h^{-1}, H_2/Guaiacol = 1 (mol/mol), and gas flow comprised by 13% H_2 in Ar. The catalyst $Pt/20\%Nb_2O_5–Al_2O_3$ was reactivated after 35 h TOS by a H_2 flow for 12 h, then the reaction was retaken for more 60h**.**

F. Nitrogen physisorption (Chapter 5)

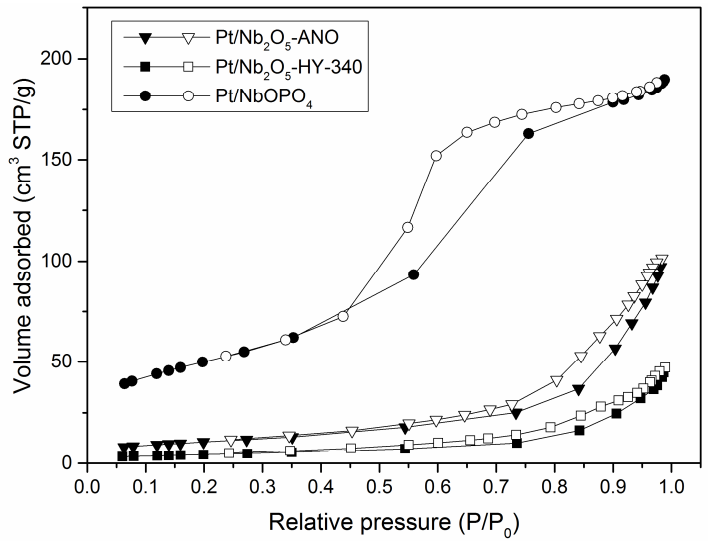

Fig. F – Nitrogen adsorption (filled points) and desorption (unfilled points) isotherms at 77 K for the Pt/Nb_2O_5-ANO, Pt/Nb_2O_5-HY-340, and $Pt/NbOPO_4$ catalysts.

G. Temperature-programmed desorption of isopropylamine (Chapter 5)

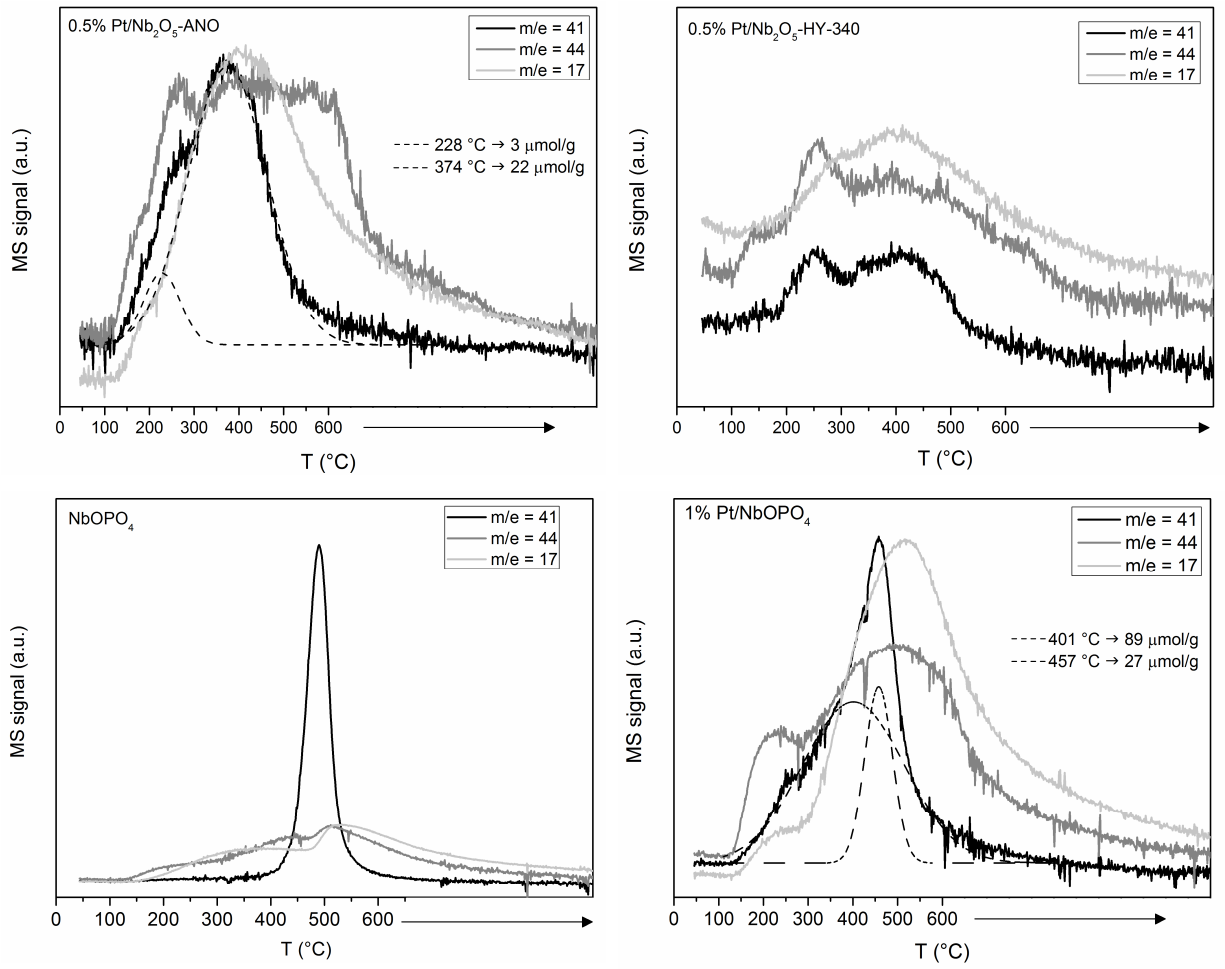

Fig. G – Isopropylamine TPD profiles for the Pt/Nb_2O_5 and $Pt/NbOPO_4$ catalytic system corresponding to Brønsted acid site catalyzed decomposition of isopropylamine (m/e = 44) into propylene (m/e = 41) and ammonia (m/e = 17).